INNOVATIVE APPROACH FOR LIFETIME EXTENSION OF AN AGING INVENTORY OF VULNERABLE BRIDGES

A DISSERTATION
SUBMITTED TO THE FACULTY OF THE GRADUATE SCHOOL
OF THE UNIVERSITY OF MINNESOTA
BY

ANDREW J. GASTINEAU

IN PARTIAL FULFILLMENT OF THE REQUIREMENTS
FOR THE DEGREE OF
DOCTOR OF PHILOSOPHY

STEVEN F. WOJTKIEWICZ; ARTURO E. SCHULTZ

DECEMBER 2013

Acknowledgements

I would like to thank my advisors Dr. Steven F. Wojtkiewicz and Dr. Arturo E. Schultz for their guidance and patience throughout my graduate work. I extend my appreciation to the Center for Transportation Studies and the Department of Civil Engineering at the University of Minnesota for financially supporting me during my time at the University. I would also like to thank David Thompson for the initial numerical model of the Cedar Avenue Bridge as well as the countless other graduate students who have given me advice and allowed me to bounce ideas around the office. I would like to acknowledge my parents and grandparents who have always encouraged me to continue learning and supported me during my extended time as a student. Lastly, I would like to thank Sonja for putting up with me during the ups and downs of my research.

Abstract

Many of the bridges in the United States are being used beyond their initial design intentions, classified as structurally deficient, and are in need of rehabilitation or replacement. A portion of these bridges suffer from specific bridge vulnerabilities that have been categorized as fracture prone. The safe operating life of fracture prone details is governed by the stress range experienced by the detail. Providing alternate load paths through a supplemental apparatus attached to the bridge structure can relieve high stress ranges, and the limited safe bridge service life due to these vulnerabilities may be safely extended. As part of the apparatus, the utility of a mechanical amplifier, the scissor jack, is carefully investigated; the amplifier allows for a very localized application and much smaller stiffness and damping device demands. The mathematical relationships for the apparatus, in particular the magnification factor for displacement and force, are formulated analytically and verified through numerical modeling. The effects of the mechanical amplifier are investigated on a simple beam numerical model as well as through more comprehensive parameter studies on numerical bridge models of an in-service fracture critical bridge. The parameter studies reveal that longer apparatuses and larger cross-sectional member area improve performance. A relatively small passive stiffness and damping device provides adequate safe life extension when employing the mechanical amplifier and vastly outperforms an apparatus without the amplifier. The apparatus parameters are optimized through a series of simulations, and small amounts of device damping with no stiffness perform the best. Much larger damping and stiffness coefficients are necessary to achieve similar performance without the mechanical amplifier. Safe life extension of over 100 percent can be achieved with apparatus member cross-sectional area of 25 percent of the bridge girder area. For implementation on a general bridge, a long and slender mechanically amplified RM apparatus is

recommended for safe life extension. For a passive system, a RM device with a small damping coefficient and no stiffness should be employed. The cross-sectional area of the RM apparatus members will need to be sufficiently large to provide adequate safe life extension and will have to be evaluated on a case-by-case basis. A simple bridge model should be used to gauge initial member size. Frequency response analyses of the modified bridge structures show response amplification at some loading frequencies. Analyses also found different optimal device characteristics for decreasing the magnitude of the maximum or minimum moment range experienced at the vulnerability. These findings lend support to the hypothesis that semi-active control strategies allowing for changes in device characteristics may ultimately be more beneficial and should be further investigated.

Table of Contents

List of Tables

List of Figures

List of Symbols

A = cross-sectional area;

A_f = constant depending on the fatigue vulnerable detail;

A = modified state space matrix used for simulations;

$\check{A}$ = MR damper parameter;

a_{co} = modified matrix area coefficient;

a_{des} = desired member cross-sectional area;

$\mathbf{A_i}$ = initial state space matrix;

$a_{initial}$ = initial member cross-sectional area;

$Axial_{local}$ = local member axial force;

$Axial_{Global}$ = global member axial force;

$ADTT_{SL}$ = average daily truck traffic for a single lane;

A_1 = bridge skew stress formula constant;

A_2 = bridge skew stress formula constant;

A_3 = bridge skew stress formula constant;

C = damping matrix;

c = damping coefficient;

c_{co} = modified matrix damping coefficient;

c_{cr} = critical speed;

c_{des} = desired RM device damping coefficient;

C_i = constant of integration;

$c_{initial}$ = initial RM device damping coefficient;

$\mathbf{C_r}$ = reduced damping matrix;

$\check{c_0}$ = viscous damping at large velocities;

$\check{c_1}$ = viscous damping for force rolloff at low frequencies;

d = horizontal projection of a side of the undeflected scissor jack quadrilateral;

E = young's modulus of elasticity;

F = force;

f = loading vector of the reduced order bridge model;

$\check{F}$ = MR damper force;

F_d = force of RM stiffness device;

F_i = force at the respective degree of freedom;

F_j = force at end of scissor jack;

$f_{(j)}$ = jth natural frequency of beam;

f_{re} = effective stress range at fatigue vulnerable detail;

G = shear modulus;

g = web gap;

H = magnetic field;

I = moment of inertia;

$\check{\imath}$ = MR damper electric current;

J = torsional stiffness;

j = frequency index;

K = stiffness matrix;

k = stiffness coefficient;

k_{co} = modified stiffness coefficient;

k_d = stiffness of RM device in PIA apparatus;

k_{des} = desired RM device stiffness coefficient;

k_{eff} = effective stiffness of PIA apparatus;

k_{ext} = stiffness of horizontal member in PIA apparatus;

$\mathbf{K_i}$ = global stiffness matrix for a specified member;

$k_{initial}$ = initial RM device stiffness coefficient;

k_{jack} = equivalent stiffness of the scissor jack;

$k_{leg,des}$ = the desired extension stiffness for the PIA apparatus;

$k_{leg,i}$ = the initial extension stiffness for the PIA apparatus;

$\mathbf{k_{mem}}$ = local member stiffness matrix;

k_{PIA} = the stiffness coefficient for the PIA apparatus;

$\mathbf{K_r}$ = reduced stiffness matrix;

k_s = spring stiffness coefficient;

$k_{s,des}$ = the desire RM device stiffness for the PIA apparatus;

$k_{s,i}$ = the initial RM device stiffness for the PIA apparatus;

$\mathbf{K_{static}}$ = stiffness matrix after static reduction;

$\widetilde{k_0}$ = stiffness at large velocities;

$\widetilde{k_1}$ = accumulator stiffness;

L = bridge span length;

L = length of a side of the scissor jack quadrilateral;

l = length of beam;

l = length of frame element;

l = length of beam;

$\tilde{L}$ = distance between attachment points for PIA apparatus;

$\mathbf{LR_k}$ = stiffness matrix for degrees of freedom with zero entry in the mass matrix;

$\mathbf{LR_m}$ = mass matrix for degrees of freedom with zero entry in the mass matrix;

M = moment;

$\mathbf{M}$ = mass matrix;

m = mechanical magnification value for the scissor jack;

m_f = mechanical force magnification for the scissor jack;

M_{left} = moment at the left end of a frame element;

$\mathbf{M_r}$ = reduced mass matrix;

M_{right} = moment at the right end of a frame element;

$\mathbf{M_{static}}$ = mass matrix after static reduction;

n = number of stress range cycles per truck;

$\check{n}$ = MR damper parameter;

P = point load at midpoint of beam;

p = loading vector of the bridge model;

q = generalized modal displacements;

r = joint rotations calculated from displacements;

r_L = frame element left end rotation;

R_R = resistance factor;

r_R = frame element right end rotation;

R_{red} = stress range percent moment reduction;

R_s = partial load factor;

S = global structural stiffness matrix;

t_w = girder web thickness;

u_i = displacement at the respective degree of freedom;

$\mathbf{UL_k}$ = stiffness matrix for degrees of freedom with non-zero entry in the mass matrix;

$\mathbf{UL_m}$ = mass matrix for degrees of freedom with non-zero entry in the mass matrix;

v = vertical displacement of frame element;

w = vertical displacement of frame element;

x = one half of height of vertical height within the scissor jack;

x = global displacements;

$\dot{x}$ = velocity of *x*;

$\hat{x}$ = horizontal position beginning from the left end of the element;

$\breve{x}$ = MR damper accumulator displacement;

x_i = one half of height of vertical height within the undeflected scissor jack;

X_L = frame element left end horizontal global displacement;

x_L = frame element left end horizontal local displacement;

X_R = frame element right end horizontal global displacement;

x_R = frame element right end horizontal local displacement;

Y = fatigue life;

y = vertical deflection of a simple beam;

$\breve{y}$ = MR damper system displacement;

Y_f = remaining fatigue life;

Y_N = fatigue life based on future volume;

Y_P = present bridge age;

Y_1 = fatigue life based on past volume;

z = distance from the centerline of the beam to the horizontal end of the scissor jack;

$\check{z}$ = evolutionary variable in MR damper model;

Z_L = frame element left end vertical global displacement;

z_L = frame element left end vertical displacement;

Z_R = frame element right end vertical global displacement;

z_R = frame element right end vertical displacement;

α = rotational stiffness equivalent of scissor jack;

$\check{\alpha}$ = MR damper parameter;

β = angle between the horizontal and one side of the quadrilateral in the scissor jack;

$\check{\beta}$ = MR damper parameter;

γ = fatigue load factor;

$\check{\gamma}$ = MR damper parameter;

$\dot{\gamma}$ = shear strain rate;

γ_k = non-dimensional rotational stiffness constant for beam with RM apparatus;

λ = stiffness matrix coefficient;

$\mathbf{\Delta A_{area}}$ = state space matrix for unit change in RM apparatus member axial area;

$\mathbf{\Delta A_{k,device}}$ = state space matrix for unit change in RM device stiffness;

$\mathbf{\Delta A_{c,device}}$ = state space matrix for unit change in RM device damping;

Δf = live load stress range;

$(\Delta F)_n$ = nominal fatigue resistance;

$(\Delta F)_{TH}$ = nominal stress threshold for infinite fatigue life;

η = post-yield plastic viscosity;

θ = rotation at RM apparatus attachment point;

μ = mass matrix coefficient;

ξ = damping ratio;

σ_{wg}= web gap stress;

τ = shear stress;

τ_0 = yield stress;

$\mathbf{\Phi}$ = mode shapes;

φ = slope of frame element;

χ = non-dimensional matrix shear beam element constant;

Chapter 1: Introduction

1.1 Discussion of Infrastructure

Many of the bridges in the United States are being used beyond their initial design intentions, classified as structurally deficient, and in need of rehabilitation or replacement. The most recent American Society of Civil Engineers (ASCE) infrastructure report (2013) gives the bridge system in the United States a rating of C+. While this is an improvement over the previous report card grade of C, the average age of the 607,380 bridges in the United States is 42 years old; many bridges have an initial design life of 50 years. According to Minnesota Department of Transportation (Mn/DOT) records, as of July 2010, 270 trunk highway bridges in Minnesota are classified as structurally deficient or obsolete. Of those, 99 are structurally deficient signifying that one or more members or connections of the bridge should be repaired or replaced in the near future. Additionally, the Federal Highway Administration (FHWA) reports that out of the 13,121 local and trunk highway bridges in Minnesota, 1,613 bridges are structurally deficient or functionally obsolete. Nationally, 151,497 bridges, 25 percent of the highway bridge inventory in the United States, are categorized as deficient (2012). Included in the deficiency classification are bridges that that do not meet design specifications for current loading conditions and bridges that have members or connections that should be replaced or repaired. ASCE estimates a funding deficit of $76 billion for deficient bridges alone over the next 15 years. The majority of these bridges were built in the 1950s and 60s and are at or near the end of their intended design life. This situation prompts one to pose the questions: How can bridge owners extend the life of these bridges while funds are allocated for bridge replacement? What options are both safe and affordable?

1.2 Motivation

A large portion of bridges that are structurally deficient have details that are prone to fatigue damage. The National Cooperative Highway Research Program (NCHRP) did not begin comprehensive fatigue testing until the late 1960s so that most bridges designed before the mid 1970s and some even later were not adequately designed for fatigue (Mertz 2012). Due to the fiscal constraints of many bridge owners, the replacement of these bridges is cost prohibitive, and it will be necessary to extend the life of these bridges in a safe and cost effective manner. The service life of these fatigue prone details is governed by the size and number of cyclic stress ranges experienced by the detail. As a result, if the stress ranges encountered by the detail can be reduced, the safe extension of bridge life may be accomplished. This dissertation aims to show that by using bridge health monitoring and structural response modification techniques, it may be possible to achieve stress range reduction and safely extend bridge fatigue life.

Before continuing, a few important terms used throughout the dissertation will be defined. A *response modification (RM) device* is a piece of equipment that provides additional stiffness and/or damping which can be passive, semi-active, or active in nature. A *RM apparatus* is a group of components, including a RM device and its attachment to the structure, which can apply response modification forces to the bridge to improve bridge response.

1.3 Outline of Dissertation

Chapter 2 presents an overview of bridge health monitoring and structural response modification techniques to explore the components of health monitoring and recent control strategies. The chapter addresses previous research as well as mathematical representations in four main categories: 1) common bridge vulnerabilities, 2) bridge loading models, 3) RM and control devices, and 4) bridge health monitoring systems, which are all critical elements for successful bridge structural response modification. Defining these mathematical models allows for modeling to be formulated and analyses carried out. Fig. 1.1 depicts the interactions between the four components and presents a concise picture of general bridge response modification approaches.

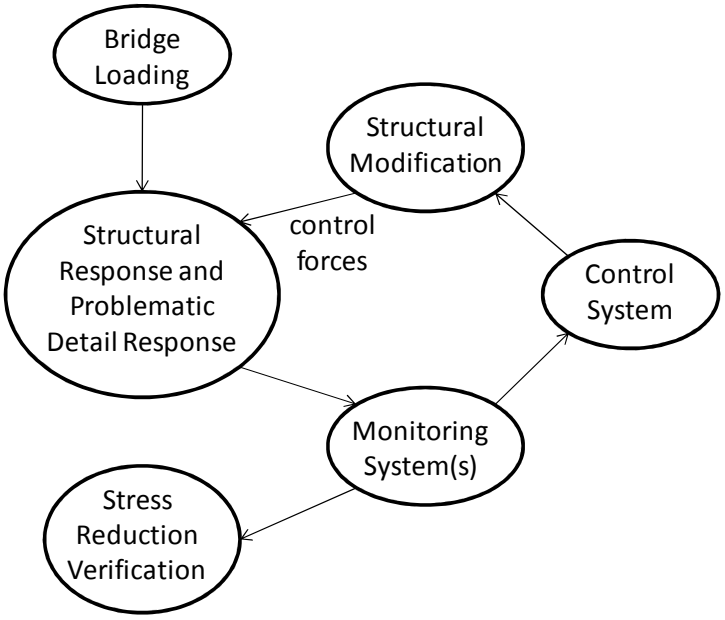

Figure 1.1 Structural response modification flowchart for addressing vulnerabilities

Chapter 3 presents the proposed bridge response modification approach. A mechanical amplifier, known as a scissor jack, for novel use on bridges is introduced and mathematically analyzed. The mathematical derivations are validated using a numerical 2-D beam finite element model. The RM apparatus is fully described and its effects are briefly investigated on the simple numerical model.

Chapter 4 introduces a prospective bridge candidate for structural response modification, the Cedar Avenue Bridge in Minnesota. The Cedar Avenue Bridge is a fracture critical tied arch bridge, and due to the non-redundant nature of a fracture critical steel bridge, fatigue failure is a concern. To explore the RM apparatus, finite element numerical models of the Cedar Avenue Bridge are developed and described in detail.

Chapter 5 demonstrates the efficacy of the response modification approach on the numerical model of the Cedar Avenue Bridge through several parameter studies. While gaining an understanding of the advantages and limits of the approach, it will be shown that stress ranges can be locally reduced on specific fatigue vulnerable details.

Chapter 6 further develops the response modification approach through optimizations of various RM apparatus properties. Optimizations for loading scenarios with either a single truck or five trucks traveling in succession are carried out.

Chapter 7 explores the frequency responses of a simple beam outfitted with the response modification apparatus as well as the vulnerable bridge outfitted with the apparatus. Response amplifications could occur at some frequencies and may warrant the need for a device that has the ability to change characteristics depending on loading conditions so that amplification does not occur.

Chapter 8 offers conclusions and recommendations regarding the proposed response modification approach. Additionally, future directions and other possible extensions for the response modification apparatus approach are discussed.

Chapter 2: Bridge Structural Response Modification and Health Monitoring

To successfully implement structural response modification techniques and bridge health monitoring for the purpose of bridge safety and life extension, the theoretical concepts and mathematical formulations of four main components are considered: 1) common bridge vulnerabilities, 2) bridge loading models, 3) RM devices, and 4) bridge health monitoring systems. The thoughtful combination of these four attributes should lead to a productive system yielding successful safe life extension.

2.1 Common Bridge Vulnerabilities

The identification of bridge vulnerabilities can be a difficult task because of the diversity of factors that can contribute to bridge failure. These vulnerabilities range from possible vehicle or barge impacts to stress concentrations at a specific bridge detail; the wide variety of issues can be problematic to classify and recognize. The goal of this section is to identify vulnerabilities that could decrease safe bridge life and that could be modified to safely extend bridge life. To help identify these vulnerabilities that affect bridge safety, it is important to understand previous bridge collapses and their causes. It is also essential to identify other issues such as bridge components that decrease the operational life of the bridge.

2.1.1 Bridge Failures

Historically, bridge collapses have been caused by many different problems. Most collapses have been closely scrutinized and reasons for the collapse are generally agreed upon. Akesson (2008) outlines five key bridge collapses that have changed the way engineers understand bridges as well as documenting other important collapses. The key

collapses identified are: the Dee Bridge, the Tay Bridge, the Quebec Bridge, the Tacoma Narrows Bridge, and the multiple box-girder bridge failures from 1969-1971. In addition to the collapses highlighted by Akesson, other bridge failures are of interest for particularly dangerous issues and have been documented by others. Some of these collapses include: the Cosens Memorial Bridge, the Silver Bridge, the Hoan Bridge, the Grand Bridge, the I-35W bridge in Minnesota, and, most recently, the I-5 Skagit River Bridge in Washington. Each of these failures provided insight and caution for incorporation into bridge designs and maintenance.

2.1.1.1 Dee Bridge – Brittle Fracture Collapse

Following the success of the first iron bridge, Ironbridge, in 1779, more iron bridges were erected including the Dee Bridge. A three span iron girder train bridge built in 1846, the design incorporated tension flanges reinforced with a Queen Post truss system (tension bars attached with a pin to the girder). Prior to the bridge's collapse, cracking had been found in the lower flanges during inspections, and it was realized that the tension bars had not been properly installed and the bars were reset; however, in 1847, the bridge collapsed as a train crossed, killing five people. While lateral instability and fatigue cracking (Petroski 2007) have been proposed as potential causes of the failure, Akesson (2008) believes that repeated loadings caused the pin holes in the web plate to elongate. This elongation negated the composite action of the girders and tension rods, leaving the girder to carry the entire load. Regardless of the actual cause of the collapse, the failure of the Dee Bridge caused engineers to realize that the brittle and weak nature of cast iron in tension is undesirable; consequently, more ductile materials like wrought iron and, eventually, steel replaced cast iron. Additionally, this collapse highlighted the fact that a bridge designer's assumptions are not always correct, and if problems such as cracking occur, all possibilities of their cause should be investigated.

2.1.1.2 Tay Bridge – Stability Issues Due to Load Combinations

The Tay Bridge was built in 1878 to cross the Firth of Tay in Scotland. The bridge was the longest train bridge in the world at the time and consisted of wrought iron trusses

and girders supported by trussed towers. In 1879, while a mail train was crossing at night, the bridge collapsed during a storm with high winds killing 75 people. Thirteen of the tallest spans, having higher clearances to allow for ship passage beneath, collapsed. It was determined that wind loading had not been taken into account in the design of the bridge. The open truss latticework was assumed to allow the wind to pass through; however, it was not considered that, when loaded with a train, the surface area of the train would transfer wind loading to the structure. During the gale, the extremely top heavy portion of the bridge, upon which the train rode, acted like a mass at the end of a cantilever. The narrow piers could not withstand the lateral thrust and collapsed into the water (Biezma and Schanack 2007; Akesson 2008). In addition, defective joints also led to fatigue cracking, which aided in the collapse of the bridge (Lewis and Reynolds 2002). This collapse highlighted problems with tall structures in windy environments, which require that the stability of the structure be considered, the need to consider the effects of load combinations, and continued problems with fatigue in iron structures.

2.1.1.3 Quebec Bridge – Buckling Failure

During construction of the cantilever steel truss Quebec Bridge in 1907, a compression chord was found to be distorted out of plane, and the designer ordered construction to be halted. However, the contractor was falling behind schedule and continued construction, which resulted in a complete collapse, killing seventy-five workers. Multiple reasons led to the collapse; first, the bridge had been designed using higher working stresses, and second, the designers underestimated the self-weight of the steel. The large stresses caused the buckling of a compression member that led to the complete collapse ("Quebec Bridge Disaster" 1908; Biezma and Schanack 2007; Akesson 2008). A new bridge was planned and erected using compression chords with almost twice the cross-sectional area to avoid buckling; however, the bridge partially collapsed again in 1916 killing an additional 13 workers. The second collapse was blamed on a weak connection detail, which was redesigned, and the bridge was finally completed in 1917. These collapses highlighted the need for not only economical, but also safe

designs. Increasing working stresses without proper testing and safety precautions can lead to devastating consequences.

2.1.1.4 Tacoma Narrows Bridge – Stability Issues Due to Wind

The collapse of the Tacoma Narrows Bridge in 1940 is one of the most well known and well studied (Reissner 1943; Billah and Scanlon 1991; Larsen 2000; Green and Unruh 2006; Biezma and Schanack 2007; Subramanian 2008; Petroski 2009). A Google™ search yields multiple videos of the collapse with millions of views. The narrow and elegant suspension bridge spanned the Puget Sound, and a gale caused the bridge to begin to oscillate out of control. Vortices formed on the leeward side of the deck causing oscillations at one of the natural frequencies of the very flexible bridge deck, and the bridge resonated, causing extremely large deflections (Akesson 2008). The bridge had been designed to withstand a static wind pressure three times the one that resulted in collapse, but the dynamic effects of the wind loading on the bridge had not been taken into account. After the collapse, the bridge was rebuilt with a wider bridge deck and deeper girders to yield a much stiffer design. The new bridge was also tested in a wind tunnel prior to erection. These design changes helped form the standard for future suspension bridge design.

2.1.1.5 Various Box-Girder Failures – Local Buckling Failures

A series of box-girder bridge failures occurred in the late 1960s and early 1970s with the majority of failures occurring during erection (Biezma and Schanack 2007; Subramanian 2008; Akesson 2008). By using the cantilever method during erection, high moment regions at the supports produced a buckling failure in the Fourth Danube Bridge in Austria. As the final piece was placed to close the gap between the two segments, the piece had to be shortened on the top due to the sag of the cantilevers. The inner supports needed to be lowered to reduce the stress distribution to the designed continuous span distribution; however, this was planned for the next day. As the bridge cooled that evening, tension was introduced in the shortened region and compression in the bottom flange. Areas designed to be in tension for in-service loads were instead in compression,

causing buckling failures. Four other box girder failures occurred in the next four years, all of which had buckling issues during erection (one was kept secret for over 20 years due to the controversy). Because of the large number of collapses in a small period of time, it was clear that erection loads and practices needed to be included in the design process and that local buckling problems were not well understood.

2.1.1.6 Cosens Memorial Bridge – Brittle Fracture Due to Structural Change

The Sgt. Aubrey Cosens VC Memorial Bridge in Ontario, Canada, a tied arch bridge built in 1960, partially collapsed in 2003 when a large truck was crossing (Biezma and Schanack 2007; Akesson 2008). Previously, other pieces of the bridge had failed but had gone unnoticed and, when the truck crossed, the first three vertical hangers connecting the girder to the arch failed in succession. When the first two hangers failed, the next few were able to redistribute and carry the load; however, when the third hanger finally fractured, a large portion of the deck displaced. The hangers were designed with the ends free to rotate, but these ends had seized up over time with rust and become fixed. When fixed, they were subjected to bending, which caused fracturing to occur on the portions of the hangers hidden inside the arch. Fortunately, no lives were lost in this collapse, but this failure highlighted the necessity of understanding initial bridge design assumptions and ensuring that these original design assumptions continue to hold true through maintenance and inspections.

2.1.1.7 Silver Bridge – Cleavage Fracture in Eyebar

Constructed in the late 1920s, the Silver Bridge connecting Ohio and West Virginia was the first suspension bridge in the United States to use heat-treated steel eyebars as the tension members connecting the stringers to the suspension cable. During rush hour in 1967, an eyebar fractured at its head that caused a complete collapse of the bridge and killed 46 people. Corrosion and design issues of the eyebars were the major reasons for failure (Lichtenstein 1993; Subramanian 2008). This tragedy led Congress to adopt systematic inspections of all bridges in the United States and made engineers aware of the consequences of cutting corners on design specifications to save money.

2.1.1.8 Hoan Bridge Failure – Brittle Fracture Due to Stress Concentrations

In 2000, the Hoan Bridge failed in Wisconsin. This steel bridge built in 1970 had full depth cracking in two of three girders, with at least some cracking in all three (Fisher et al. 2001). The cracks initiated where the diaphragm connected to the girder near the tension flange because stress concentrations led to stress levels 60 percent above the yield level for the steel in the girder web. Steel toughness levels met the American Association of State Highway and Traffic Officials (AASHTO) requirements, but due to the excessive stress levels, cracking still occurred. This stress concentration led to brittle fracture, and the failure has shown that details that amplify stress levels are problematic.

2.1.1.9 Grand Bridge and I-35W Bridge Failure – Gusset Plate Design

Issues with gusset plate design have caused some more recent collapses (Richland Engineering Limited 1997; Subramanian 2008; Hao 2010; Liao et al. 2011). In 1996, the Grand Bridge, a suspended deck truss bridge built in 1960 near Cleveland, Ohio, suffered a gusset plate failure. The failed gusset plate buckled under the compressive load and displaced, but the bridge only shifted three inches both laterally and vertically and did not completely collapse. The FHWA found that the design thickness of the plate was only marginal and had been decreased due to corrosion. An independent forensic team concluded that the plates had lost up to 35 percent of their original thickness in some areas. On the day of the failure, the estimated load compared to the design load was approximately 90 percent, and it was concluded that sidesway buckling occurred in the gusset plates. The damaged gusset plates were replaced and other plates throughout the bridge deemed inadequate were retrofitted with supporting angles.

The I-35W Bridge in Minneapolis, Minnesota collapsed on August 1, 2007 killing 13 people. Undersized gusset plates were determined by the NTSB to be the cause of the collapse (Subramanian 2008; Hao 2010; Liao et al. 2011). The design forces in the diagonal members were not correctly incorporated into the initial gusset plate design and significantly higher forces dominated the actual stresses in the gusset plates. These higher stresses in the undersized plates led to significant yielding under service loadings

and ultimately collapse (Liao et al. 2011). These two collapses indicated that gusset plates on bridges designed during the 1960s need to be analyzed for sufficient design and load capacity strength.

2.1.1.10 Skagit River Bridge Collapse – Clearance Issues

Most recently, a span of the I-5 Skagit River Bridge collapsed north of Seattle, Washington (Lindblom 2013; Johnson 2013). While no one perished in this collapse, individuals had to be rescued and travel times along the Washington coast were impacted significantly. The initial reports indicate that an oversize load struck an overhead support girder causing complete collapse of the span (Lindblom 2013). Clearances and weight issues are clearly an issue for many bridges, especially those with non-redundant above-deck truss systems.

Engineers have learned many lessons from the bridge collapses described in this section. These lessons included the necessity of careful consideration of new materials, wind stability, safety factors, local buckling, construction practices, inspections practices, and connection design flaws. Although these collapses have provided many insights into bridge design and construction, other problems that have not caused major collapses also exist.

2.1.2 Bridge Fatigue Vulnerabilities

The collapses of the I-35W Bridge, I-5 Skagit River Bridge, and the Hoan Bridge highlighted issues with the aging steel bridges that were built in the late 1950s, 1960s, and 1970s. In addition to the problems observed from these collapses, recent information on steel bridge vulnerabilities and issues specifically in Minnesota has been compiled (Lindberg and Schultz 2007). Although these vulnerabilities do not cause immediate collapse, high cycle fatigue issues can reduce safe bridge life. Fifteen state departments of transportation were surveyed and responded that transverse stiffener web gaps, insufficient cope radius, and partial length cover plates were the most common details displaying fatigue cracking (Lindberg and Schultz 2007). Diaphragm distortional fatigue (due to web gapping) is also frequent, and a list of common problems with steel bridges

is repeated in Table 2.1. Additionally, Thompson and Schultz (2010) indicated through numerical modeling that connections of floor beams to box girders of steel tied arch bridges have high stress concentrations. Decreasing stresses at these particular details could lead to increased bridge life for aging steel girder bridges in Minnesota and throughout the United States.

For high cycle fatigue, AASHTO requires a design check and has classified many connections types as being vulnerable. The AASHTO Manual for Bridge Evaluation (2008) offers the following formula to estimate the finite fatigue life of fatigue damage prone details

$$Y = \frac{R_R A_f}{365n(ADTT_{SL})(R_s f_{re})^3} \tag{2.1}$$

where Y = fatigue life (years), A_f = constant depending on the detail in question found in Table 2.2, R_R = resistance factor, n = number of stress range cycles per truck, $ADTT_{SL}$ = average daily truck traffic for a single lane, R_s = partial load factor, and f_{re} = effective stress range at detail. Fatigue behavior and failure has been heavily studied (Miner 1945; Schilling et al. 1978; Keating and Fisher 1986; Moses et al. 1987; Chung et al. 2003), and a variety of methods exist for estimating the effective stress range at the detail. If truck data is present for a particular bridge, more rigorous methods for calculating fatigue life can be used (Miner 1945; Moses et al. 1987; Chung et al. 2003). For steel bridge details, an effective stress range, S_r, can be written as:

$$S_r = (\Sigma f_i S_{ri}^3)^{1/3} \tag{2.2}$$

where f_i = fraction of stress ranges within an interval, S_{ri} = midwidth of stress interval (Schilling et al. 1978; Moses et al. 1987). However, a simplified method for estimating the effective stress range is provided by AASHTO utilizing a fatigue truck load and reducing the range by 25 percent to obtain the effective stress range.

Table 2.1 Steel details with fatigue problems

Steel Detail	Description	Collapse/Cracking Example
Partial length cover plate	Welded plate to flange for increased moment resistance with fatigue issues near welds. Crack begins at plate joint and initiates into the beam flange then proceeds to web. The cover plate is one of the most common problems.	Yellow Mill Pond Bridge (Connecticut)
Transverse stiffener web gap	Stiffeners used to be placed with a gap between the stiffener and bottom tension flange. Cracks begin in or near welds due to distortion. 50% of bridges with the detail have cracking.	I-480 Cuyahoga River Bridge (Ohio)
Insufficient cope radius	Copes with small radii have stress concentrations causing cracking.	Canadian Pacific Railroad Bridge No. 51.5 (Ontario)
Shelf plate welded to girder web	Cracking initiates near welded plate, stiffener and web girder.	Lafayette Bridge (Minnesota)
Welded horizontal stiffener	Insufficient welding causes a fatigue crack that propagates as a brittle failure.	Quinnipiac River Bridge (Connecticut)
Stringer or truss floor beam bracket	Suspension bridges and truss bridges have seen issues of cracking in the beam floor bracket near expansion joints.	Walt Whitman Bridge (Delaware River)
Haunch insert	Cracks began near a poor transverse weld. However, at point near zero moment so generally not a large issue (many cycles, but low stress range).	Aquasabon River Bridge (Ontario)
Web penetration	Cracking near backing bar of welds for beams that penetrate box stringers.	Dan Ryan Train Structure (Illinois)
Tied arch floor beam	Cracks between beam flange (tie) and plate due to unexpected rotation.	Prairie Du Chien Bridge (Wisconsin)
Box girder corner	Continuous longitudinal weld had cold cracking in the core, undetectable to the naked eye. Fatigue caused cracking, but quite small due to small stress range.	Gulf Outlet Bridge (Louisiana)
Cantilever floor-beam bracket	Cracking occurs near tack welds used for construction purposes.	Allegheny River Bridge (Pennsylvania)
Cantilever: lamellar tear	Lamellar tear occurred in highly restrained connection. Cracks occurred prior to erection.	I-275 Bridge (Kentucky)

For the response modification and health monitoring applications described herein, $R_s f_{re}$ will be considered the stress range calculated by simulations utilizing the fatigue truck load. Finite life estimation will be based on only changes in these ranges and the reduction can be ignored since no direct safe life calculations using Eq. 2.1 are undertaken. In addition, the number of stress cycles per truck can be taken conservatively as two as long as long as a cantilever is not present; however, by examining the number of stress cycles larger than a particular value, it may be found that this number could be lower. From Eq. 2.1, to successfully increase the safe fatigue life, either the problematic detail needs to be replaced (i.e., increase *A*), traffic needs to be limited on the bridge (i.e., reduce $ADTT_{SL}$), or the stress ranges seen by the detail need to be decreased (i.e., reduce f_{re}). While methods to improve detail category by introducing residual stresses have been evaluated with some success (Takamori and Fisher 2000), an intrusive modification of the detail is often not feasible. Decreasing daily truck traffic by limiting bridge traffic is unpopular and disruptive. The fatigue life of the vulnerable detail is inversely proportional to the cube of the stress range, and consequently, decreasing the stress range will have the largest effect of the three options that can be used to increase safe fatigue life; a 10 percent reduction in stress range leads to a fatigue life increase of 37 percent.

Another way to increase the life at a fatigue vulnerable detail could be to have infinite fatigue life. According to Section 6 of the AASHTO LRFD Bridge Design Specifications (2010), the fatigue load must satisfy:

$$\gamma(\Delta f) \leq (\Delta F)_n \tag{2.3}$$

where γ = fatigue load factor = 0.75 for finite fatigue life or 1.50 for infinite fatigue life; Δf=live load stress range; $(\Delta F)_n$ = nominal fatigue resistance. The nominal fatigue resistance, $(\Delta F)_n$, can be defined in two ways: $(\Delta F)_{TH}$ for infinite fatigue life and, similar to Eq. 2.1, for finite fatigue life

$$(\Delta F)_n = \left(\frac{A_f}{365(75)n(ADTT)_{SL}}\right)^{\frac{1}{3}} \quad (2.4)$$

where A_f can be found in Table 2.2 (AASHTO 2010) and $(\Delta F)_{TH}$ can be found in Table 2.3 (AASHTO 2010).

Table 2.2 Stress resistance constants by detail category

Detail category	Constant, A_f x10^8 (ksi^3)
A	250.0
B	120.0
B'	61.0
C	44.0
C'	44.0
D	22.0
E	11.0
E'	3.9
A 325 bolts in tension	17.1
A 490 bolts in tension	31.5

Table 2.3 Nominal stress thresholds by detail category

Detail category	Threshold (ksi)
A	24.0
B	16.0
B'	12.0
C	10.0
C'	12.0
D	7.0
E	4.5
E'	2.6
A 325 bolts in tension	31.0
A 490 bolts in tension	38.0

Another useful form of the fatigue life equation is expressed in terms of remaining fatigue life. Lindberg and Schultz (2007) restate the equations from NCHRP-299 for remaining fatigue life for a bridge already in-service as

$$Y_f = Y_N \left[1 - \frac{Y_P}{Y_1}\right] \tag{2.5}$$

where Y_f = remaining fatigue life, Y_N = fatigue life based on future volume, Y_P = bridge age, and Y_1 = fatigue life based on past volume. This equation will have to be utilized to calculate the remaining fatigue life for current in-service bridges that undergo response modification and health monitoring.

2.1.2.1 Cover Plates

Two of the most commonly identified vulnerabilities, cover plates and web gaps have undergone extensive evaluation. Minnesota bridges known to have examples of cover plates include: #9779, #9780, #19843, #82801, #02803, and #27015 (Lindberg and Schultz 2007). The AASHTO classifications state that cover plates are in a fatigue stress category of E', the worst category. This stress category would need to be used for the calculation of the remaining fatigue life once the stress ranges have been decreased using response modification and bridge health monitoring.

2.1.2.2 Web Gap (Distortional Fatigue)

In Minnesota, multiple bridges with distortional fatigue vulnerabilities exist, such as bridge #9330. Many studies have been completed to evaluate competing web gap stress formulas (Jajich et al. 2000; Berglund and Schultz 2002; Severtson et al. 2004; Li and Schultz 2005; Lindberg and Schultz 2007). The most recent formula reported by Lindberg and Schultz (2007) is

$$\sigma_{wg} = 2.5E\left(\frac{t_w}{g}\right)\left(\frac{A_1L^2 + A_2L + A_3}{L}\right) \tag{2.6}$$

where E is the modulus of elasticity, t_w is the girder web thickness, A_1, A_2, and A_3, are constants for bridge skew (see Table 2.4), g is the web gap, and L is the bridge span length. This equation can be used to help identify which bridge layouts have the largest

stress ranges due to skew and can also be used as verification for computer models used in response modification.

Table 2.4 Bridge skew constants for Lindberg stress concentration formula

Deg. skew	A_1 (1/in)	A_2	A_3 (in)
20	-3.3700E-07	0.001486	-0.3399
40	-3.1150E-07	0.001522	-0.4065
60	-4.3520E-07	0.002185	-0.9156

2.1.3 Other Bridge Vulnerabilities

In addition to steel bridge vulnerabilities, Enright and Frangopol (2008) surveyed damaged concrete bridges and found that the majority of damage was caused by corrosion. Water ingress at deck joints caused most of the corrosion problems, and other issues were typically caused by shear cracking as opposed to flexural cracking. Deck joints (generally over supports) were found to be the most likely locations on concrete bridges to have damage and need particular attention.

Taking both steel and concrete bridge vulnerabilities into account, O'Conner (2000) described a safety assurance plan implemented for New York State's bridge infrastructure. Bridges in the New York state inventory were rank ordered using six collapse categories: hydraulic (scour), collision, steel details, concrete details, overload, and seismic. In a separate, related program, the bridges were ranked using an additional category of deterioration.

2.2 Bridge Loading

Bridge loading models are another critical component for the successful response modification of a bridge structure. Many different types of loading for bridge structures are possible such as vehicles, vehicle impacts, earthquake loadings, high wind, as well as other extreme events. Defining the way vehicles and other loads interact with the bridge is necessary for computer modeling of the structure. Due to the fatigue vulnerabilities of the steel details that are focused on in this dissertation, the most important bridge loading is heavy truck loading.

Nowak (1991) describes the necessary components of general loading, but also states the need for better loading models for extreme events such as scour, vessel collisions, and earthquakes. The dead load, or self-weight, can be subdivided into three categories: weight of prefabricated elements, cast-in-place elements, and wearing surfaces. These are treated as bridge dependent, normal random variables. The live loadings include both static and dynamic effects from vehicles (specifically trucks) crossing the bridge and are affected by span length, position of vehicles, truck weight, axle positions and loads, and structural layout. Truck weights have a general trend, but can be very site specific, and the dynamic loads induced by the trucks depend on vehicle dynamics (shocks), bridge dynamics, and wearing surfaces. Dynamic deflection is generally constant and independent of truck weight and the extra dynamic load does not exceed 15 percent of the static live load of a single truck. Extreme loading cases such as scour, vessel collisions, and earthquakes that need to be considered are very site specific and can be quite difficult to quantify due to the rarity of occurrence and their large range of possible loading situations.

Bridge loading models for static live loadings can be further refined (Nowak 2003). The parameters that affect the live load model are: span length, position of vehicles, truck weight, axle positions and loads, structural layout (stiffness), and future bridge/traffic growth. Using a major truck survey of 10,000 heavily loaded trucks from 1975, probabilities based on a 75-year design period were calculated. For spans less than around 100 feet, a single truck heavily loaded governs the response, and for anything larger, two heavily loaded trucks govern the response. A similar study was performed for two lane bridges and it was found that two heavily loaded trucks traveling side-by-side governs the response.

The effects of heavy truck loading have recently been studied (Altay et al. 2003). Suggestions from NCHRP 12-51 were utilized and improved upon to refine loading and girder analysis. Truck tests were used to verify the results and beam grillage models were suggested as the easiest way to define and distribute truck loading; however, finite element modeling was found to be the best way to define truck loading but was very time consuming. Additionally, truck loading defined by AASHTO seems to be fairly

reasonable, but local weigh in motion (WIM) data for actual truck weights should be used when available. For steel bridge details, an effective truck weight, W, can be written as:

$$W = (\Sigma f_i W_i^3)^{1/3} \quad (1.1)$$

where f_i = fraction of gross weights within an interval, W_i = midwidth of interval (Moses et al. 1987). In Minnesota, over 70% of trucks are five axle trucks around the 60 kip range for effective weight (Altay et al. 2003). It may be necessary to increase this average weight depending on the types of trucks travelling over a particular bridge considering that average weights around 70 kip are possible. Increasing truck weights by only 10 percent could reduce fatigue life by 25 percent and, for an increase in legal truck weight of 20 percent, the reduction in the remaining life in older steel bridges could be as high as 42 percent.

Loading models vary around the world (Miao and Chan 2002). Countries use models consisting of a concentrated load representing the truck, a distributed load, or a combination of the two. The United States standard uses a concentrated truck load plus a distributed load for bridge strength design; some countries forgo the distributed load. The use of WIM data was investigated for live load design characteristics and a statistical analysis of the data was used to find design loads instead of the traditional normality assumption. For Hong Kong bridges, the WIM loads were found to be less than typical design loads.

The bridge loading suggested by AASHTO is another model for evaluating structural response modification and bridge health monitoring techniques. The model comes from multiple researchers and is loosely based on Miner's rule. The fatigue equations that govern bridge life are evaluated using the AASHTO loading criteria, but if more loading data is present for a particular bridge, such as WIM, the AASHTO model could be modified. AASHTO (2010) standards for fatigue loading state that the "fatigue load shall be one design truck or axles thereof specified in Article 3.6.1.2.2, but with a constant spacing of 30 feet between the 32 kip axles. The dynamic load allowance specified in Article 3.6.2 shall be applied to the fatigue load." The standard truck has three point

loads: the front axle is 8 kip, the second axle is 14 feet back and 32 kip, and the third axle is 32 kip 30 feet back from the second axle (see Fig. 2.1 (From AASHTO LRFD Bridge Design Specifications, 2010, by the American Association of State Highway and Transportation Officials, Washington, DC. Used by permission.)); the width of the truck is 6 feet. The dynamic load allowance or impact factor is meant to amplify the static load to account for two effects: the dynamic interaction of the suspension system and the pavement and also the deflection amplification caused by dynamic versus static loading; the impact factor is 15 percent for the fatigue loading state. According to article 3.6.1.4.3a the "truck shall be positioned transversely and longitudinally to maximize stress range at the detail under consideration, regardless of the position of traffic or design lanes on the deck." Therefore, it is necessary to consider a range of possible placements of the truck to find the worst-case scenario.

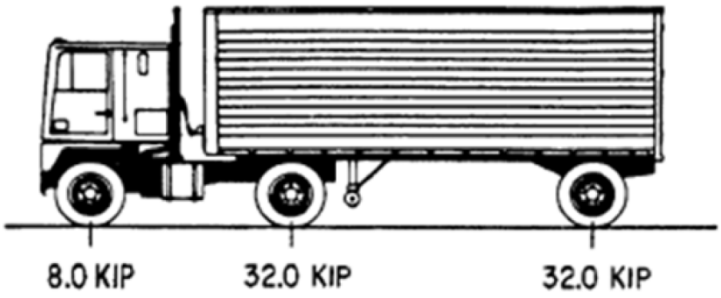

Figure 2.1 AASHTO standard truck

Another bridge loading model that should considered is a dynamic truck load. Using the AASHTO standard truck, the finite element program SAP2000 (SAP2000 v14.2.3) can be used for a time-stepped dynamic analysis of the bridge due to truck loads. For the moving point loads, SAP2000 uses a triangular pulse that starts at zero at the previous time step, goes to the maximum value of the load at the current time step, and back to zero at the next time step. The placement of the point loads depends upon the speed of the truck and the time step that the analysis is currently calculating. Then, SAP2000 uses Hilber-Hughes-Taylor (1977) direct linear integration to calculate the bridge response

and saves each time step. Any typical finite element quantity can be calculated for any member including the moment range.

Bridge loading models can vary widely depending on which loads are most important. Truck configurations and weights are very important characteristics for defining vehicle loadings for fatigue life calculations and may be very site specific. If WIM data is present for a particular bridge, this data can be used to refine the truck loading models.

2.3 Response Modification and Control Devices

Response modification can be applied to many types of structures. Cheng et al. (2008) outline many systems suitable for seismic control, and though not focused specifically on bridge applications, passive, active, and semi-active RM devices are presented. All of these RM devices focus on energy dissipation to decrease overall displacements. Passive RM devices are generally engineered to help resist either the most likely or the most dangerous loading conditions and require no external power; however, these passive devices cannot adapt to changing conditions making them act similar to a retrofit. The passive RM devices described are tuned mass dampers, tuned liquid dampers, friction devices, metallic yield devices, viscoelastic dampers, and viscous fluid dampers. A retrofit to stiffen a member or the replacement of a connection, would also be considered a passive RM device. Passive devices modify bridge behavior and, once installed, become a permanent change in the bridge structure.

An active RM device requires external power and generally uses large equipment to provide larger controlling forces. The active systems use sensors and a control computer to change the characteristics of the system to "smartly" apply a damping force to the structure. Active systems are usually more expensive than passive or semi-active systems, but can control multiple vibration modes simultaneously. One problem with these active systems is that they require large amounts of power and can become unstable; however, these systems are the most adaptable and have the ability to greatly change structural responses. Another problem is the complexity of the active system that leads to a higher probability of usability issues. The active RM devices described are

mass damper systems, tendon systems, brace systems, and pulse generation systems. Active RM devices, as well as semi-active RM devices, have the ability to adapt to different loading conditions unlike their passive counterparts.

The semi-active RM device uses minimal power and can adapt to changing structural conditions. The semi-active systems are similar to active systems and use sensors and a control computer to change the characteristics of the system to "smartly" apply a damping force to the structure, but these systems cannot add energy to the system and controlling forces are limited. An advantage of semi-active devices is that when power is lost, the system is still stable and acts like a passive device. Another advantage is that their required power can be supplied by battery and that is advantageous at a bridge site where power access may be limited. The semi-active devices described are mass dampers, liquid dampers, friction dampers, vibration absorbers, stiffness control devices, electro-rheological dampers, magneto-rheological (MR) dampers, and viscous fluid dampers.

Hybrid systems combine both passive and active devices are the most reliable because the active system can maintain the most control, but in the event of a power failure, the passive system would completely take over and maintain a stable environment. Passive, active, semi-active, and hybrid systems can all be applied to many different types of civil structures to provide a wide variety of response modification scenarios.

2.3.1 Response Modification in Civil Structures

Response modification and control in civil structures has been an active area of research for the last few decades. Yao (1972) presents a short history on initial efforts concerning the control of civil structural systems and encourages others to continue the exploration of structural control as a way to mitigate problems due to unknown or variable loading conditions, especially complex systems such as long span bridges and tall buildings. The use of active response modification for large civil structures was suggested by Miller et al. (1988) in the late 1980s as another way to reduce dynamic deflections in structures. Subsequently, response modification and structural health

monitoring techniques have been applied to reduce structural responses in many seismic and wind loading applications (Dyke et al. 1996; Housner et al. 1997; Symans and Constantinou 1999; Soong and Spencer 2002; Yang and Agrawal 2002; Erkus et al. 2002; Spencer and Nagarajaiah 2003). Soong and Spencer (2002) summarize a wide range of energy dissipation approaches using RM devices that have been applied to civil structures, including response modification through passive, active, and semi-active RM devices.

While many response modification efforts have been focused on building structures, others have focused specifically on bridges. Kim et al. (2000) investigated a retrofit using passive restrainers for bridge abutments to resist seismic unseating. Using SAP2000 and nonlinear finite element modeling, the authors showed that a spring and nonlinear viscous damper connected in parallel can be effective in restraining the expansion joints. Andrawes and DesRoches (2005) investigated an interesting passive RM device that uses an alloy called nitinol to control the unseating of girders during excessive ground motions. This alloy remains elastic throughout loading while still dissipating energy and, because the alloy does not fail and remains elastic, the device can easily re-center the displaced girder joint. Typical steel restrainers can either yield or break, causing the joint to not return to the original position. Vukobratovic (2000) suggests active control strategies that could have been applied to the Tacoma Narrows Bridge collapse and the St. Francis Dam collapse, among others. Each of these collapses was caused by different problems, but all involved dynamic effects that had been ignored in design. Particularly interesting was the description of controlling of suspension bridge vibrations similar to the Tacoma Narrows Bridge vibrations that caused the failure. It was suggested that by adding a damping RM device, one could induce the eigenvalues of the torsional modes to change sign thus stabilizing unstable modes of the uncontrolled structure. For a damping RM device, it is suggested that either spring mass dampers are installed between girders or a set of dampers be installed on the hangers. Interestingly, the Akashi-Kaikyo Bridge presently incorporates tuned mass dampers (passive) and hybrid mass dampers (semi-active and passive) in the support towers to mitigate wind

vibrations. It is noted that while active systems are best at mitigating dangerous responses, they also require more equipment, maintenance, and power.

While these are all good examples of structural response modification, most applications to bridge structures have concerned seismic and wind hazard mitigation; there have been few investigations of the application of structural response modification and control to reduce the response in bridge structures due to typical traffic service loads. Researchers have tried to decrease bridge responses by tuning smart damping devices in heavy vehicles to a known road roughness pattern with some success (Harris et al. 2007). Although the modification of the vehicle is an intriguing possibility, outfitting millions of trucks with semi-active suspension systems would be costly and would only mitigate the amplification of bridge response due to a known road roughness profile. Das and Dey (1992) investigated how tuned mass dampers can mitigate random bridge vibrations with some success, but did not look specifically at moving loads. Siwiecki and Derby (1972) outfitted a simple bridge with tuned mass dampers, but found that passive tuned mass dampers only reduced vibrations for a narrow range of loading conditions.

Due to the variability of passive device results and the impracticality of active devices, Patten et al. (1996) improved these efforts and demonstrated a semi-active system for bridge application in the laboratory with good results. Further, Patten et al. (1999) implemented a semi-active stiffening RM device as part of an RM apparatus directly attached to a bridge to show that reduction in bridge stresses due to traffic loads can be achieved. In Fig. 2.2 (reprinted with permission of ASCE (Gastineau et al. 2013)), a schematic of an RM apparatus and an RM device placed in parallel to a fatigue vulnerable member that can provide additional stiffness and/or damping similar to that employed by Patten et al. (1999) is depicted on a simple beam; this type of RM apparatus will be referred as to as PIA (Patten Inspired Apparatus) throughout the remainder of the dissertation. The PIA reduces displacements and stresses in the beam between attachment points by applying opposing moments where the system is fastened to the structure. An on-off algorithm to control the semi-active RM device was developed and implemented. When in the on position, the RM device locks and acts as a supplemental stiffener. In the off position, the RM device acts like a supplemental viscous damper.

The PIA achieved predicted safe life extension of bridge girder members for a simple highway crossing of up to 50 years for 10% of the cost of replacing the bridge.

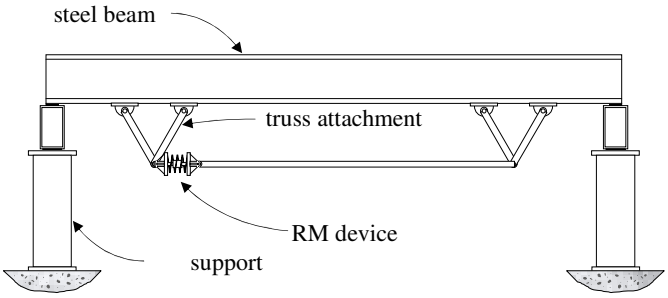

Figure 2.2 PIA attached to a simple beam

Work in progress on semi-active control strategies has been reported by Christenson and co-workers at the University of Connecticut (2009). The equations that govern fatigue life used by AASHTO are described and it is noted that there are three ways to increase fatigue life: 1) truck traffic reduction, 2) replacing fatigue critical details, and 3) stress range reduction. Replacing the problematic details of the bridge is quite expensive and limiting truck use would be unacceptable in many highway networks. Stress range reduction can be achieved by altering the dynamic response of the bridge to reduce deflections. Reduced deflections mean reduced strains and reduced stresses, which could safely extend bridge life. In the AASHTO equations, fatigue life is inversely proportional to the cube of the stress range so that decreasing stress ranges would have a profound effect. To accomplish the reduced deflections, different RM devices are discussed and semi-active control applications are described as ideal due to their small power consumption and adaptable nature. Semi-active control seems to the most logical type of control system because it is both stable and uses minimal power. The system modeled involves a semi-active resettable damping system with a mass that vibrates as the bridge vibrates and helps dissipate vibratory energy in the bridge. The damper has two chambers and, when moving in one direction, the valve closes to resist movement until maximum displacement is reached. As the direction of motion reverses, the valve opens and the other valve closes to resist motion in the new direction. By dissipating

some energy and adding stiffness, the deflections in the bridge can be reduced, inducing a reduced strain or, equivalently, a reduced stress. Decreasing stress ranges can lead to bridge life extension in most cases. Many of the steel bridges built in the 1960s have finite fatigue lives due to particular details included in the bridge (cover plates, welding issues, diaphragm connections, etc.). If these stress ranges can be reduced, the life of the bridge could possibly be increased to nearly infinite (in terms of fatigue life). Some generic and basic bridge configurations were modeled and deflection reductions of close to 50% were found in simulations (Christenson et al. 2009).

2.3.2 Magneto-Rheological Damping Devices

Many types of RM devices could possibly help to modify and control deflections. One popular semi-active RM device has received recent scrutiny (Dyke et al. 1996; Carlson et al. 1996; Spencer et al. 1997; Lee and Choi 2000; Erkus et al. 2002; Yang et al. 2002; Bolandhemmat et al. 2010); it is an attractive potential RM device due to the small amount of power required to run the equipment and the relative simplicity of the mechanics in the device. A commercialized system MagneRide™ of the device has even been implemented in high-end car suspension systems (Bolandhemmat et al. 2010). Magneto-Rheological (MR) devices use magnetic particles suspended in a fluid to cause damping forces. These devices use a variable magnetic field to induce polarization of these particles, and, in turn, change the yield stress of the fluid. The devices have large temperature operating ranges (-40 to 150 ºC) and yield stresses of at least 2.09 ksf depending on the type of magnetic suspension. Yang et al. (2002) analyzed one large scale MR damping device, the LORD Rheonetic™ Seismic Damper (MRD-9000) (Fig. 2.3, Yang et al. 2002). MR damping devices generally are modeled to follow a simple Bingham plasticity representation (Fig. 2.4, Yang et al. 2002) which can be written mathematically as:

$$\begin{gathered} \tau = \tau_0(H)sgn(\dot{\gamma}) + \eta\dot{\gamma};\ |\tau| > |\tau_0| \\ \dot{\gamma} = 0;\ |\tau| < |\tau_0| \end{gathered} \tag{1.2}$$

where $\tau_0$is the yield stress and a function of the applied field H, $\dot{\gamma}$ is the shear strain rate, and η is the post-yield plastic viscosity, which is the shear stress divided by the shear strain rate (Yang et al. 2002). The *sgn* in the equation is the signum function which is defined as:

$$\operatorname{sgn}(\tilde{x}) = \begin{cases} -1 \text{ if } \tilde{x} < 0 \\ 0 \text{ if } \tilde{x} = 0 \\ 1 \text{ if } \tilde{x} > 0 \end{cases} \tag{1.3}$$

The Bingham plasticity model is the simplest way to represent the behavior and to initially design the device; however, this equation used in conjunction with a parallel plate theory correctly predicts quasi-static forces at higher velocities, but at low velocities it fails to be accurate. More complicated mathematical representations exist but are cumbersome for use in design; yet, to correctly predict the dynamic behavior, a numerical approach is necessary. This approach uses the Bouc-Wen hysteresis model and assumes the mechanical model shown in Fig. 2.5 (Yang et al. 2002). Yang et al. (2002) found that the force imparted by the damper follows

$$\begin{aligned} \check{F} &= \check{\alpha}\check{z} + \check{c_0}\left(\dot{\check{x}} - \dot{\check{y}}\right) + \widetilde{k_0}(\check{x} - \check{y}) + \widetilde{k_1}(\check{x} - \widetilde{x_0}) \\ &= \check{c_1}\dot{\check{y}} + \widetilde{k_1}(\check{x} - \widetilde{x_0}) \end{aligned} \tag{1.4}$$

where

$$\dot{\check{y}} = \frac{1}{\check{c_0} + \check{c_1}}\left\{\check{\alpha}\check{z} + \check{c_0}\dot{\check{x}} + \widetilde{k_0}(\check{x} - \check{y})\right\} \tag{1.5}$$

and the evolutionary variable $\check{z}$ is governed by

$$\dot{\check{z}} = -\check{\gamma}\left|\dot{\check{x}} - \dot{\check{y}}\right|\check{z}|\check{z}|^{\check{n}-1} - \check{\beta}\left(\dot{\check{x}} - \dot{\check{y}}\right)|\check{z}|^{\check{n}} + \check{A}\left(\dot{\check{x}} - \dot{\check{y}}\right) \tag{1.6}$$

The parameters $\check{\alpha}$, $\check{c_0}$, and $\check{c_1}$ are all functions of the current, $\check{\imath}$, and are assumed to be third order polynomials. For the particular damper used by Yang et al. (2002), the parameters are as follows:

$$\check{\alpha}(\check{\imath}) = 16566\check{\imath}^3 - 87071\check{\imath}^2 + 168326\check{\imath} + 15114$$
$$c_0(\check{\imath}) = 437097\check{\imath}^3 - 1545407\check{\imath}^2 + 1641376\check{\imath} + 457741 \quad (1.7)$$
$$c_1(\check{\imath}) = -9363108\check{\imath}^3 + 5334183\check{\imath}^2 + 48788640\check{\imath} - 2791630$$

and $\check{A}$ = 2679 m^{-1}, $\check{\gamma}$ and $\check{\beta}$ = 647.46 m^{-1}, $\widetilde{k_0}$ = 137810 N/m, $\check{n}$ = 10, $\widetilde{x_0}$ = 0.18 m, $\widetilde{k_1}$ = 617.31 N/m. To design these devices, it is necessary to identify the range of forces that need to be imparted on the system. The controllable force in the system is inversely proportional to the gap size in the damper; therefore, a small gap size is ideal for larger forces. However, a smaller gap size leads to a smaller overall range of possible forces so there is a tradeoff to achieve larger force capacities.

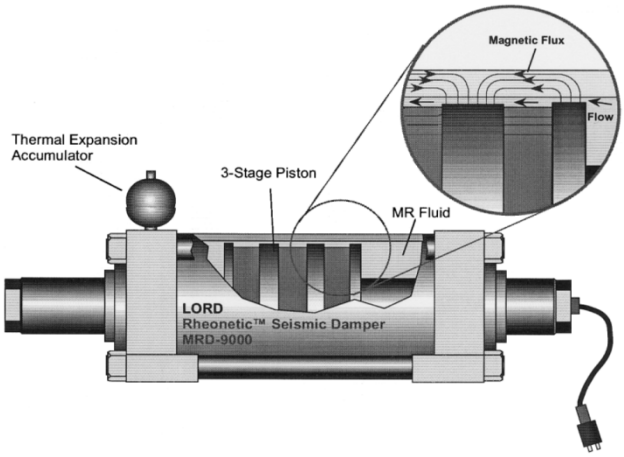

Figure 2.3 Magneto-rheological device

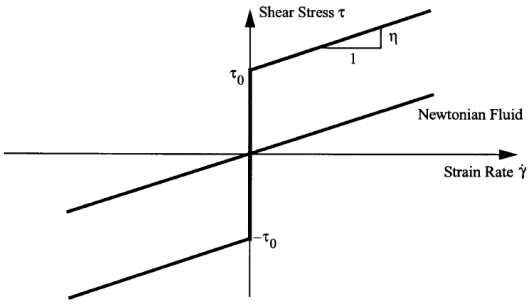

Figure 2.4 Bingham plasticity model

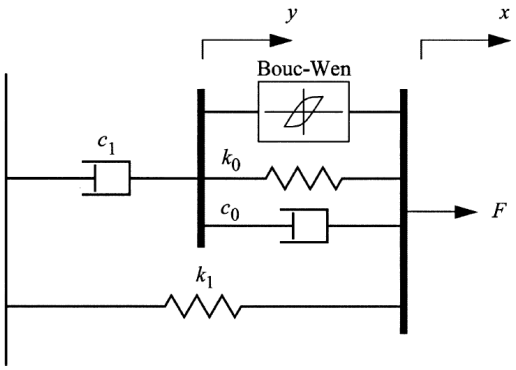

Figure 2.5 Mechanical device used to approximate MR system

The MR damper is just one of many possible choices for RM devices available for response modification. Each have their own advantages and disadvantages and the ideal approach will vary depending on the structure and site conditions.

2.4 Bridge Health Monitoring Systems

The goals of bridge health monitoring, the last component for structural response modification, can vary. One may choose to monitor a bridge globally to identify changes in structural behavior and can then process these results to find possible damage or predict impending failure. Yet, data interpretation can be very difficult and consistent results seem to be variable at the current time. For response modification applications, one system to locally monitor the bridge vulnerability to verify response reduction would be beneficial. If semi-active or active devices are present, it may be necessary to use additional systems to monitor a global bridge response and the RM device to provide feedback for the control system. Understanding the available bridge health monitoring systems will guide the selection of a proper monitoring system for a particular bridge vulnerability.

In a series of two reports, researchers at Iowa State University have surveyed bridge health monitoring technologies (Phares et al. 2005a; 2005b). The first report provides the background and history of the different classifications of sensing technology and explains that the technology needs to serve two purposes: (1) the technology should monitor the

global system to see how it is functioning overall and (2) should monitor the local system as to detect damage (i.e., cracks). A "smart" system is defined as one that can detect and automatically determine whether or not some action needs to be taken concerning the bridge. The second volume describes the existing commercial monitoring products, which range from monitoring services to sensing equipment to complete monitoring systems, and further classifies these products by their intended purpose.

A report by Gastineau et al. (2009) presents a large sampling of monitoring systems that are commercially available and able to monitor a wide variety of bridge metrics. The researchers also compiled a searchable database for the selection of systems with particular characteristics. The available systems can be lumped into three categories: inspection, short-term, and long-term monitoring systems. For the purpose of response modification and, in particular safe life extension, the long-term monitoring solutions seem to be the most appropriate. For lifetime extension, inspection systems that require a human controller would not work particularly well and will not be further investigated. Short-term systems may work, but those that cannot be left on a bridge for extended periods seem unsuitable. System types that could be useful are included in Table 2.5. When selecting systems for either RM device monitoring, global monitoring, or local monitoring, it is important to consider many aspects when choosing a monitoring system including cost, accuracy, bandwidth, repeatability, resolution, range, environmental conditions, reliability, and serviceability.

Table 2.5 Common health monitoring systems

System Type	Description
Acoustic Emission	Acoustic emission systems use an array of sensors to detect energy in the form of elastic waves. From the array, position of the origin of the energy can usually be determined (if enough sensors pick up the signal). The release of the energy usually corresponds to an area where a crack has formed or is growing. This type of system could be used for trying to control crack formation and propagation in both steel and concrete bridges.
Accelerometers	Accelerometers are one of the most basic and well-known methods of monitoring. An array of sensors detects instantaneous acceleration at a particular point. Changes in vibratory properties can mean changes in the structure. The acceleration can be numerically integrated to find velocities and displacements at a particular point. Some error can be present due to integrations, but usually decent results can be achieved. This type of system could be used when trying to control particular bridge vibrations. It may be useful in displacement control, but real time displacements are difficult to obtain due to the processing needs.
Fatigue sensing	Fatigue systems try to predict the remaining fatigue life of a steel member. These systems use either a sensor that measures the growth of an initiated crack or the voltage in a fluid adjacent to the component to predict the fatigue life left in the member. Generally, these systems would be used on critical connections or members. This type of system could be used to monitor and verify a fatigue critical place on a bridge such as a critical weld or cover plate.
Fiber Optics	Fiber optics use changes in light to detect a large range of metrics. Sensors exist to monitor acceleration, corrosion, cracking, displacement, loading, pressure, slope, strain, and temperature. These systems are not affected by electromagnetic radiation. These could be used to measure loads of trucks crossing the bridge to decide when control should be initiated or used for the same purposes of acceleration and displacement type systems.
LVDTs	Linear variable differential transducers are used to measure displacement. One of the oldest, most common and reliable methods of measuring displacement, two ends of a magnetic core are attached at the endpoints of the distance to be measured. LVDTs could measure changes in expansion joints or other small displacements within a bridge. They could also be used to measure relative out of plane displacement between two girders.
Linear Potentiometer	Linear potentiometers measure displacement using a wire attached to a spool. The sensor detects the spool position and converts it into a linear distance. Potentiometers have similar uses as LVDTs but can be used over greater distances.
Tilt/Inclinometers	Tilt and inclinometer systems are used to measure relative angle changes of piers or bridge segments. Knowing these angles, deflections can be calculated for many positions on the bridge. A large number of sensors are necessary for displacement calculations to be accurate. Pier angles could be monitored during temperature loading while trying to control bridge response.

Table 2.5 Common health monitoring systems (cont.)

System Type	Description
Scour	Scour measurements can be carried out in a variety of ways. These systems measure the amount of soil that has been carried away from the pier footing. Too much riverbed loss can lead to an unstable pier. This type of system could be used to measure pier stability during high water periods while controlling bridge response.
GPS	Global positioning systems measure absolute position at discrete points by communicating with satellites orbiting the earth. Using GPS systems, global and local displacements can be measured down to the centimeter or even millimeter. These systems could be used to measure displacements at midspan (lateral and vertical) while minimizing these displacements using a control system.
Strain (vibrating wire, fiber optic, electrical resistance)	Strain gauges work in a variety of ways to measure relative strain of a member. Absolute strain can only be measured if the sensor is mounted before loading of the member. Strain gauges could be used to measure additional strains caused by traffic or temperature loading while trying to control stresses in the bridge.

2.4.1 Response System Monitoring

The response system monitoring can be subdivided into two parts: RM device monitoring and global monitoring. For semi-active systems, RM device response will need to be monitored for communication with the control algorithm and many RM devices have internal measuring capabilities. Force transducers will most likely be necessary on one side of the RM device to provide accurate response modification force measurements. It may also be helpful to place transducers at attachment points so that other forces imparted into the system can be more accurately measured. Additionally, string potentiometers or accelerometers to record displacements, velocities, or accelerations of the RM apparatus may also be beneficial depending on RM apparatus characteristics. Monitoring of the global structural response may be best accomplished by accelerometers. For many control algorithms, accelerometer data is a straightforward feedback metric and will be the most helpful for targeting the correct parameters in RM device to achieve maximum efficiency.

2.4.2 Stress Reduction Verification Monitoring

A system for monitoring the stress ranges around the vulnerable area may be best accomplished using strain gauges. Although a system to monitor the stresses at the vulnerable connection may be difficult to incorporate into the control system, it will be beneficial for verifying that these modified stress ranges are within the new targeted range. When fatigue cracking is the chief vulnerability, it may also be warranted to place acoustic emission monitoring equipment to listen for crack initiation and propagation.

Chapter 3: Proposed Response Modification Approach

Previous attempts at response modification of bridge structures have had mixed results. Patten et al. (1999) achieved laudable results using the PIA apparatus described herein. While their work concerned the overall reduction of bridge stresses to increase fatigue life of bridge members, this dissertation focuses on an improved RM apparatus that targets local details or vulnerabilities of steel bridges that reduce the overall fatigue life of the structure; it examines the application of a structural response modification approach (Gastineau et al. 2011a, 2011b, 2011c, 2012a, 2012b, 2013) to achieve the safe extension of bridge life by locally reducing stress ranges on key vulnerable components to increase the fatigue life of the component and, in turn, increase the overall fatigue life of the entire bridge structure. This proposed RM apparatus will be referred to as the GWS (Gastineau-Wojtkiewicz-Schultz) apparatus. The main difference between the PIA (Fig. 2.2) and the proposed GWS apparatus, which is shown in Fig. 3.1 (reprinted with permission of ASCE (Gastineau et al. 2013)), is the addition of a mechanical amplifier, as was suggested by researchers at the University of Connecticut (Christenson et al. 2009).

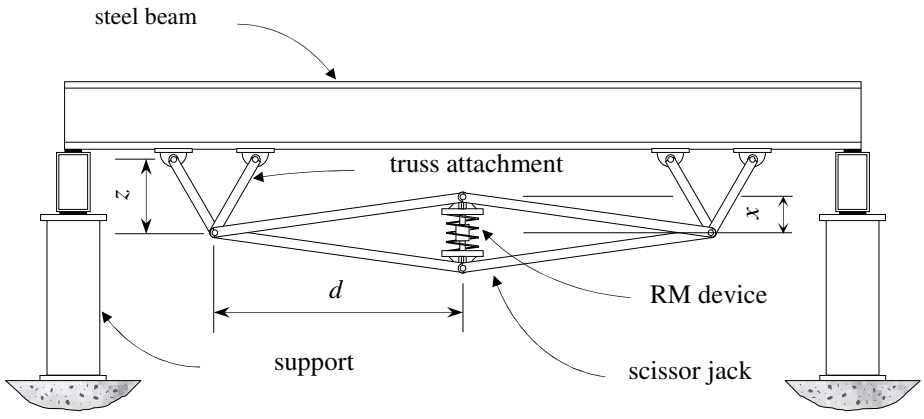

Figure 3.1 Response modification apparatus (GWS) on a simple beam

This mechanism can amplify the typically small deformations in a bridge structure to increase RM device stroke as well as amplify the force from the RM device to allow for larger overall RM apparatus control moments to the structure. By decreasing the length of the apparatus and the size of the device, a less intrusive, more feasible application to the bridge can be achieved. To the author's knowledge, the mechanical amplifier, the scissor jack, has not been investigated in detail for use in bridge structures and will be subsequently described and analyzed.

3.1 Scissor Jack Mechanical Amplifier

Typically, bridge slopes and deflections are quite small making amplification of the displacements to increase both stroke and velocities for use with RM devices desirable. Amplification will also allow these RM devices and RM apparatuses to be as small as possible, which means that the apparatuses can target a much more precise area. The scissor jack is one possible way to amplify displacements and has been proposed and tested previously in frames as a seismic energy dissipation system (Sigaher and Constantinou 2003). Christenson et al. (2009) mention the scissor jack as a possible mechanical amplifier, but do not derive and discuss the mathematics behind the scissor jack for bridge application. The RM device providing damping and stiffness is placed across the middle of the scissor jack in the vertical direction and, when the beam deflects, the slope of the beam causes a displacement at the end of the jack. This small horizontal end displacement is amplified as a larger vertical displacement across the middle of the scissor jack. The goal of displacement amplification is to allow for smaller RM apparatus sizes so that stress reduction can be targeted for very specific regions of the bridge; it also allows for smaller RM devices which should ultimately save costs.

3.1.1 Scissor Jack Displacement Magnification

An amplification factor can be derived to show the benefits of the mechanical amplifier. Fixed parameters of L, β, and z, can be used to characterize these amplifiers (Fig. 3.2, reprinted with permission of ASCE (Gastineau et al. 2012a)) where L is the length of the side of the scissor jack quadrilateral, β is the angle between the horizontal

and one side of the quadrilateral, and z is the distance from the centerline of the beam to the horizontal of the quadrilateral. In Fig. 3.3, the deformed configuration with a damper as the RM device can be seen. Note that all joints within the quadrilateral of the scissor jack are assumed to be hinged.

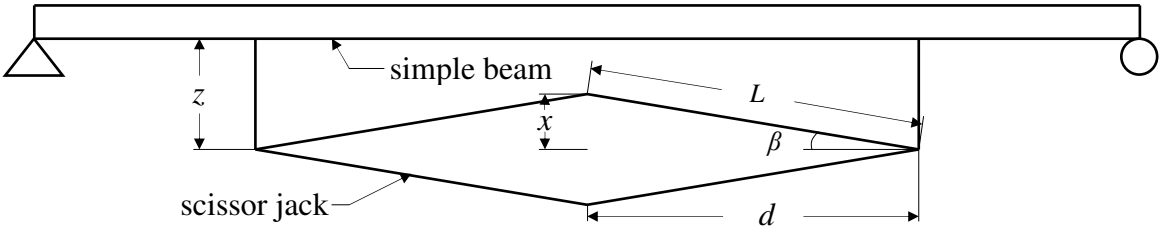

Figure 3.2 Scissor jack configuration (not to scale) on a simple beam

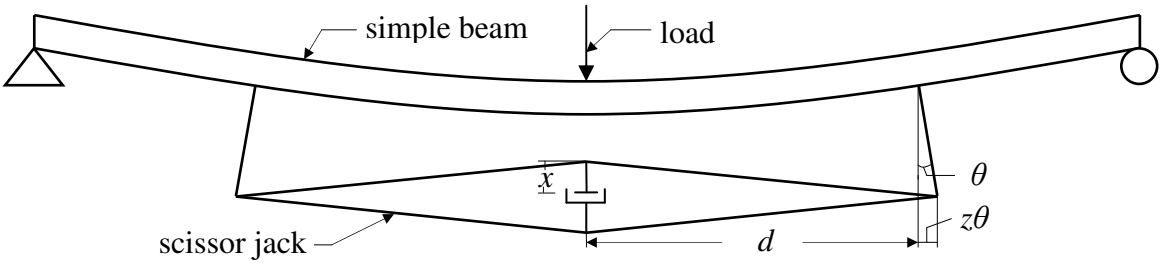

Figure 3.3 Deformed scissor jack configuration (not to scale) with damper on a simple beam

If L, β, and z are assumed to be fixed parameters, then:

$$x(\theta) = \sqrt{L^2 - (d + z\sin\theta)^2} \tag{2.1}$$

where $d = L\cos\beta$, so

$$\begin{aligned} x &= \sqrt{L^2 - (L\cos\beta + z\sin\theta)^2} \\ &= \sqrt{L^2(1-\cos^2\beta) - 2Lz\cos\beta\sin\theta - (z\sin\theta)^2} \\ &= \sqrt{L^2\sin^2\beta - 2Lz\cos\beta\sin\theta - (z\sin\theta)^2}. \end{aligned} \tag{2.2}$$

Without the scissor-jack, the RM device would be placed horizontally across the RM apparatus (Fig. 2.2) and only depend on the horizontal displacement, $z\sin\theta$. To calculate how much the scissor jack magnifies the horizontal displacement, the change in x with respect to the horizontal distance, $z\sin\theta$, should be computed. Therefore,

$$m = \frac{dx}{d(z\sin\theta)} = -\frac{1}{2}\frac{(2L\cos\beta + 2z\sin\theta)}{\sqrt{L^2\sin^2\beta - 2Lz\cos\beta\sin\theta - (z\sin\theta)^2}} = -\frac{(L\cos\beta + z\sin\theta)}{\sqrt{L^2\sin^2\beta - 2Lz\cos\beta\sin\theta - (z\sin\theta)^2}}. \tag{2.3}$$

It is possible to make small angle approximations in the analysis to simplify the analysis. Again, the exact equations are

$$x(\theta) = \sqrt{L^2 sin^2\beta - 2L\cos\beta\,(z\sin\theta) - (z\sin\theta)^2} \tag{2.4}$$

and

$$m = \left|\frac{dx}{d(z\sin\theta)}\right| = \frac{\frac{L}{z}\cos\beta + \sin\theta}{\sqrt{(\frac{L}{z})^2 sin^2\beta - 2\frac{L}{z}(\cos\beta)\,(\sin\theta) - sin^2\theta}}. \tag{2.5}$$

The small angle approximation assumes that $(z\sin\theta) \approx (z\theta)$ and higher order terms are approximately zero so that

$$x(\theta) \approx \sqrt{L^2 sin^2\beta - 2L\cos\beta\,(z\theta)} \tag{2.6}$$

and

$$m = \left|\frac{dx}{d(z\theta)}\right| \approx \frac{\frac{L}{z}\cos\beta + \theta}{\sqrt{(\frac{L}{z})^2 sin^2\beta - 2\frac{L}{z}\theta\cos\beta}}. \tag{2.7}$$

Lastly, when the beam is undeflected $(\theta = 0)$

$$m = \left|\frac{dx}{d(z\sin\theta)}\right| \approx \frac{L\cos\beta}{\sqrt{L^2 sin^2\beta}} = \cot\beta. \tag{2.8}$$

Alternately, if d and x are as defined in Fig. 3.2 and assumed to be initial fixed parameters denoted by d and x_i, the magnification can also be written as:

$$m = \cot\beta = \frac{d}{x_i}. \tag{2.9}$$

Therefore, magnification is largest when d is large and x_i is small, indicating a long and shallow scissor jack will have the largest magnification.

3.1.2 Scissor Jack RM Device Force Magnification

In addition to displacement magnification, the scissor jack mechanical amplifier also provides force magnification from the RM device to the ends of the scissor jack. To analytically study this magnification, the RM device force is assumed to be magnified by the same factor as the displacement magnification. It is then possible to treat the moment restraint provided by the scissor jack as rotational springs. For a spring as the RM device placed across the scissor jack, it is necessary to know how x is changing compared to θ to calculate the rotational spring force. Then,

$$\begin{aligned}\frac{dx}{d\theta} &= -\frac{1}{2}\frac{2Lz\cos\theta\cos\beta + z^2 2\sin\theta\cos\theta}{\sqrt{L^2 sin^2\beta - 2Lz\cos\beta\sin\theta - (z\sin\theta)^2}} \\ &= -\frac{Lz\cos\theta\cos\beta + z^2\sin\theta\cos\theta}{\sqrt{L^2 sin^2\beta - 2Lz\cos\beta\sin\theta - (z\sin\theta)^2}}\end{aligned} \tag{2.10}$$

For small θ,

$$\frac{dx}{d\theta} \approx -\frac{Lz\cos\beta + z^2\theta}{\sqrt{L^2 sin^2\beta - 2Lz\theta\cos\beta}} \tag{2.11}$$

and at neutral ($\theta = 0$),

$$\frac{dx}{d\theta} \approx -\frac{Lz\cos\beta}{\sqrt{L^2 sin^2\beta}} = -z\cot\beta. \tag{2.12}$$

If a damper is present as the RM device, it is necessary to know how quickly x is changing because the force from the damper depends on the velocity. So,

$$\begin{aligned} \frac{dx}{dt} &= \frac{dx}{d(z\sin\theta)}\frac{d(z\sin\theta)}{dt} \\ &= -\frac{L\cos\beta + z\sin\theta}{\sqrt{L^2 sin^2\beta - 2Lz\cos\beta\sin\theta - (z\sin\theta)^2}}(z\cos\theta)\dot{\theta} \end{aligned} \tag{2.13}$$

and, assuming θ is small,

$$\dot{x} \approx -\frac{L\cos\beta + z\theta}{\sqrt{L^2 sin^2\beta - 2L\cos\beta\,(z\theta)}} z\dot{\theta}. \tag{2.14}$$

Then, at $\theta = 0$

$$\dot{x} \approx -\frac{L\cos\beta}{\sqrt{L^2 sin^2\beta}}\dot{\theta} = -\cot\beta\, z\dot{\theta}. \tag{2.15}$$

Next, it is necessary to examine how much force is exerted by the RM device and to translate that into the moment experienced by the bridge member. The geometry of the scissor jack necessitates that the change in distance *dx* needs to be multiplied by two in order to get the change in the distance across the whole RM device (*x* is only half the height); therefore, for the spring, the force is (see Fig. 3.4),

$$F_d = 2kdx \tag{2.16}$$

where k is the spring stiffness of the RM device. If we approximate at $\theta = 0$, then the force exerted at the end of the scissor jack is (see Fig. 3.4):

$$F_j \approx F_d \cot\beta \approx 2k \cot\beta \, dx = -2kz \cot^2\beta \, d\theta. \tag{2.17}$$

Therefore, the moment is (see Fig. 3.5),

$$M \approx 2kz^2 \cot^2\beta \, d\theta. \tag{2.18}$$

For the damper, using small angle approximations and assuming the apparatus starts from $\theta = 0$, the force is:

$$F_d = 2c\frac{dx}{dt} = -2c\frac{L\cos\beta + z\theta}{\sqrt{L^2 sin^2\beta - 2L\cos\beta\,(z\theta)}}z\dot{\theta} \approx -2c\cot\beta\, z\dot{\theta} \tag{2.19}$$

where c is the damping coefficient. Then, the force exerted at the end of the scissor jack is

$$F_j \approx -2c\cot^2\beta\, z\dot{\theta} \tag{2.20}$$

so that the moment is

$$M \approx 2cz\cot^2\beta\,\dot{\theta}. \tag{2.21}$$

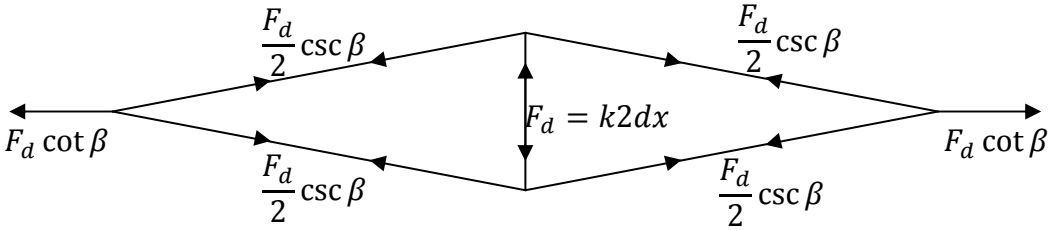

Figure 3.4 Forces within the scissor jack due to spring placed across the jack

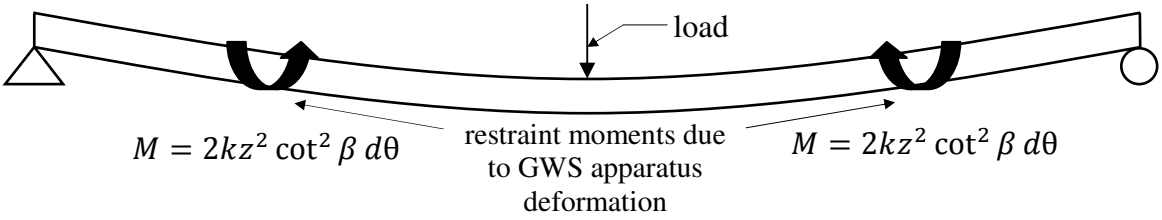

Figure 3.5 Moments imparted on the system due to a scissor jack with a spring

The simplest example of the GWS apparatus fitted with a spring as the RM device would be to assume the RM apparatus spans the whole length of the bridge with a point load, *P*, at midspan. For the analogous beam with rotational springs, the spring constant would be $\alpha = 2kz^2 \cot^2 \beta$ and the deflection, *y*, can be solved exactly from a fourth order differential equation,

$$EI \frac{d^4 y}{d\hat{x}^4} = -P\delta\left(\hat{x} - \frac{l}{2}\right) \tag{2.22}$$

where *l* is the length of the entire beam and with boundary conditions

$$y(0) = 0;\ y(l) = 0;\ EIy''(0) = \alpha y'(0);\ EIy''(l) = -\alpha y'(l). \tag{2.23}$$

Solving for the deflection of the beam,

$$y = \frac{-P}{48EI}\left(8\left(\hat{x} - \frac{l}{2}\right)^3 u\left(\hat{x} - \frac{l}{2}\right) - 4\hat{x}^3 + 3l\hat{x}^2\left(\frac{\gamma_k}{\gamma_k + 2}\right) + 6l^2\hat{x}\frac{1}{\gamma_k + 2}\right) \tag{2.24}$$

where *u* is the Heavyside function and

$$\gamma_k = \frac{\alpha l}{EI};\ \alpha = 2kz^2 \cot^2 \beta. \tag{2.25}$$

For $0 < \hat{x} < \frac{l}{2}$

$$y = \frac{-P}{48EI}\left(-4\hat{x}^3 + 3l\hat{x}^2\left(\frac{\gamma}{\gamma+2}\right) + 6l^2\hat{x}\frac{1}{\gamma+2}\right) \tag{2.26}$$

and the solution for no springs where $\gamma = 0;\ \alpha = 0$ is the same as for a simple beam with the point load at the center

$$y = \frac{-P}{48EI}(-4\hat{x}^3 + 3l^2\hat{x}). \tag{2.27}$$

3.2 Simple Beam Response Modification

To verify the derived analytical solutions and explore the GWS apparatus attached to a simple beam, a finite element numerical model of the GWS apparatus was created in the structural analysis program SAP2000. To make the comparison, values will be assumed for *E, I, l,* and α since γ depends on each. The analytic solution assumes perfectly rigid scissor jack components and perfectly rigid connections to the beam. The example SAP2000 frame model uses a W40x324 (I = 25,600 in^4, E = 29,000 ksi) to span the l = 50 ft between the simple supports and rigid elements (E = 1x10^{10}ksi) for all members in the GWS apparatus. The fixed parameters for the GWS apparatus are: L = 25.08 ft, β = 4.574º, and z = 4 ft and the spring placed across the scissor jack has a stiffness of k = 120 kip·ft. Additionally, a force P = 60 kip is applied at midspan. All connections within the GWS apparatus are pin connections except for the rigid moment connection to the wide flange section that transfers the response modification forces to the beam. The RM device is modeled as a two joint link that only transfers force in the axial direction of the link.

3.2.1 Displacement Magnification Verification

Planar analyses assuming Euler beam theory were carried out for four different GWS apparatus configurations, which varied magnification factor and connection type; connections to the beam were either an ideal rigid moment connection (Fig. 3.6) or more practical pinned truss connection (Fig. 3.7). Table 3.1 compares the analytic magnification values from Eq. 3.9 to the numerical magnification factors obtained from

the beam configurations. The numerical magnification factor was calculated using the vertical displacement of the middle of the scissor jack and dividing by the horizontal displacement of the end of the scissor jack.

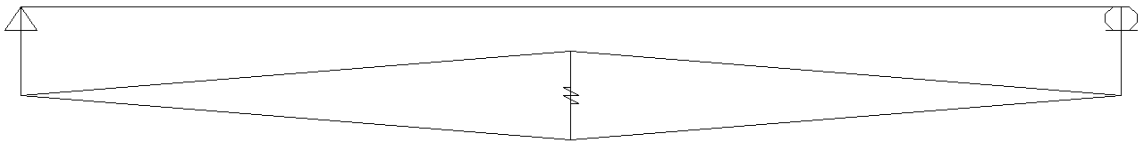

Figure 3.6 SAP2000 GWS apparatus with fully restrained moment connections configuration

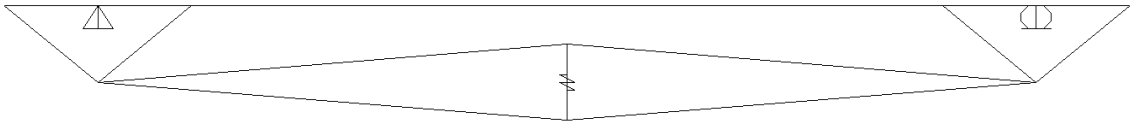

Figure 3.7 SAP2000 GWS apparatus with truss connections configuration

For all four GWS configurations, the results show close agreement. The differences between the analytical magnification factor and the numerical magnification factor arise because the rotation at the end of the GWS apparatus is no longer zero in static equilibrium when the beam is subjected to a point load. This can be seen more clearly before the neutral theta approximation is introduced in Eq. 3.7. As theta increases, the magnification factor increases slightly as well.

Table 3.1 Displacement magnification factor comparison

Analytical magnification factor (*m*)	Connection type	Vertical displacement (in)	Horizontal displacement (in)	Numerical magnification factor
12.5	Moment	0.279	0.0223	12.52
12.5	Truss	0.289	0.0231	12.52
7.5	Moment	0.332	0.0442	7.5
7.5	Truss	0.343	0.0458	7.5

3.2.2 Force Magnification Verification

To verify the force magnification assumption, the deflection (Eq. 3.27) from the analytical solution for the beam with rotational springs was compared to the numerical beam example with rigid moment connections and m = 12.5. In this configuration, the parameters defined in Eq. 3.25 are $\gamma = 5.819$ and $\alpha = 600000$ kip·ft. The beam deflection solutions are plotted in Fig. 3.8 and the numerical example matches the analytical solution closely; therefore, the assumed force magnification, m_f, is the same as the deflection magnification (Eq. 3.9)

$$m_f = m = \cot\beta = \frac{d}{x_i}. \tag{2.28}$$

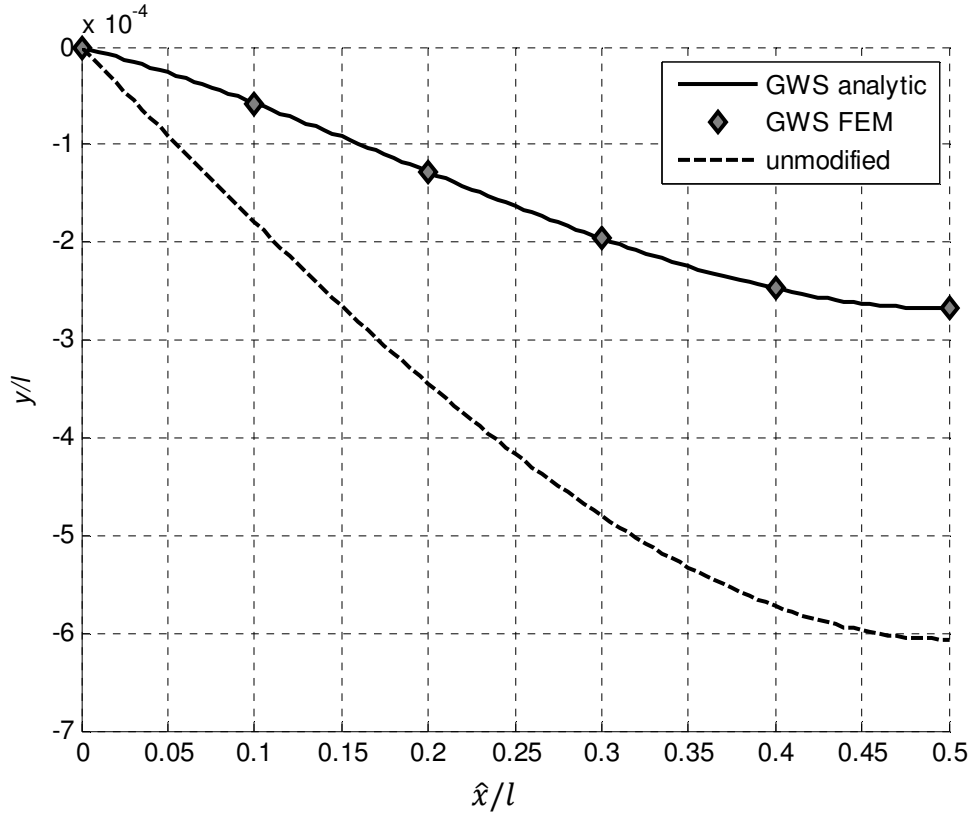

Figure 3.8 Beam deflection comparison for the analytic rotational spring equivalent, beam GWS apparatus FEM, and unmodified beam

3.2.3 Simple Beam Safe Life Extension

In addition to confirming the analytical magnification factors, the numerical model examples demonstrate the utility of the response modification approach when applied to a simple beam. Table 3.2 shows that midspan moment can be decreased from 750 kip·ft for an unmodified system to 470.92 kip·ft using the GWS apparatus, which results in a static moment reduction of 37 percent. Employing the same RM device, the PIA apparatus (no mechanical amplifier) described in Chapter 2 would achieve moment reduction of only 1 percent. The moment diagrams for the GWS apparatus with moment connections and with the more practical truss connections are shown in Fig. 3.9 and Fig. 3.10.

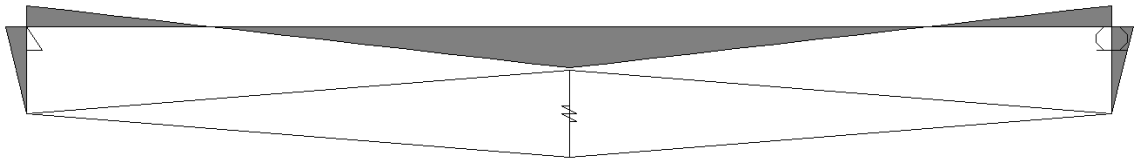

Figure 3.9 Moment diagram in SAP2000 for GWS apparatus with fully restrained moment connections

The moment diagram is transformed from all positive bending in the simply supported beam case to a combination of positive and negative bending similar to a fixed-fixed beam case. Notice that for the truss connections, no moment is present in any of the members of the GWS apparatus. While the truss connection cannot be compared exactly to the analytical solution due to the moment being applied as a force couple, its performance closely mirrors the moment connection.

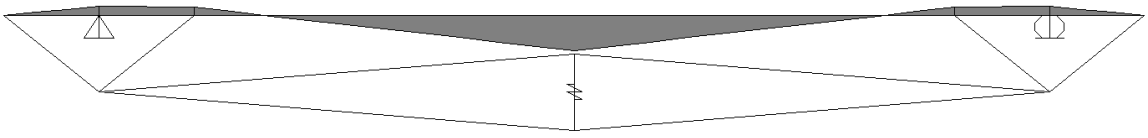

Figure 3.10 Moment diagram in SAP2000 for GWS apparatus with truss connections

Also, assuming that moment reduction is directly related to stress reduction, the AASHTO equations for fatigue life would predict a safe life increase of over 300 percent for the GWS apparatus compared with only 3 percent for the PIA apparatus. While these were static rather than dynamic analyses, the moment (i.e., stress) reduction still provides insight into the utility of the GWS apparatus.

Table 3.2 SAP2000 Results for response modification applied to a simple beam

Response modification	m	Moment (kip·ft)	Reduction (%)	Safe life increase (%)
None	-	750.00	-	-
GWS apparatus	12.5	470.92	37	304
PIA apparatus	0	743.14	1	3

3.3 Simple Beam Apparatus Parameter Study

Prior to modeling the GWS apparatus on a vulnerable bridge, a parameter of the scissor jack was carried out to investigate the performance of different scissor jack configurations. This study was performed to gain insight for the design a scissor jack for an in-service vulnerable bridge.

The GWS apparatus and scissor jack mechanical amplifier (Fig. 3.2) were already fully described but a few details will be again presented for clarity. Fixed parameters of d, x_i, and z can be used to characterize the scissor jack where d is the width of one half of the scissor jack, x_i is one half the initial height of the scissor jack, and z is the distance from the centerline of the beam to the horizontal end of the scissor jack. The magnification factor from Eq. 3.9 relates the distances x_i and d where x_i is half the vertical span of the scissor jack before deflection. Again, the magnification factor is

$$m = \frac{d}{x_i}. \tag{2.29}$$

By varying d and x_i, different magnification factors can be achieved for different scissor jack configurations. In this dynamic numerical parameter study, a sinusoidal load with a

peak value of 60 kips was placed at the quarter point of a simply supported beam. An RM device of stiffness 15 kip/in and damping 10 kip·s/in was placed across the GWS apparatus. The simulations were carried out in both SAP2000 and Simulink (*MATLAB*) and the results are very similar. In general, Simulink uses a smaller, automatically chosen variable time step to ensure that results are accurate whereas SAP2000 uses a constant time step to speed up simulation time. Table 3.3 shows the results of this parameter study which demonstrate that the magnification factor plays a significant role in reducing the maximum deflection at midspan. While magnification plays a large role, comparing trials 3 and 7 shows that length of the GWS apparatus also plays a significant role. Cutting the total length of the GWS apparatus from 50 to 20 feet decreases the performance in deflection reduction from 60.7 to 42.4 percent. It can also be seen that z, the moment arm distance, is important in determination of the deflection as well. Cutting the length of z in half from 4 to 2 feet decreases the performance in deflection reduction from 42.4 to 29 percent. Interestingly, a deeper device, corresponding to a larger x_i, does not translate into better magnification or better performance. A long narrow RM apparatus provides the largest amplification and best performance.

Table 3.3 Scissor jack parameter study results

Trial	d	x_i	z	m	Deflection at midspan (in)				Range	Reduction (%)
					SAP2000		*Simulink*			
	(ft)				*Max*	*Min*	*Max*	*Min*		
-	No jack				0.2799	0.2799	-	-	0.5598	-
1	25	3.33	4	7.5	0.1107	0.1151	0.1101	0.1236	0.2337	58.3
2	25	2.5	4	10	0.1078	0.1086	0.1069	0.1170	0.2239	60.0
3	25	2	4	12.5	0.1067	0.1071	0.1064	0.1137	0.2201	60.7
4	25	1	4	25	0.1056	0.1059	0.1070	0.1094	0.2164	61.3
5	10	2	4	5	0.1816	0.1941	0.1842	0.1988	0.383	31.6
6	10	1	4	10	0.1556	0.1666	0.1587	0.1691	0.3278	41.4
7	10	.8	4	12.5	0.1547	0.1625	0.1576	0.1647	0.3223	42.4
8	10	1	2	10	0.2006	0.2115	0.1977	0.2120	0.4097	26.8
9	10	.8	2	12.5	0.1934	0.2042	0.1921	0.2054	0.3975	29.0

From the parametric study, it is clear that larger values for z, m, and d improve performance (i.e., reduce the displacement). In some cases, the reduction in displacement

range is more than 60% compared to the case with no response modification. From the analytical derivation of the scissor jack mechanical amplifier, it was implied that a larger z and m should improve performance and the parametric study verifies this assumption. Additionally, a larger d would not only increase magnification since m depends on x_i and d, but also provide larger RM device displacements. This is because, thinking back to a simply supported member, the farther apart the location is on the member, the larger the slope difference will be. A larger slope difference will cause larger displacement that will in turn be magnified by the scissor jack. For bridges with multiple vulnerabilities, it may be advantageous to increase the length of the RM apparatus to span more than one vulnerability to exploit the increased performance of longer RM apparatuses.

The mathematical concepts for the GWS apparatus employing the scissor jack mechanical amplifier have been derived and verified using finite element analysis in SAP2000. The GWS approach can achieve significantly better performance over the PIA approach in terms of decreases in moment ranges on static analyses of a numerical model of a simple beam. During dynamic numerical analyses of a simple beam, the GWS apparatus performed best when the apparatus is wider horizontally and narrower vertically; additionally, better performance was achieved when the connections from the scissor jack to the beam are longer. Due to the preliminary success of the GWS apparatus, the response modification approach was applied to a realistic model of an in-service bridge structure.

Chapter 4: Application of GWS Approach to an In-Service Bridge

While the application of the GWS apparatus response modification approach to a simple beam model provides promising results, applying the approach to a numerical model of an in-service fracture critical bridge would provide further insight into the efficacy of the method. To demonstrate this approach, it is necessary to identify a bridge with critical vulnerable elements such as those enumerated in Chapter 2 and correctly apply bridge response modification to safely extend the life of these vulnerabilities. This chapter seeks to further demonstrate the benefits of the GWS apparatus response modification approach applied to a realistic bridge system using the Cedar Avenue Bridge in Minnesota (Fig. 4.1) as a specific example.

(photo credit: Arturo Schultz)

Figure 4.1 Cedar Avenue Bridge

4.1 Cedar Avenue Bridge

Built in 1979, the Cedar Avenue Bridge (Fig. 4.2, Schultz and Thompson 2010) is a dual span fracture critical steel tied arch bridge spanning 358.5 feet over the Minnesota River in the Minneapolis-St. Paul metropolitan area and is a candidate for structural

response modification. Although this bridge currently shows no sign of visible damage, due to its fracture critical nature, bridge member connections are of the utmost importance and this study uses response modification to safely extend bridge life. The floor beam-to-girder-to-hanger connections are critical to bridge performance and a diagram of these connections is shown in Fig. 4.3 (reprinted with permission of ASCE (Gastineau et al. 2013)).

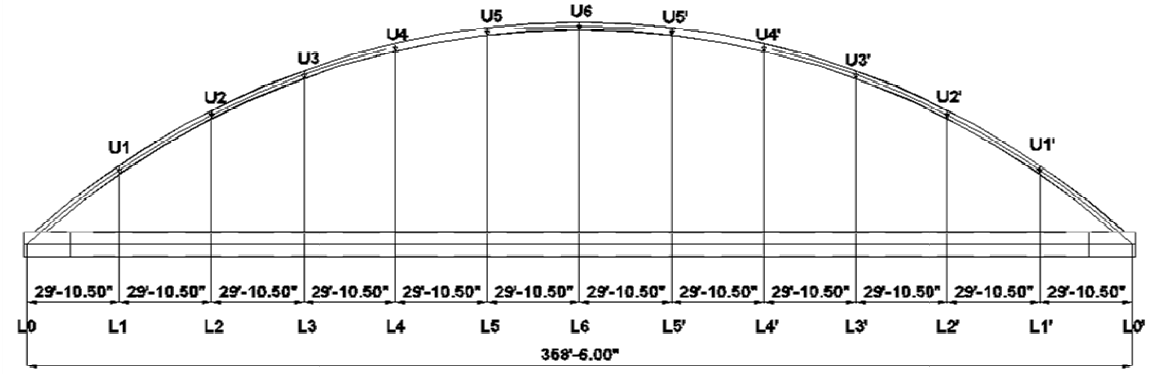

Figure 4.2 Elevation view of the Cedar Avenue Bridge

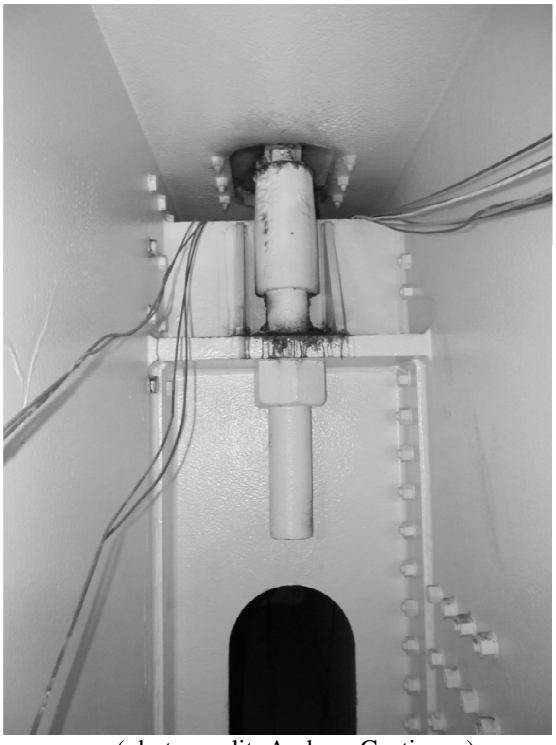

(photo credit: Andrew Gastineau)

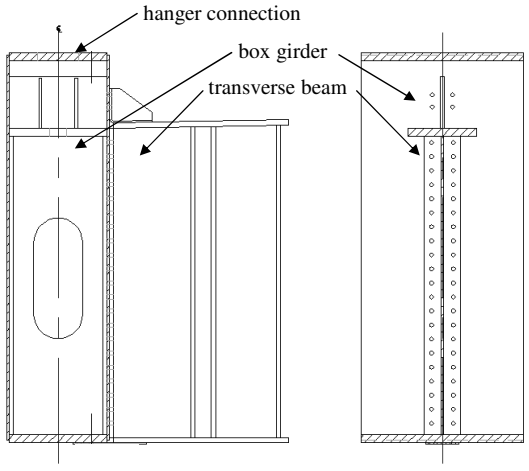

Figure 4.3 Cedar Avenue Bridge floor beam to box girder to hanger connection

Schultz and Thompson (2010) created a finite element numerical model of the Cedar Avenue Bridge and performed analyses using the structural analysis program SAP2000 to identify connections that had the highest stress ranges. The model was verified by comparing moments and axial forces presented by the designers in the bridge plans to those moments and axial forces reported from analyses using SAP2000. A global frame element analysis of the bridge was conducted to determine the connections with the highest combined moment, shear, and axial forces (Fig. 4.4 and Fig. 4.5, Schultz and Thompson 2010).

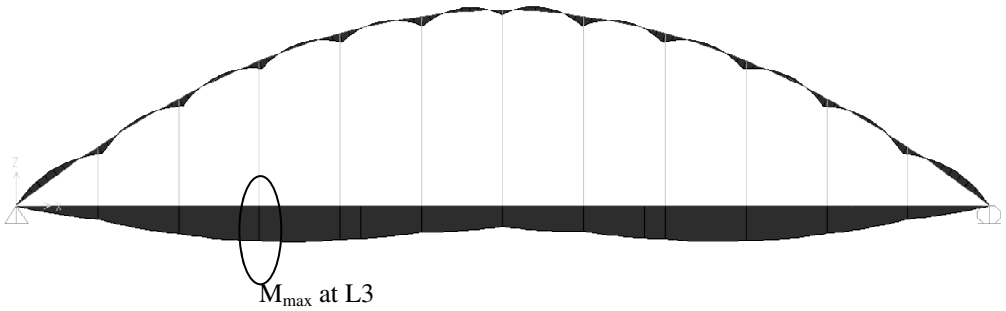

Figure 4.4 Moment distribution in global SAP2000 model for dead load

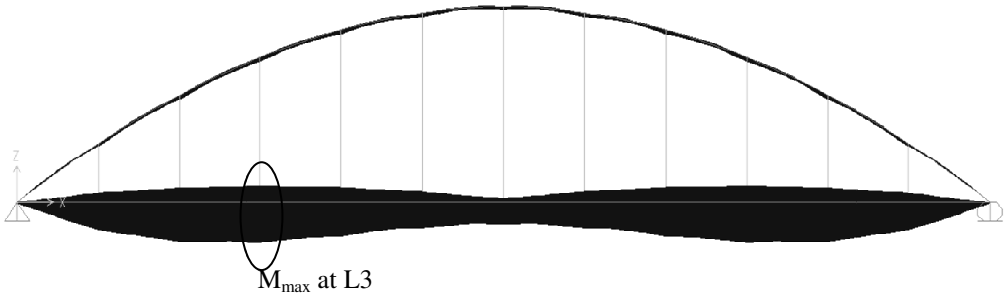

Figure 4.5 Moment envelope in global SAP2000 model for dead and live load

The areas with the highest stresses due to the combined axial, moment, and shear were modeled locally using 3D shell elements and Fig. 4.6 and Fig. 4.7 (Schultz and Thompson 2010) show the stress concentrations at the L3 connection (darkest spots).

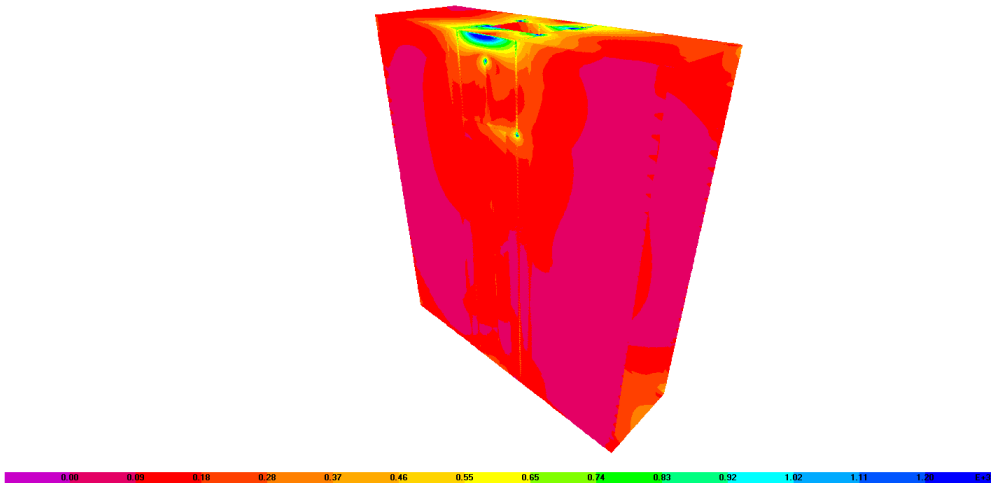

Figure 4.6 Von Mises stresses at L3 connection (box girder exterior)

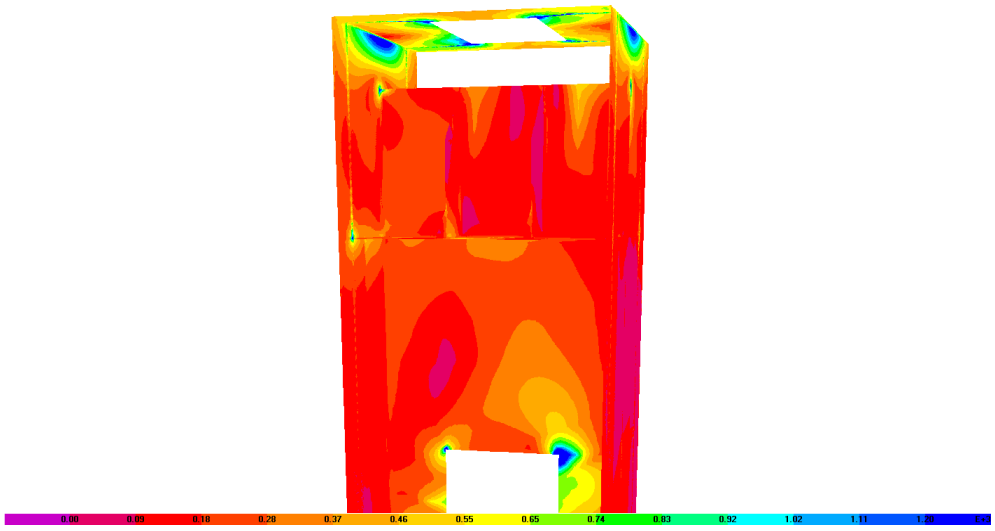

Figure 4.7 Von Mises stresses at L3 connection (box girder interior)

Given these findings by Schultz and Thompson (2010), a reduction in stress range at the critical connection location on the Cedar Avenue Bridge would be advantageous to alleviate the severity of the stress concentrations; therefore, the L3 joint would be a good candidate for response modification to reduce the risk of high cycle fatigue failure. The GWS apparatus (Fig. 4.8, reprinted with permission of ASCE (Gastineau et al. 2013)) described in Chapter 3 can be attached on either side to span the vulnerable joint to

provide counter moments, thereby potentially reducing the moment range experienced by the joint.

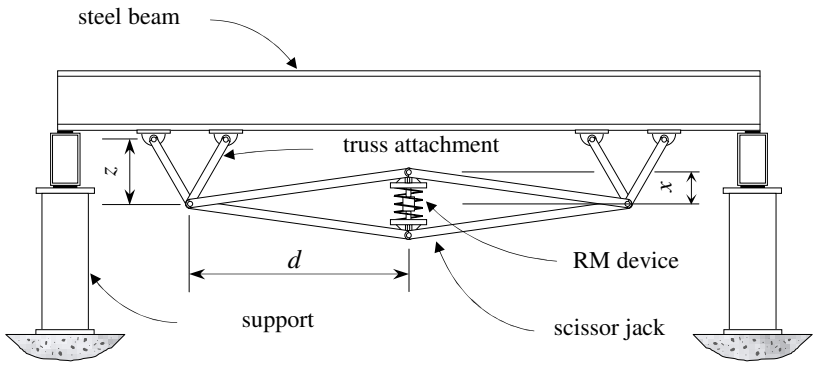

Figure 4.8 GWS apparatus attached to a simple beam

The parameter study of scissor jack performance in Chapter 3 showed that a larger horizontal RM apparatus provides better performance, and although the problem area is local, the high stress range region extends to multiple floor beam-to-box girder-to-hanger connections. Therefore, it may be advantageous to extend the GWS apparatus across multiple connections to increase *d* and also increase the number of vulnerable connections that are modified by the RM apparatus. Additionally, in some cases the GWS apparatus may not be feasible due to clearance concerns, but for the Cedar Avenue Bridge clearance issues are not anticipated and the GWS apparatus has potential.

4.2 Cedar Avenue Bridge Numerical Model

To study the effects of the GWS apparatus response modification approach, a numerical model of the Cedar Avenue Bridge was developed and refined in the structural analysis program SAP2000. The initial model was supplied by Schultz and Thompson (2010), but was subjected to multiple updates and improvements. Evolving models were used in analyses during various stages of the response modification approach development. The model progression will be subsequently described.

4.2.1 Steel Components

Schultz and Thompson (2010) developed the initial Cedar Avenue Bridge numerical model in the structural analysis program SAP2000 from existing bridge plans and included the global steel members. To provide safe life extension, GWS apparatuses were added to the numerical model spanning the L2 and L3 joints on the two transverse sides of the Cedar Avenue Bridge (Fig. 4.9). Due to the initial parameter studies on the simple beam, the apparatuses were made to span multiple joints because of the finding that a longer apparatus performs better. Additionally, the moment ranges at joints L2 and L3 are fairly similar (although the range at L3 is slightly larger), which implies that L2 is also a vulnerable joint. The material properties of the RM apparatus members were considered to be rigid for early comparisons and all joints within the RM apparatus were modeled as pin connections. The RM device is modeled as a two joint link that only transfers force in the axial direction of the link.

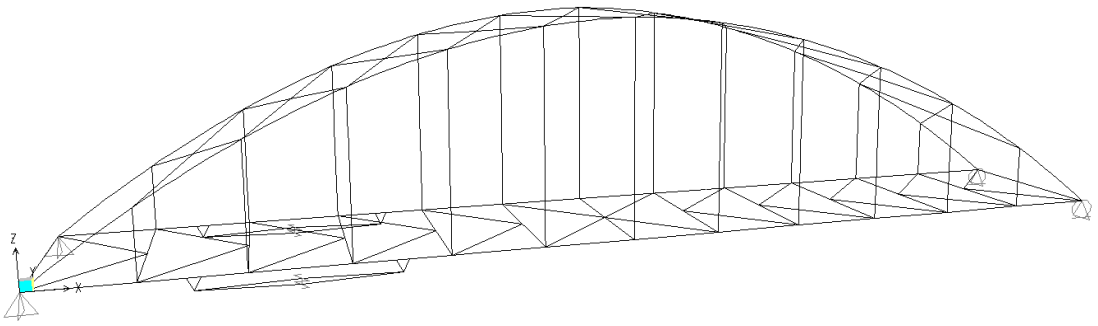

Figure 4.9 Cedar Avenue Bridge steel only model with the GWS apparatuses

The steel numerical model consisted of 89 joints, 134 frames, 22 cables, and 2 links and 1928 degrees of freedom. Initial analyses showed large transverse (out of plane) deformations in the structure when each node had six degrees of freedom (three translational and three rotational). Therefore, early analyses were conducted with planar degrees of freedoms where each node possesses three degrees of freedom, displacement in the *x* direction, displacement in the *z* direction and rotation about the *y* direction. Very

brief parameter studies (see Chapter 5) were carried out to ensure continued efficacy of the GWS apparatus approach before further refinement of the bridge model.

While performing modal analyses of the bridge model, it was discovered that unrestrained torsional modes of the GWS apparatus were present. After some investigation, it was realized that the torsional rigidity of one section of the box girders was incorrect and the problem was remedied. The torsion issue solution also remedied the large out of plane deformations that were occurring in early space frame analyses.

4.2.2 Concrete Bridge Deck Incorporation

In addition to fixing the torsional rigidity of the box girder, a more refined bridge model including the concrete bridge deck was developed and incorporated into the finite element model in SAP2000. The original model only included the steel elements of the bridge superstructure and employed only planar degrees of freedom. Therefore, the concrete bridge deck was added and full spatial analyses were implemented to assure that the moment reduction seen at the vulnerable joint was not negatively impacted by the additional stiffness and load redistribution due to the concrete deck or by the constrained degrees of freedom. Additionally, the dynamic analyses necessary for capturing the damping effects of the RM device take into account the mass of the entire bridge structure; leaving out the mass of the bridge deck would invariably change the dynamics of the bridge. The deck was added as shell elements connected to the steel frame elements with many rigid links (Fig. 4.10). Since frame elements do not have physical depth in the model, the rigid elements were necessary to achieve a geometric likeness to the overall depth from the floor beams to the concrete bridge deck of the actual bridge structure. The density of these links connecting the deck to the steel structure was increased until the bridge response remained constant from one iteration to the next, resulting in eight deck segmentations per section of the bridge.

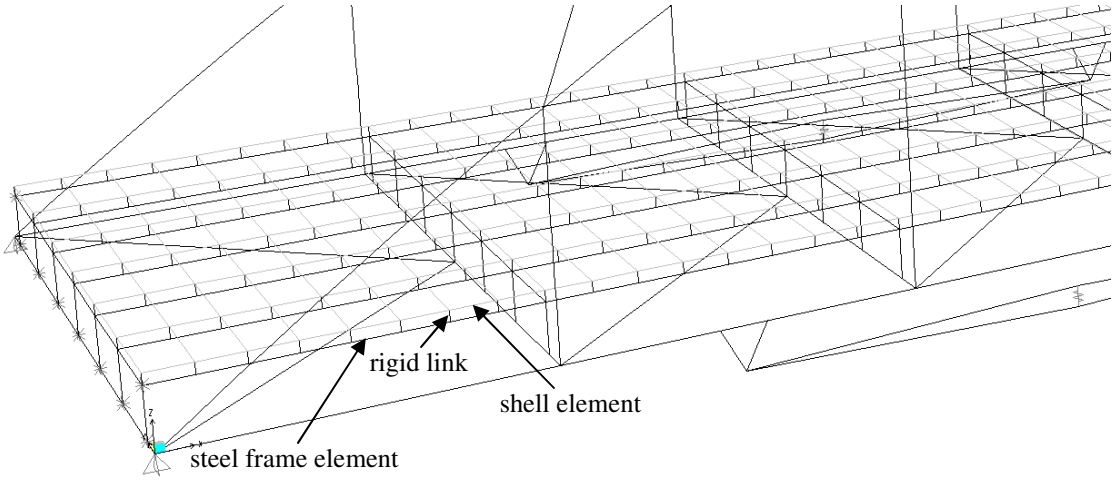

Figure 4.10 Rigid links connecting steel frame elements to deck shell elements

Furthermore, because it is expected that the Cedar Avenue Bridge exhibits a symmetric moment envelope, the moment range at the vulnerable joint L3 is similar to the range at joint L3' (Fig. 4.2 and Fig. 4.5). Therefore, two more RM apparatuses were added to the model for a total of four RM apparatuses (Fig. 4.11), one set of RM apparatuses at each potentially vulnerable joint.

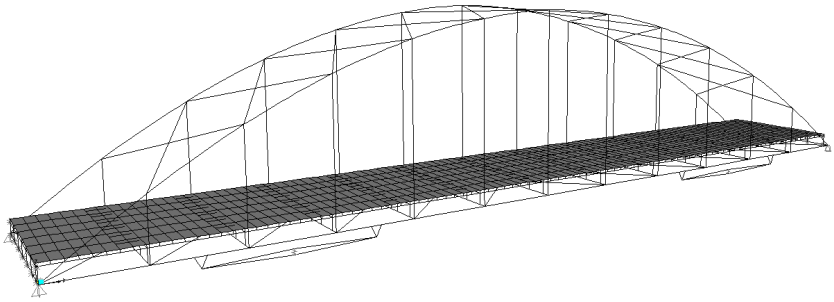

Figure 4.11 Cedar Avenue Bridge numerical model with bridge deck and four GWS apparatuses

Additional model constraints were added to the final version of the Cedar Avenue Bridge numerical model to eliminate spurious mode shapes. For instance, the deck ends were constrained to eliminate a deck shearing mode that was previously present as a result of the deck's attachment to the superstructure in the numerical model (Fig. 4.12).

Additionally, the transverse members at each end of the bridge deck were constrained to eliminate another non-physical mode shape at a low frequency.

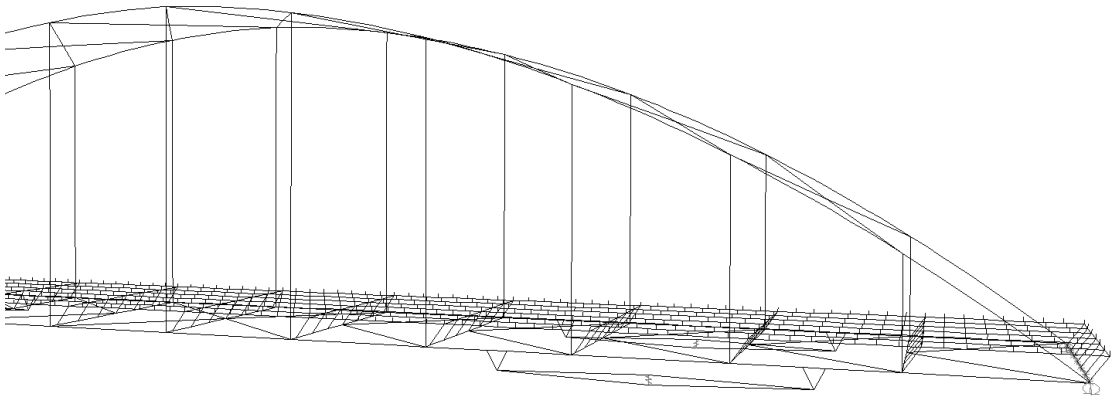

Figure 4.12 Deck shearing mode that was eliminated in new modeling

As well as eliminating these spurious modes, damping in the superstructure, which was neglected in the original model, was added to yield a more realistic model. Damping was added to the superstructure model in the form of Rayleigh damping where the damping matrix, **C**, is:

$$\mathbf{C} = \mu\mathbf{M} + \lambda\mathbf{K} \tag{3.1}$$

where μ and λ are determined using $\xi = 0.5(\mu/\omega + \lambda\omega)$ using the natural frequencies, ω, of first two vertical modes of the unmodified bridge with a damping ratio, ξ, of two percent and **M** and **K** are the mass and stiffness matrices of the bridge. The coefficients and natural frequencies were calculated from the updated numerical model in SAP2000 and are tabulated in Table 4.1.

Table 4.1 Cedar Avenue Bridge damping criteria

Mode	Period (s)	Frequency (rad/s)	Damping	Stiffness coefficient λ	Mass coefficient μ
1	0.6086	10.32	2%	0.00163	0.2392
2	0.4422	14.21	2%		

In addition to the bridge deck shell elements and superstructure frame elements, the hanging cables from the arch were modeled as tension only elements. The final bridge model consisted of 1,543 joints, 1,082 frame elements, 22 cable elements, 576 shell elements, and 4 links. After automatic meshing, these elements yielded a total of 35,402 degrees of freedom in the model with each joint allowing translation and rotation in all three coordinate directions unless actively constrained.

4.2.3 Truck Loading

The numerical bridge model was loaded with a specified truck configuration similar to the design truck identified by AASHTO in section 3.6 of the LRFD design code (2010). The vehicle traveled South to North (left to right in Fig. 4.13) at 1144 in/s (65 mph) in one of three specified lanes, specifically the East lane (near lane in Fig. 4.13). The lane is specified in SAP2000 and the loading points were automatically generated; however, the members to be loaded were limited to the spandrel beams in the steel only model and the shell concrete deck elements for the model which incorporated a concrete deck (Fig. 4.13).

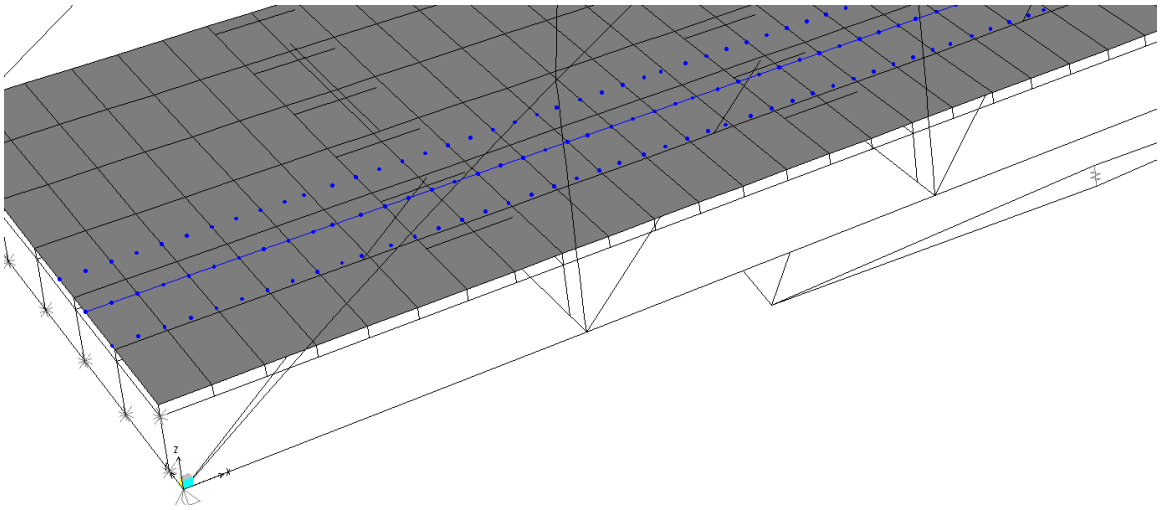

Figure 4.13 Truck lane loading points for model with concrete deck

The truck loading pattern consisted of 6 point loads, 2 per axle representing the wheel contact points. The point loads for each axle were 6 feet apart. The distance from the

front axle to the second axle is 14 feet while the distance from the second axle to the third axle is 30 feet which is consistent with the loading conditions for fatigue in the AASHTO (2010) specifications (see Fig. 4.14 (From AASHTO LRFD Bridge Design Specifications, 2010, by the American Association of State Highway and Transportation Officials, Washington, DC. Used by permission.)). The total weight of the front axle is 8 kip and the second and third axles each weigh 32 kip.

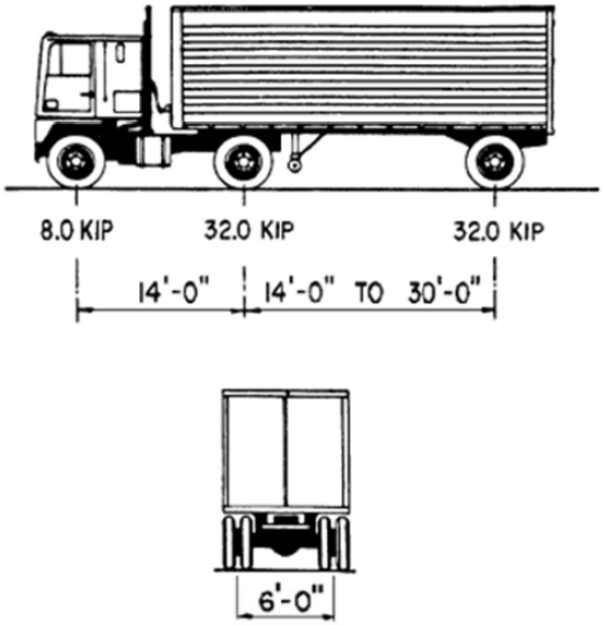

Figure 4.14 AASHTO standard truck

To model moving point loads on a bridge, SAP2000 employs a triangular pulse that starts at zero at the previous time step, goes to the max of the load at the current time step, and back to zero at the next time step. The placement of the point loads depends upon the speed of the truck and the current time step that the analysis is currently calculating. Initial simulations were run using linear direct integration time histories with time steps of 0.05 seconds for a 10 second loading period. Results indicated that vibration response, especially during the free vibration period, was being under sampled with the large time step. Final simulations were carried out using a 0.005 second time step for a 5 second loading period and these results were better behaved. For trucks

traveling at 65 mph (1144 in/s), the distance to cross the bridge is 358.5 feet plus 44 feet of truck length; the simulation needed to be at least 4.2 seconds to allow the truck to fully exit the bridge.

4.2.4 Flexibility of RM Apparatus Members

The mathematical relationships for the GWS apparatus were derived for an RM apparatus with perfectly rigid axial members. In reality, the RM apparatus members will be flexible, and the relationship between the stiffness of the RM apparatus and both the flexibility of the RM apparatus members and the stiffness of the RM device is important. By using matrix analysis for a simple truss, the equivalent stiffness of the scissor jack based on member flexibility and RM device stiffness can be derived. Although only for the static case, the derivation shows the amount of force that the flexible members are able to impart on the structure. Since the magnification factors were derived using the lateral deflection of one end of the scissor jack, the equivalent stiffness will be derived in a similar manner. The member layout and degrees of freedom for the matrix analysis derivation can be seen in Fig. 4.15.

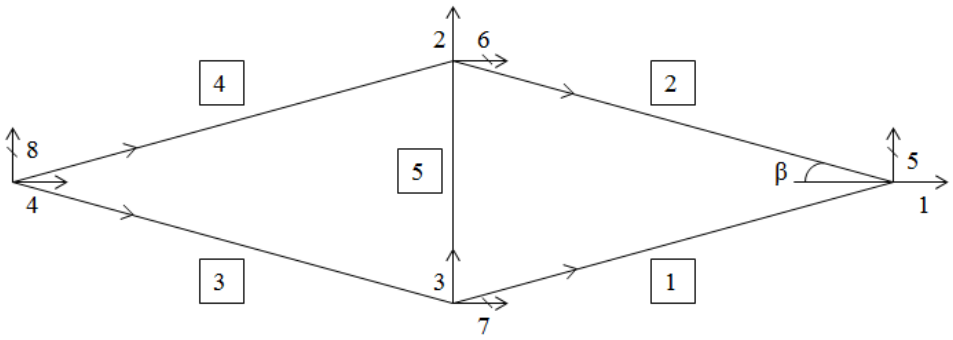

Figure 4.15 Member layout for the matrix analysis of the flexible scissor jack

The local stiffness matrix, $\mathbf{k}_{mem}$, for each flexible member looks like:

$$\mathbf{k_{mem}} = \frac{EA}{L}\begin{bmatrix} 1 & 0 & -1 & 0 \\ 0 & 0 & 0 & 0 \\ -1 & 0 & 1 & 0 \\ 0 & 0 & 0 & 0 \end{bmatrix} \tag{3.2}$$

where E is Young's Modulus, A is the cross sectional axial area, and L is the length of the member. If it is assumed that $\cos\beta = 1$ and $\sin\beta \approx \beta$ so that good magnification values for magnified displacements can be achieved, the global stiffness matrices, $\mathbf{K_i}$, for the five members look like:

$$\mathbf{K_{1,4}} = \frac{EA}{L}\begin{bmatrix} 1 & \beta & -1 & -\beta \\ \beta & \beta^2 & -\beta & -\beta^2 \\ -1 & -\beta & 1 & \beta \\ -\beta & -\beta^2 & \beta & \beta^2 \end{bmatrix} \tag{3.3}$$

and

$$\mathbf{K_{2,3}} = \frac{EA}{L}\begin{bmatrix} 1 & -\beta & -1 & \beta \\ -\beta & \beta^2 & \beta & -\beta^2 \\ -1 & \beta & 1 & -\beta \\ \beta & -\beta^2 & -\beta & \beta^2 \end{bmatrix} \tag{3.4}$$

and for the RM device across the middle as member five with k_s as the spring stiffness coefficient

$$\mathbf{K_{5,spring}} = k_s\begin{bmatrix} 0 & 0 & 0 & 0 \\ 0 & 1 & 0 & -1 \\ 0 & 0 & 0 & 0 \\ 0 & -1 & 0 & 1 \end{bmatrix}. \tag{3.5}$$

The indices for members 1, 2, 3, and 4 are [7,3,1,5], [6,2,1,5], [4,8,7,5], [4,8,6,2], and for the RM device [6,3,5,2] respectively. Therefore the global structural stiffness matrix, **S**, is

$$\mathbf{S} = \begin{bmatrix} \mathbf{K_{1,[3,3]}} + \mathbf{K_{2,[3,3]}} & \mathbf{K_{2,[3,2]}} & \mathbf{K_{1,[3,2]}} & \mathbf{[0]} \\ \mathbf{K_{2,[2,3]}} & \mathbf{K_{2,[2,2]}} + \mathbf{K_{4,[4,4]}} + \mathbf{K_{5,[4,4]}} & \mathbf{K_{5,[4,2]}} & \mathbf{K_{4,[4,1]}} \\ \mathbf{K_{1,[2,3]}} & \mathbf{K_{5,[2,4]}} & \mathbf{K_{1,[2,2]}} + \mathbf{K_{3,[4,4]}} + \mathbf{K_{5,[2,2]}} & \mathbf{K_{3,[4,1]}} \\ \mathbf{[0]} & \mathbf{K_{4,[1,4]}} & \mathbf{K_{3,[1,4]}} & \mathbf{K_{3,[1,1]}} + \mathbf{K_{4,[1,1]}} \end{bmatrix} \tag{3.6}$$

or

$$\mathbf{S} = \begin{bmatrix} \frac{EA}{L} + \frac{EA}{L} & \beta\frac{EA}{L} & -\beta\frac{EA}{L} & 0 \\ \beta\frac{EA}{L} & 2\left(\beta^2\frac{EA}{L}\right) + k_s & -k_s & -\beta\frac{EA}{L} \\ -\beta\frac{EA}{L} & -k_s & 2\left(\beta^2\frac{EA}{L}\right) + k_s & \beta\frac{EA}{L} \\ 0 & -\beta\frac{EA}{L} & \beta\frac{EA}{L} & \frac{EA}{L} + \frac{EA}{L} \end{bmatrix} \tag{3.7}$$

so that

$$\left(2\frac{EA}{L}\right)u_1 + \left(\beta\frac{EA}{L}\right)u_2 - \left(\beta\frac{EA}{L}\right)u_3 = F_1 \tag{3.8}$$

$$\left(\beta\frac{EA}{L}\right)u_1 + \left(2\left(\beta^2\frac{EA}{L}\right) + k_s\right)u_2 - (k_s)u_3 - \beta\frac{EA}{L}u_4 = F_2 \tag{3.9}$$

$$-\left(\beta\frac{EA}{L}\right)u_1 - (k_s)u_2 + \left(2\left(\beta^2\frac{EA}{L}\right) + k_s\right)u_3 + \beta\frac{EA}{L}u_4 = F_3 \tag{3.10}$$

$$-\left(\beta\frac{EA}{L}\right)u_2 + \left(\beta\frac{EA}{L}\right)u_3 + \left(2\frac{EA}{L}\right)u_4 = F_4 \tag{3.11}$$

where F_i and u_i are the forces and displacements at the respective degree of freedom. For comparison, it would be convenient to have the equation in the form of $F_1 = k_{jack}u_1$ where k_{jack} is the equivalent stiffness of the scissor jack. Notice for the scissor jack

$F_2 = F_3 = 0$, $u_2 = -u_3$, and $F_1 = -F_4$ because the only external forces come from the two end attachment points. Rearranging and substituting,

$$F_1 = \left(2\frac{EA}{L} - \frac{2\left(\beta\frac{EA}{L}\right)^2}{\left(\beta^2\frac{EA}{L}\right) + k_s} \right) u_1 \tag{3.12}$$

so that

$$k_{jack} = \left(2\frac{EA}{L} - \frac{2\left(\beta\frac{EA}{L}\right)^2}{\beta^2\frac{EA}{L} + k_s} \right). \tag{3.13}$$

From Eq. 4.13, it is clear that the overall stiffness of the scissor jack is limited mostly by the size of the scissor jack members. The scissor jack stiffness is reduced from the stiffness of a beam the size of the four legs combined by a value depending on geometry, member size, and RM device stiffness. A brief analysis of solely the scissor jack portion of the apparatus using both finite elements and the derived analytical solution shows that a small amount of RM device stiffness makes for a fairly stiff scissor jack (Table 4.2). The slight discrepancies between the finite element model and the predicted are due to the small angle approximations and rounding of the displacement outputs from the finite element model before calculating the effective stiffness. For comparison, the PIA stiffness with the same amount of total cross-sectional area is also listed (see section 4.2.6 for PIA modeling description). Notice how much stiffer the apparatus with the scissor jack is compared to the apparatus without the scissor jack (PIA).

Table 4.2 Numerical verification of analytic effective stiffness of the scissor jack

k_{device} (kip/in)	k_{member} (kip/in)	sinβ	cotβ = *m*	k_{jack} (kip/in)	k_{FE}(kip/in)	k_{PIA} (kip/in)
1	369	0.0797	12.5	220	220	0.997
10	369	0.0797	12.5	598	595	9.74
100	369	0.0797	12.5	721	715	78.7
1000	369	0.0797	12.5	736	730	270
10000	369	0.0797	12.5	738	735	357

To explore the effect of changes in axial area for the GWS apparatus members including the attachments, it is convenient to identify the stiffness change matrix for a change in axial area. For the numbered joints shown in Fig. 4.16, the stiffness matrix entries will vary for the entries marked with an x as shown in Table 4.3 where U1 is horizontal and U3 is vertical.

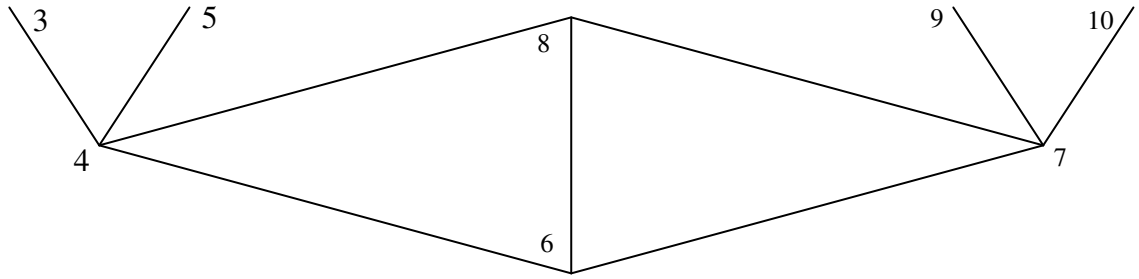

Figure 4.16 Joint numbering for the matrix analysis of the flexible scissor jack

Table 4.3 Stiffness matrix variation for a change in GWS apparatus member area

Joint		3		4		5		6		7		8		9		10	
	DOF	U1	U3	U1	U3	U1	U3	U1	U3	U1	U3	U1	U3	U1	U3	U1	U3
3	U1	x	x	x	x												
	U3	x	x	x	x												
4	U1	x	x	x		x	x	x	x			x	x				
	U3	x	x		x	x	x	x	x			x	x				
5	U1			x	x	x	x										
	U3			x	x	x	x										
6	U1			x	x			x		x	x						
	U3			x	x				x	x	x						
7	U1							x	x	x		x	x	x	x	x	x
	U3							x	x		x	x	x	x	x	x	x
8	U1			x	x					x	x	x					
	U3			x	x					x	x		x				
9	U1									x	x			x	x		
	U3									x	x			x	x		
10	U1									x	x					x	x
	U3									x	x					x	x

There are 88 unique entries in the matrix. The DOFs that are not on the superstructure affect itself and U1 and U3 of all adjacent joints, but not the perpendicular displacement of the joint DOF itself. Joint DOFs attached to the superstructure affect itself and U1 and U3 of all adjacent joints as well as the perpendicular DOF at the joint.

4.2.5 Reduced Order Numerical Model

The full 3-dimensional numerical bridge model of the Cedar Avenue Bridge was developed using the finite element software SAP2000 and underwent many modeling updates and improvements that were enumerated in the preceding sections of Chapter 4. However, to fully investigate the flexibility of the RM apparatus members and RM device characteristics, a reduced order model was necessary. The full SAP2000 model with the bridge deck and four 717 inch long GWS apparatuses with a magnification value of 30 placed across two consecutive joints (Fig. 4.17) requires approximately 540 seconds (9 minutes) to complete one analysis, and SAP2000 is not well suited for interfacing with other programs and performance design optimizations. To optimize the system to multiple loading scenarios manually would invariably take a large amount of time, and a reduced order model in MATLAB (MATLAB Release 2011a) that can effectively capture the necessary behavior of the bridge would be advantageous for implementation with DAKOTA (Adams et al. 2009) optimization techniques.

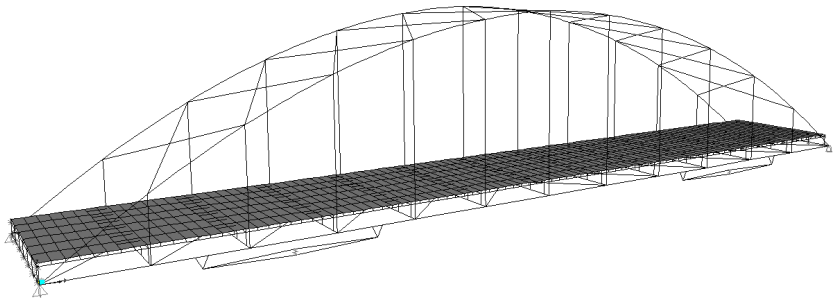

Figure 4.17 Cedar Avenue Bridge numerical model with GWS apparatuses

The first step for creating the reduced order model was transferring the model from SAP2000 to MATLAB. SAP2000 outputs the mass and stiffness matrices for the structure into a text file which can be imported into MATLAB; however, rotational degrees of freedom are assigned zero mass in SAP2000. To analyze the bridge structure in MATLAB using a state space representation, zeros in the diagonal of the mass matrix will cause instabilities when inverting the mass matrix to write the problem in state space

form. Therefore, it is necessary to perform a static condensation to remove the zeros in the mass matrix. The mass matrix, **M**, can be organized into

$$\mathbf{M} = \begin{bmatrix} \mathbf{UL_m} & [\mathbf{0}] \\ [\mathbf{0}] & \mathbf{LR_m} \end{bmatrix} \tag{3.14}$$

where

$\mathbf{UL_m}$ = mass matrix for degrees of freedom with non-zero diagonal values in the mass matrix

$\mathbf{LR_m}$ = mass matrix for degrees of freedom with values of zero in the mass matrix diagonal

Note that $\mathbf{LR_m}$ is made up of all zeros. The stiffness matrix, **K**, can be organized into

$$\mathbf{K} = \begin{bmatrix} \mathbf{UL_k} & \mathbf{UR_k} \\ \mathbf{LL_k} & \mathbf{LR_k} \end{bmatrix} \tag{3.15}$$

where

$\mathbf{UL_k}$ = stiffness matrix for degrees of freedom with non-zero diagonal values in the mass matrix

$\mathbf{LR_k}$ = stiffness matrix for degrees of freedom with zero diagonal values in the mass matrix

The static condensation is then carried out for the reduced matrices for stiffness and mass:

$$\mathbf{K_{static}} = \mathbf{UL_k} - \mathbf{LL_k}^{\mathrm{T}}(\mathbf{LR_k}^{-1}\mathbf{LL_k}) \tag{3.16}$$

and

$$\mathbf{M_{static}} = \mathbf{UL_m}. \tag{3.17}$$

Once the static reduction was complete, a modal reduction was necessary to reduce the large size of the model. To achieve a modal reduction, modes that capture the

behavior of the structure must be found and a decision about which modes to represent the model must be made. First, the original equations of motion are

$$\mathbf{M\ddot{x} + C\dot{x} + Kx = p} \tag{3.18}$$

where **M** is the mass matrix, **C** is the damping matrix, **K** is the stiffness matrix, and **p** is the loading vector of the bridge model. Then, a substitution for the global displacements in terms of modal displacements is performed using

$$\mathbf{x = \Phi q} \tag{3.19}$$

where

x = global displacements

Φ = mode shapes

q = generalized modal displacements

so that

$$\mathbf{M\ddot{x} + C\dot{x} + Kx = M\Phi\ddot{q} + C\Phi\dot{q} + K\Phi q = p} \tag{3.20}$$

and then premultiplying by the transpose of the mode shapes gives

$$\mathbf{\Phi}^{\mathrm{T}}\mathrm{M}\mathbf{\Phi}\ddot{\mathrm{q}} + \mathbf{\Phi}^{\mathrm{T}}\mathrm{C}\mathbf{\Phi}\dot{\mathrm{q}} + \mathbf{\Phi}^{\mathrm{T}}\mathrm{K}\mathbf{\Phi}\mathrm{q} = \mathbf{\Phi}^{\mathrm{T}}\mathrm{p} \tag{3.21}$$

and

$$\mathbf{M_r\ddot{q} + C_r\dot{q} + K_rq = f} \tag{3.22}$$

where $\mathbf{M_r}$ is the reduced mass matrix, $\mathbf{C_r}$ is the reduced damping matrix, $\mathbf{K_r}$ is the reduced stiffness matrix, and **f** is the loading vector of the reduced order bridge model. Additionally, the damping in the superstructure was represented using a Rayleigh damping model of the form

$$\mathbf{C} = \mu\mathbf{M} + \lambda\mathbf{K} \tag{3.23}$$

where μ and λ (see Table 4.1) are determined from the relationship $\xi = 0.5(\mu/\omega + \lambda\omega)$ using the natural frequencies of first two vertical modes of the unmodified bridge with a damping ratio, ξ, of two percent.

Initial attempts at the reduced order model used the first nine vertical mode shapes of the bridge structure that were obtained using modal analysis on the full order SAP2000 model. However, these did not adequately capture the bridge response due to: 1) moving truckloads, 2) changes in stiffness in either the RM apparatus members or the RM device, or 3) changes in RM device damping. Subsequently, a series of eight static deflected shapes were calculated from static point loads along the truck loading line and were added to the modes as basis vectors in the reduced order model. To capture the effects of changes in device properties, four static deflected shapes for each individual RM apparatus were calculated using opposing unit loads at the RM device two joint link attachment points. The last set of mode shapes was obtained using changes in the stiffness matrices for changes in axial area of the RM apparatus members. The difference between the stiffness matrices for two distinct SAP2000 models with different axial area for the GWS apparatus members was calculated, and the result was used to calculate an orthonormal basis. Since each GWS apparatus was made up of eight axial members and with the use of four GWS apparatuses, 32 unique modes were obtained. Similarly, each PIA apparatus contains five distinct members leading to 20 unique modes. Using these bases as the loading matrices, deflected shapes were calculated and added to the reduced order model. In total, the reduced order model consisted of 53 degrees of freedom for the bridge model with GWS apparatuses, and 41 for the bridge model with PIA apparatuses.

The load model is based on the fatigue truck configuration specified in the AASHTO LRFD Bridge Design Specifications (2010) traveling at 65 mph (1144 in/s) in the northbound right lane of the 3-lane Cedar Avenue Bridge. To ease modeling difficulties, the truck is modeled as 3 moving point loads (instead of the previous 6) applied proportionally to the joints of the concrete deck along the loading line. The distance from the front axle to the second axle was 14 feet while the distance from the second axle to the third axle was 30 feet, and the front point load was 8 kips while the second and third loads were 32 kips each. The loading matrix for a point load at each node was pre-

calculated and a linear combination of these matrices was then used to approximate the truck loading at a given time step. The solver ODE23 in MATLAB was used to carry out the analyses for a 5.12 second loading duration.

To vary RM apparatus characteristics in the reduced order model, separate state space matrices were created corresponding to changes in RM apparatus member axial area ($\mathbf{\Delta A_{area}}$), changes in RM device stiffness ($\mathbf{\Delta A_{k,device}}$), and changes in RM device damping ($\mathbf{\Delta A_{c,device}}$) respectively. The base matrix describing the system already has inherent RM device damping and stiffness as well as RM apparatus member flexibility. This base matrix, $\mathbf{A_i}$, can be modified by the change matrices such that a final state space matrix $\mathbf{A}$ can be formed with multiplicative coefficients defining new parameters. The coefficients are found such that for a desired RM device stiffness,

$$k_{co} = k_{des} - k_{initial} \tag{3.24}$$

desired RM device damping,

$$c_{co} = c_{des} - c_{initial} \tag{3.25}$$

and desired RM apparatus member axial area,

$$a_{co} = a_{des} - a_{initial} \tag{3.26}$$

where the subscripts represent the matrix coefficient, desired, and initial values respectively. These state change matrices were either added or subtracted from the base state matrix of the bridge model calculated using RM apparatus area member areas of 35.2 in^2, RM device stiffness of 110 kip/in, and RM device damping of 3 kip·s/in. The final state space matrix takes the form

$$\mathbf{A} = \mathbf{A_i} + k_{co}\left(\Delta\mathbf{A_{k,device}}\right) + c_{co}\left(\Delta\mathbf{A_{c,device}}\right) + a_{co}\left(\Delta\mathbf{A_{area}}\right) \tag{3.27}$$

The accuracy of the reduced order model was verified for a wide range of GWS apparatus characteristics. Fig. 4.19 through Fig. 4.24 show that the reduced order model can predict displacements and moments at the vulnerable joint L3W for both increases and decreases in axial member area, RM device stiffness, and RM device damping. Similarly, the accuracy of the reduced order model in predicting the displacement and moment range at other important bridge locations was also verified for a wide variety of RM apparatus characteristic variations (Fig. 4.19-4.24). In addition, Fig. 4.18 compares the moment range computed using the reduced order model and computed using the full SAP2000 finite element model at the L3W vulnerable joint for an area reduction of 87.5% to 4.4 in^2 and a stiffness and damping increase in the RM device from 110 to 11000 kip/in and 3 to 300 kip·s/in respectively; the reduced order model also accurately predicts the moment history for changes of multiple characteristics simultaneously.

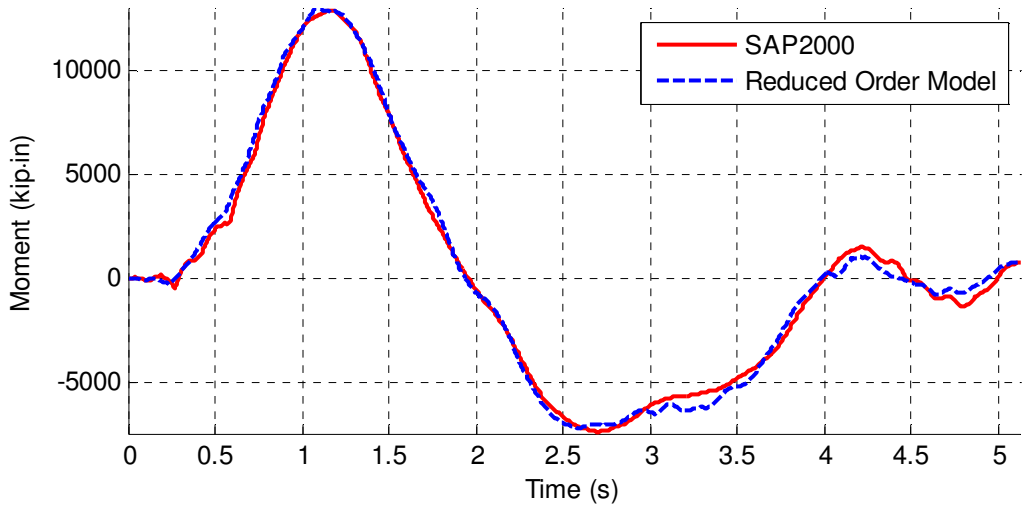

Figure 4.18 Reduced order model and SAP2000 model for one-eighth the original member axial area and one hundred times the original RM damping and stiffness

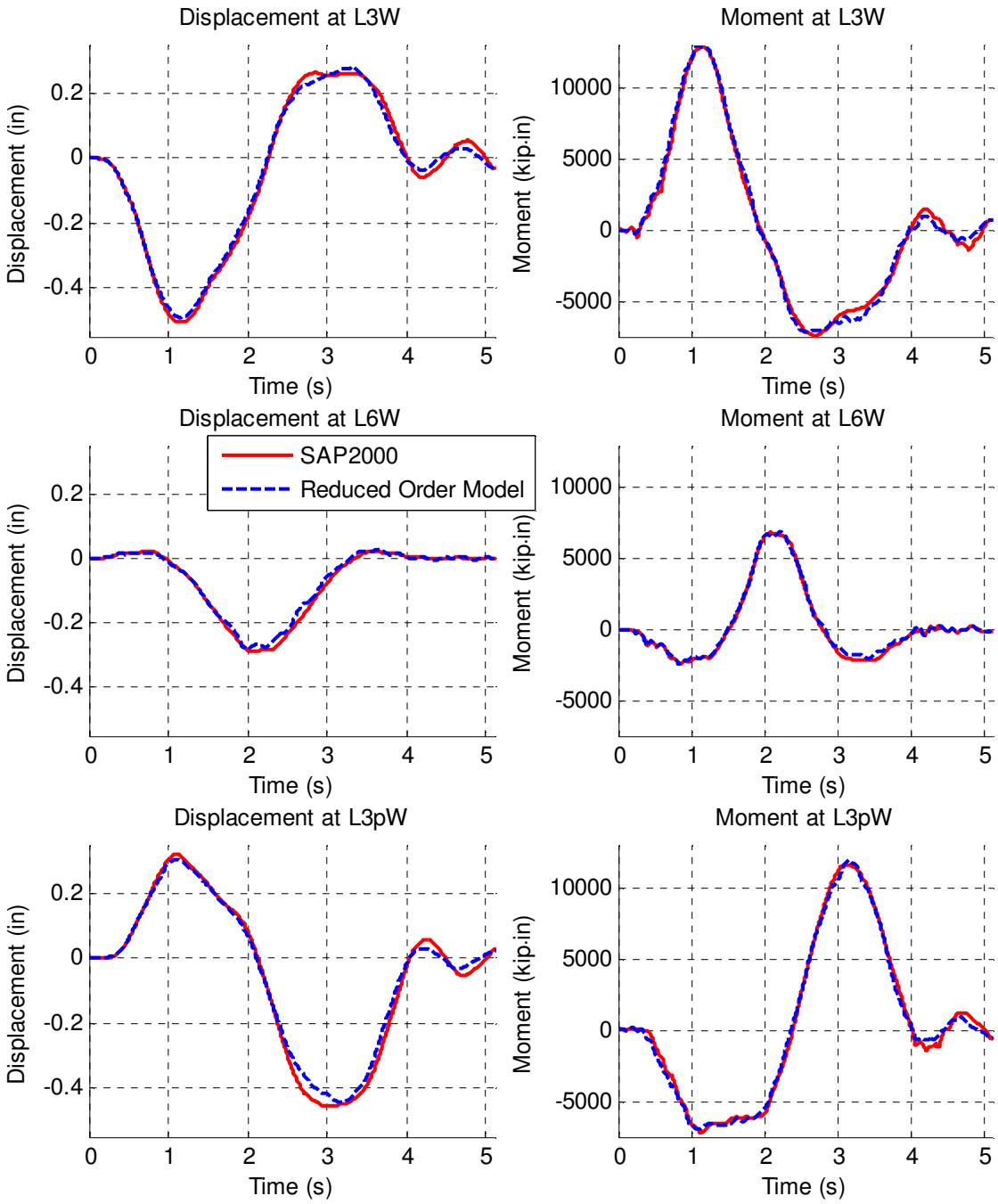

Figure 4.19 Reduced order model and SAP2000 model comparison for one-eighth the original member axial area

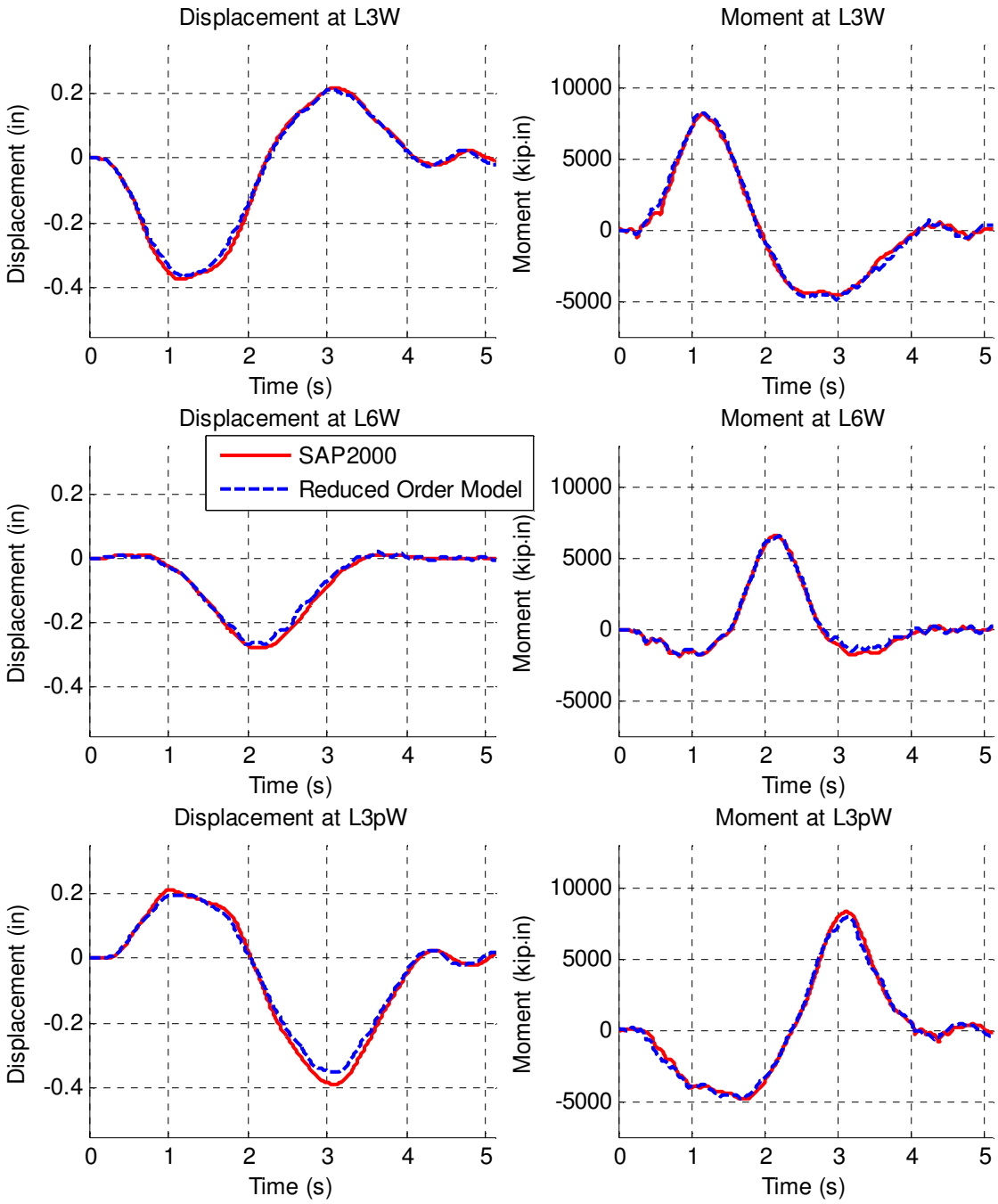

Figure 4.20 Reduced order model and SAP2000 model comparison for ten times the original member axial area

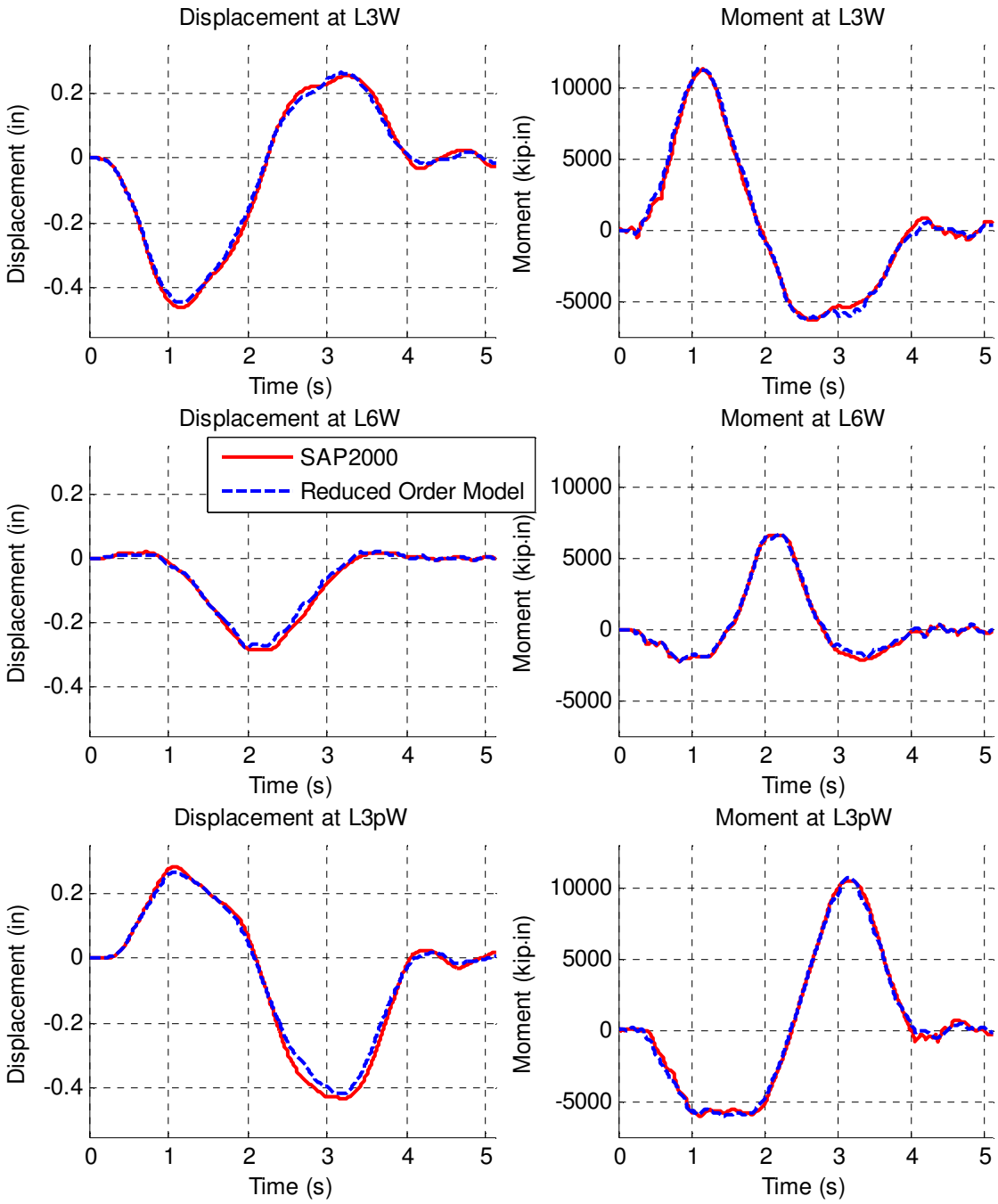

Figure 4.21 Reduced order model and SAP2000 model comparison for one hundred times the original RM stiffness

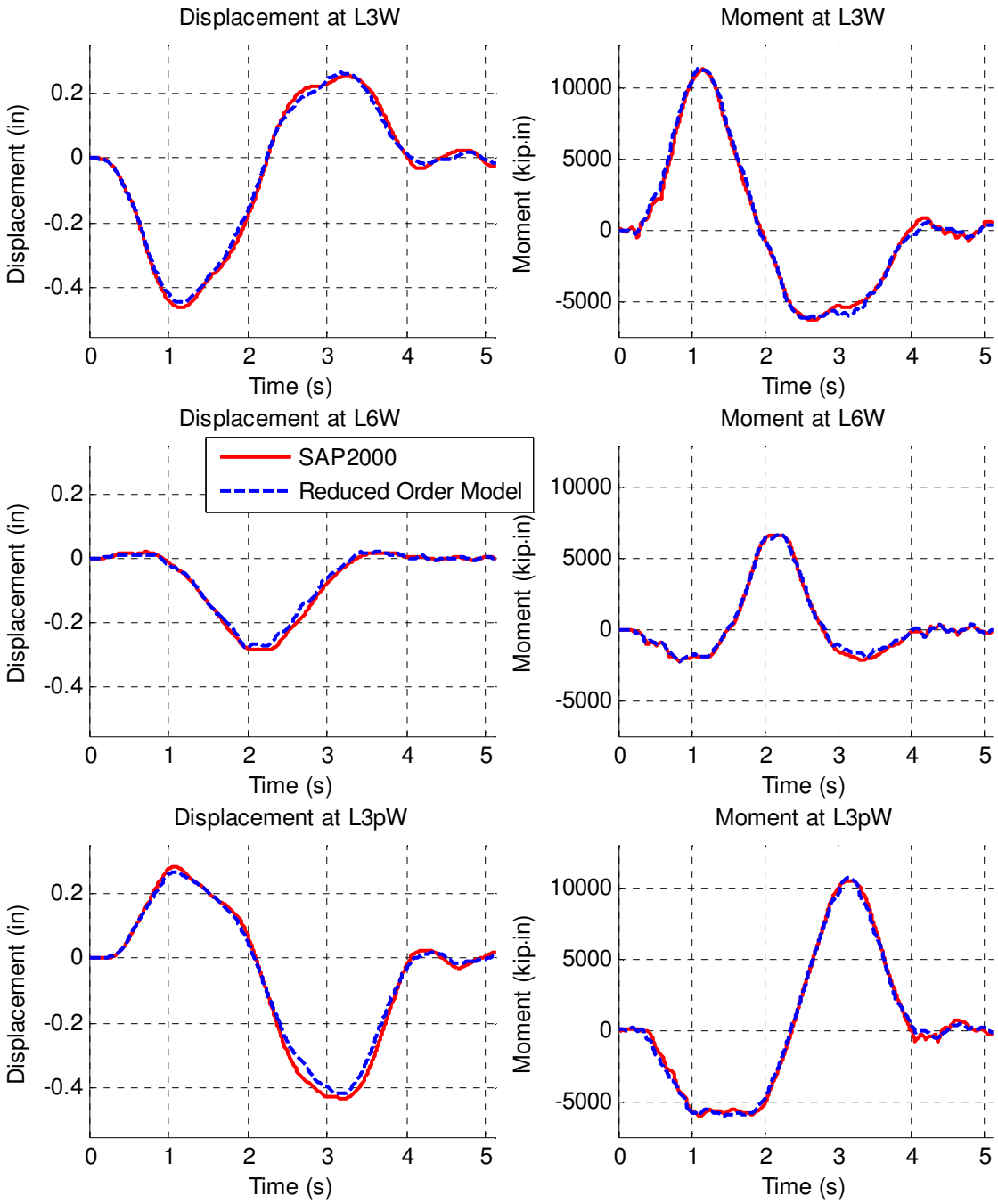

Figure 4.22 Reduced order model and SAP2000 model comparison for one hundred times the original RM damping

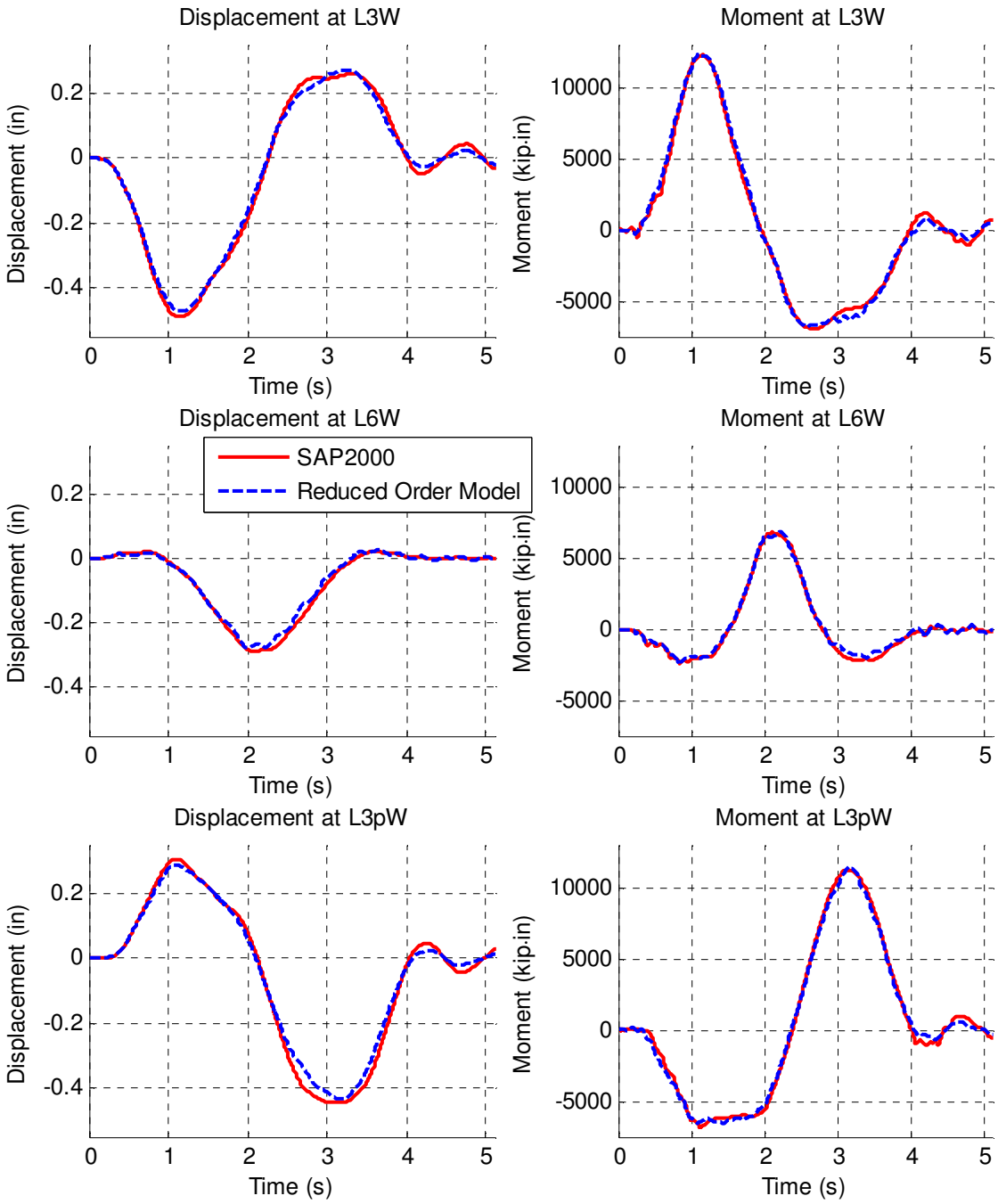

Figure 4.23 Reduced order model and SAP2000 model comparison for one-hundredth the original RM stiffness and damping

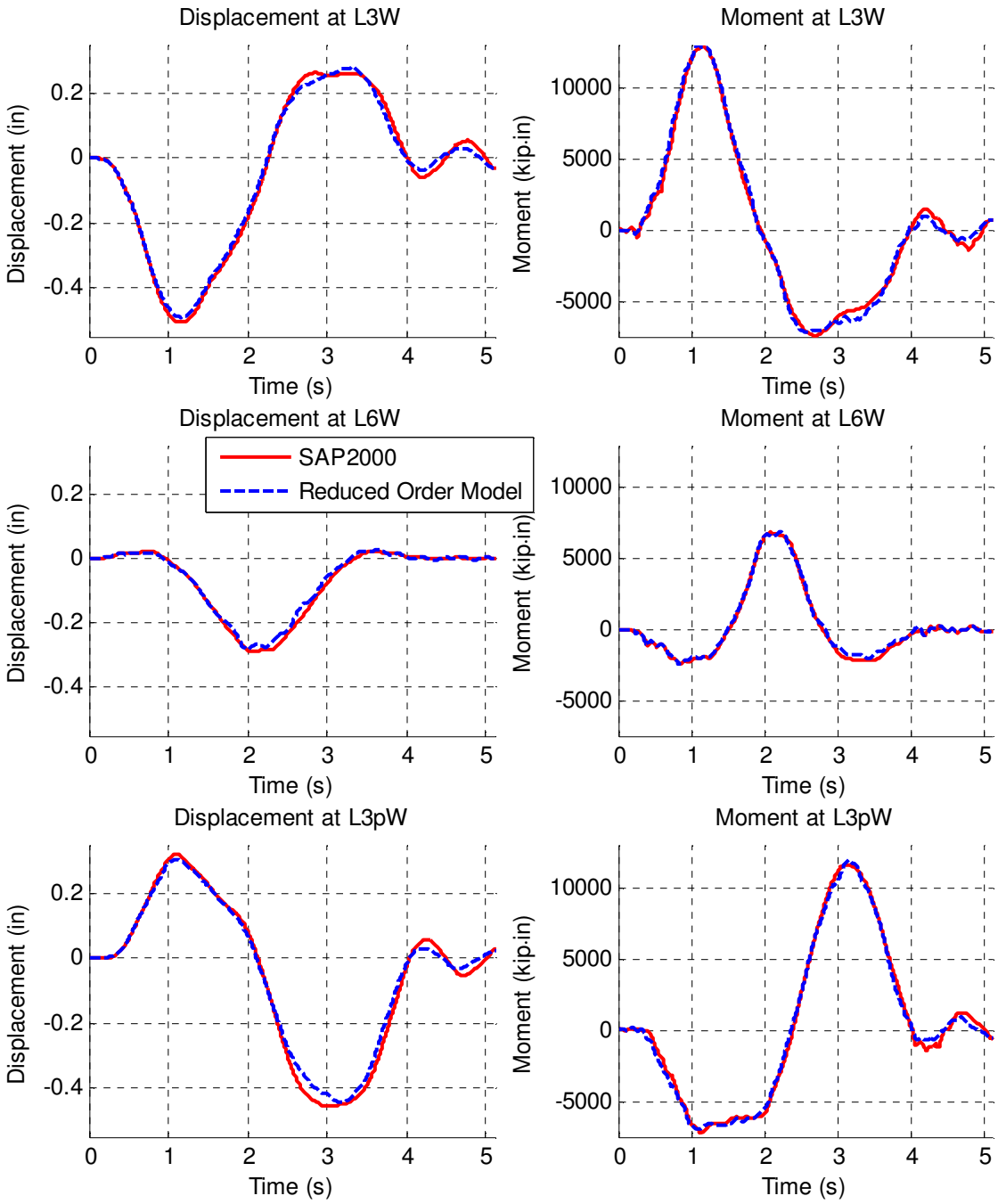

Figure 4.24 Reduced order model and SAP2000 comparison for one-eighth the original member axial area and one hundred times the original RM stiffness

A comparison of responses arising when varying characteristics of the GWS apparatuses (Fig. 4.25) shows the differences in moment range that can be achieved with various RM apparatus member axial areas, RM device damping values, and RM device

stiffness values. Notice the local nature of the response modification; very little changes are present in both displacement (not pictured) and moment at the L6 midspan joint that is not spanned by an RM apparatus, but large changes are present at the L3W and L3pW locations that are spanned by RM apparatuses.

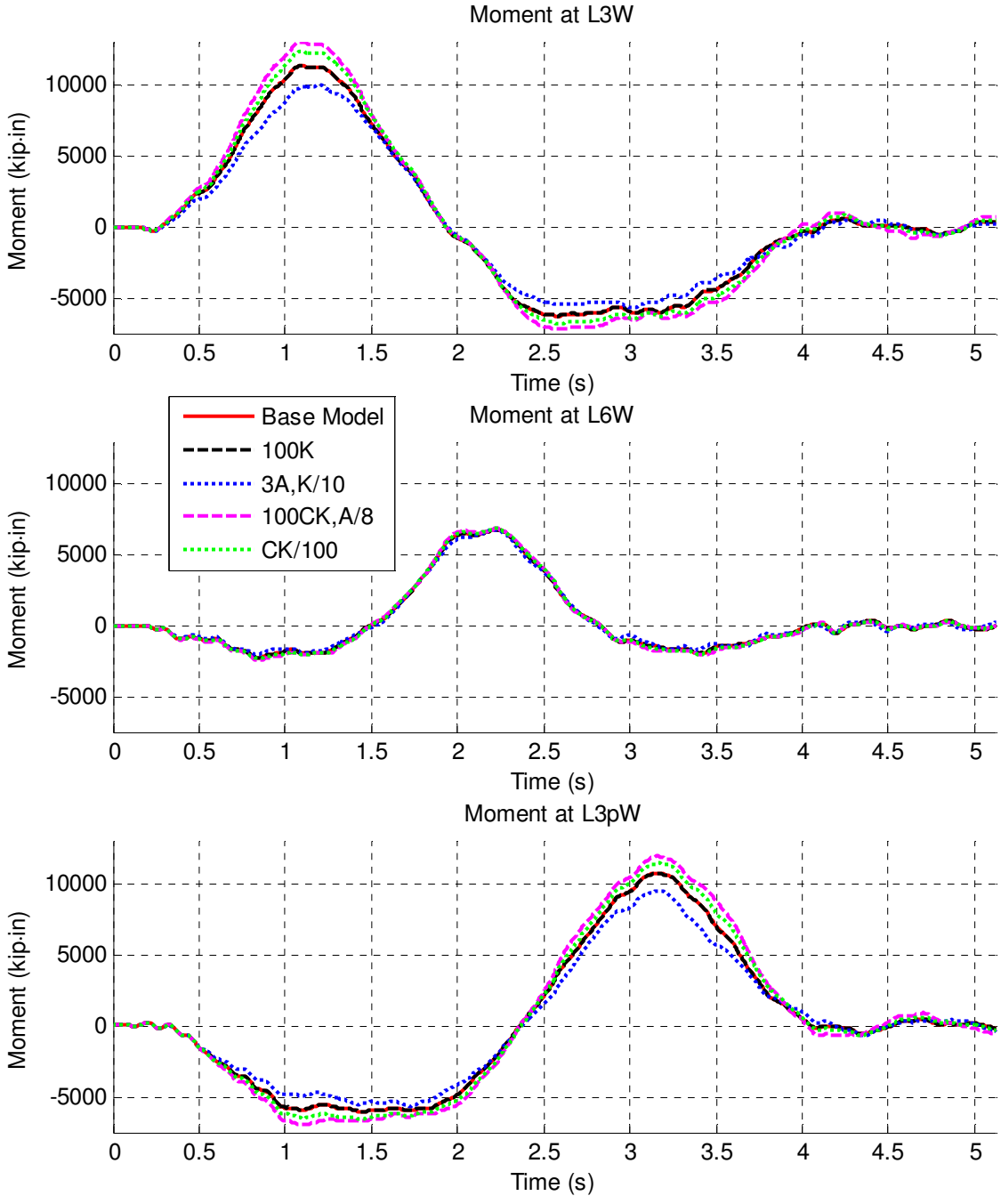

Figure 4.25 Comparison of different GWS apparatus characteristics modifying the Cedar Avenue Bridge

For model comparison and moment range results, the reduced order model needed to be able to accurately predict moments at particular joints on the bridge structure. To calculate these values, it is necessary to understand the modeling assumptions of the SAP2000 bridge model and be able to apply these to the reduced order model to obtain the correct values. Global displacements can be obtained directly from the reduced order model simply by multiplying the mode shapes used for reduction by the calculated generalized modal displacements (Eq. 4.19). Due to the static reduction, joint rotations must be calculated from joint displacements using

$$\mathbf{r} = \mathbf{LRk^{-1}(-LLk)x} = \mathbf{LRk^{-1}(-LLk)\Phi q} \tag{3.28}$$

Once global displacements and rotations are known, the moment within the frame elements can be calculated. However, there are different beam theories with slightly different kinematic assumptions that can be assumed to determine deflections.

For Euler-Bernoulli beam theory and members that are not internally loaded, the bending moment is defined by

$$M(\hat{x}) = EIv'' = C_1\hat{x} + C_2 \tag{3.29}$$

where $\hat{x}$ is the distance along the beam element from the left end. Integrating once

$$EIv' = \frac{C_1\hat{x}^2}{2} + C_2\hat{x} + C_3 \tag{3.30}$$

and again

$$EIv = \frac{C_1\hat{x}^3}{6} + \frac{C_2\hat{x}^2}{2} + C_3\hat{x} + C_4. \tag{3.31}$$

The boundary conditions are

$$v'(0) = -r_L;\ v'(L) = -r_R;\ v(0) = z_L;\ v(L) = z_R$$

where

$$r_L = left\ end\ ccw\ rotation$$

$$r_R = right\ end\ ccw\ rotation$$

$$z_L = left\ end\ vertical\ displacement$$

$$z_R = right\ end\ vertical\ displacement$$

so that

$$C_3 = C_4 = 0 \tag{3.32}$$

and

$$C_1 = \frac{6EI}{L^3}\big(2(z_L - z_R) - L(r_L + r_R)\big) \tag{3.33}$$

and

$$C_2 = \frac{2EI}{L^2}\big(L(2r_L + r_R) - 3(z_L - z_R)\big) \tag{3.34}$$

Then,

$$M(\hat{x}) = \frac{6EI}{L^3}\big(2(z_L - z_R) - L(r_L + r_R)\big)\hat{x} + \frac{2EI}{L^2}\big(L(2r_L + r_R) - 3(z_L - z_R)\big) \tag{3.35}$$

While Euler beam theory is the simplest, Timoshenko beam theory is another option and includes shear deformation of the frame members. For members that are not internally loaded, bending moment is defined by:

$$M(\hat{x}) = EI\varphi' \tag{3.36}$$

The governing differential equations for rotation and displacement are:

$$EI\varphi''' = 0 \tag{3.37}$$

and

$$GAw' = -EI\varphi'' + GA\varphi \tag{3.38}$$

where w is the vertical displacement and φ is the slope. The four boundary conditions for the member are

$$\varphi(0) = -r_L;\ \varphi(l) = -r_R;\ w(0) = z_L;\ w(l) = z_R$$

where the negative signs arise because of the rotational definitions in SAP2000. Then, integrating Eq. (4.37) twice

$$EI\varphi' = C_1\hat{x} + C_2 \tag{3.39}$$

and integrating again

$$EI\varphi = \frac{C_1\hat{x}^2}{2} + C_2\hat{x} + C_3 \tag{3.40}$$

and rearranging and integrating Eq. (4.38) and substituting in Eq. (4.39) and Eq. (4.40)

$$w = \int \varphi - \frac{EI}{GA}\varphi' = \frac{1}{EI}\left(\frac{C_1\hat{x}^3}{6} + \frac{C_2\hat{x}^2}{2} + C_3\hat{x}\right) - \frac{1}{GA}(C_1\hat{x} + C_2) + C_4 \tag{3.41}$$

Then from the first boundary condition and Eq. (4.40)

$$C_3 = -EIr_L \tag{3.42}$$

From the second boundary condition and Eq. (4.40) and substituting in Eq. (4.42)

$$C_2 = \frac{EI}{l}(r_L - r_R) - \frac{l}{2}C_1 \tag{3.43}$$

From the third boundary condition and Eq. (4.41)

$$C_4 = z_L + \frac{EI}{GAl}(r_L - r_R) - \frac{l}{2GA}C_1 \tag{3.44}$$

and from the fourth boundary condition and combining Eq. (4.41) with Eq. (4.42), (4.43) and (4.44)

$$C_1 = \frac{12GAEI}{(12EIl + GAl^3)}\left((z_L - z_R) - \frac{l}{2}(r_L + r_R)\right) \tag{3.45}$$

and it follows that

$$C_2 = \frac{EI}{l}(r_L - r_R) + \frac{l}{2}\frac{12EI}{(12EIl + GAl^3)}\left((z_L - z_R) - \frac{l}{2}(r_L + r_R)\right) \tag{3.46}$$

so

$$M(\hat{x}) = \frac{12GAEI}{(12EIl + GAl^3)}\left((z_L - z_R) - \frac{l}{2}(r_L + r_R)\right)\left(\hat{x} + \frac{l}{2}\right) + \frac{EI}{l}(r_L - r_R) \tag{3.47}$$

To determine how SAP2000 calculates moment, these different kinematic definitions were compared to the moment outputs in SAP2000, and it was determined that moments are obtained using Timoshenko beam theory or, more conveniently, matrix shear beam elements. For a beam element as depicted in Fig. 4.26, the coefficients for each degree of freedom can be found from the stiffness matrix in Table 4.4 (adapted from Przemieniecki 1968). For moment, the rows six and twelve define the left hand moment and right hand moment respectively. Notice that the SAP2000 coordinate definition differs slightly so that the displacements and rotations in the global *y* direction must be flipped in sign (S_3, S_9, S_6, S_{12}); the correct coefficients for the SAP2000 directions are denoted in the parentheses.

Rows six and twelve can be conveniently written out such that

$$M_{left} = \frac{-6EI}{l^2(1+\chi)}z_L + \frac{(4+\chi)EI}{l(1+\chi)}r_L + \frac{6EI}{l^2(1+\chi)}z_R - \frac{(\chi-2)EI}{l(1+\chi)}r_R \tag{3.48}$$

and

$$M_{right} = \frac{6EI}{l^2(1+\chi)}z_L + \frac{(\chi-2)EI}{l(1+\chi)}r_L - \frac{6EI}{l^2(1+\chi)}z_R - \frac{(4+\chi)EI}{l(1+\chi)}r_R \tag{3.49}$$

with

$$\chi = \frac{12EI}{GAl^2} \tag{3.50}$$

and where *E*, *G* are the Young's modulus and shear modulus of the material and *I*, *A*, and *l* are the moment of inertia, area, and length in the direction of the degree of freedom.

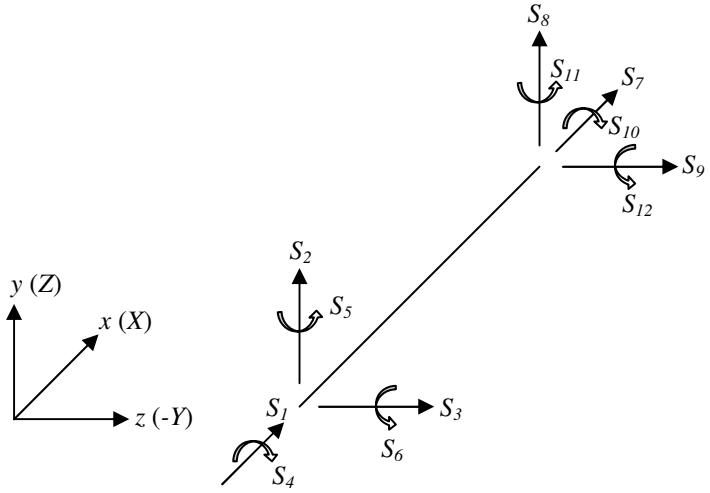

Figure 4.26 Degrees of freedom for a space frame beam element

To calculate axial forces in the members, row one or row seven can be utilized. However, due to the rotated nature of the scissor jack members, both *X* and *Z* (global) must be taken into account. Therefore:

$$Axial_{local} = \frac{EA}{L}(x_R - x_L) \tag{3.51}$$

If rotation is counterclockwise

$$Axial_{Global} = \frac{EA}{L}\left(\cos\theta\,(X_R - X_L) + \sin\theta\,(Z_R - Z_L)\right) \tag{3.52}$$

but due to the shallow angle of the scissor jack, $\cos\theta \approx 1$, so that

$$Axial_{Global} = \frac{EA}{L}\left((X_R - X_L) + \sin\theta\,(Z_R - Z_L)\right) \tag{3.53}$$

The axial forces were verified and can be seen in Fig. 4.27.

Table 4.4 Stiffness matrix for space frame beam element; (-) is the sign flip for the SAP2000 directional discrepancy

$\frac{EA}{l}$	0	0	0	0	0	$\frac{-EA}{l}$	0	0	0	0	0
0	$\frac{12EI_z}{l^3(1+\chi_y)}$	0	0	0	$\frac{(-)6EI_z}{l^2(1+\chi_y)}$	0	$\frac{6EI_z}{l^2(1+\chi_y)}$	0	0	0	$\frac{(-)6EI_z}{l^2(1+\chi_y)}$
0	0	$\frac{(-)12EI_y}{l^3(1+\chi_z)}$	0	$\frac{-6EI_y}{l^2(1+\chi_z)}$	0	0	0	$\frac{(-)-12EI_y}{l^3(1+\chi_z)}$	0	$\frac{-6EI_y}{l^2(1+\chi_z)}$	0
0	0	0	$\frac{GJ}{l}$	0	0	0	0	0	$\frac{-GJ}{l}$	0	0
0	0	$\frac{(-)-6EI_y}{l^2(1+\chi_z)}$	0	$\frac{(4+\chi_z)EI_y}{l(1+\chi_z)}$	0	0	0	$\frac{(-)6EI_y}{l^2(1+\chi_z)}$	0	$\frac{(2-\chi_z)EI_y}{l(1+\chi_z)}$	0
0	$\frac{6EI_z}{l^2(1+\chi_y)}$	0	0	0	$\frac{(-)(4+\chi_y)EI_z}{l(1+\chi_y)}$	0	$\frac{-6EI_z}{l^2(1+\chi_y)}$	0	0	0	$\frac{(-)(2-\chi_y)EI_z}{l(1+\chi_y)}$
$\frac{-EA}{l}$	0	0	0	0	0	$\frac{EA}{l}$	0	0	0	0	0
0	$\frac{-12EI_z}{l^3(1+\chi_y)}$	0	0	0	$\frac{(-)-6EI_z}{l^2(1+\chi_y)}$	0	$\frac{12EI_z}{l^3(1+\chi_y)}$	0	0	0	$\frac{(-)-6EI_z}{l^2(1+\chi_y)}$
0	0	$\frac{(-)-12EI_y}{l^3(1+\chi_z)}$	0	$\frac{6EI_y}{l^2(1+\chi_z)}$	0	0	0	$\frac{(-)12EI_y}{l^3(1+\chi_z)}$	0	$\frac{6EI_y}{l^2(1+\chi_z)}$	0
0	0	0	$\frac{-GJ}{l}$	0	0	0	0	0	$\frac{GJ}{l}$	0	0
0	0	$\frac{(-)-6EI_y}{l^2(1+\chi_z)}$	0	$\frac{(2-\chi_z)EI_y}{l(1+\chi_z)}$	0	0	0	$\frac{(-)6EI_y}{l^2(1+\chi_z)}$	0	$\frac{(4+\chi_z)EI_y}{l(1+\chi_z)}$	0
0	$\frac{6EI_z}{l^2(1+\chi_y)}$	0	0	0	$\frac{(-)(2-\chi_y)EI_z}{l(1+\chi_y)}$	0	$\frac{-6EI_z}{l^2(1+\chi_y)}$	0	0	0	$\frac{(-)(4+\chi_y)EI_z}{l(1+\chi_y)}$

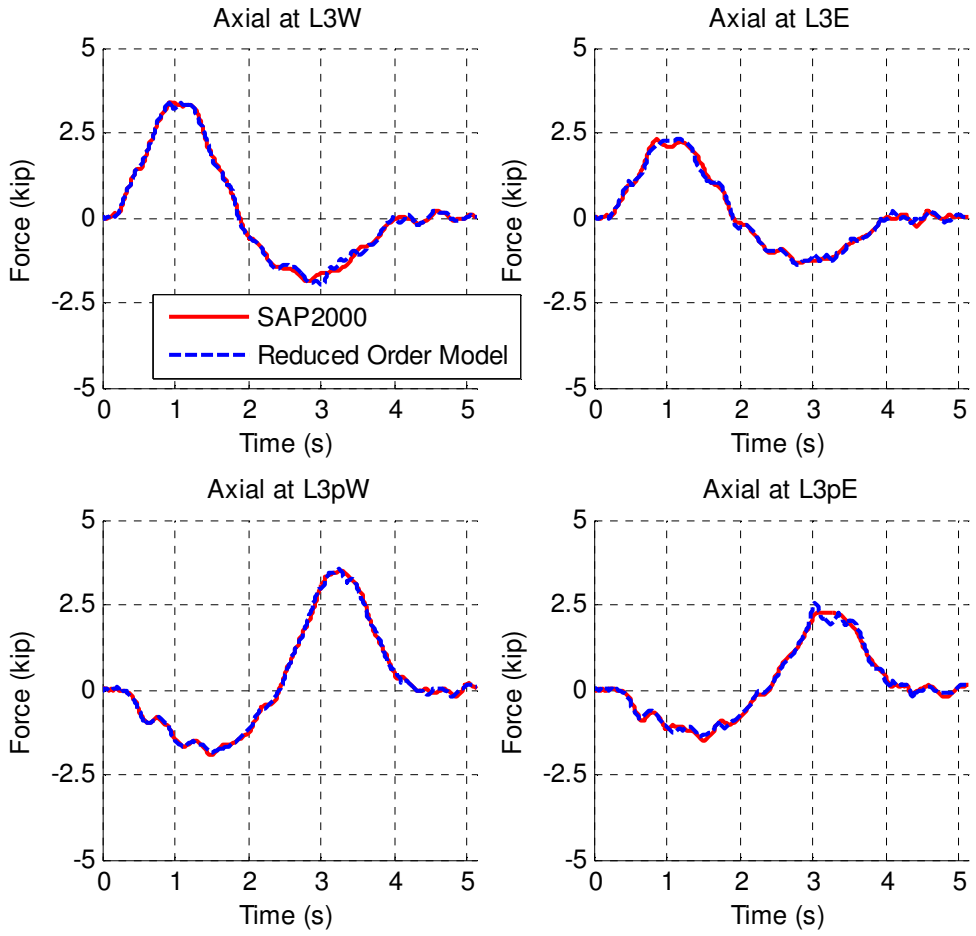

Figure 4.27 Axial force at multiple joints of the scissor jack members with one-eighth the original area

To conclude, a verified reduced order model was developed which resulted in analysis time being reduced by one or two orders of magnitude. Analyses require from 2.5 to 50 seconds depending on the parameter values compared to the 540 seconds required by a typical SAP2000 simulation yielding a speedup of 11 to 200 times. The model was reduced from a total of 35,402 degrees of freedom to 53 degrees of freedom. The reduction in required computation time is essential to perform design optimization of the RM apparatuses.

4.2.6 Modeling of the PIA Apparatus

While the main focus of this dissertation is the GWS apparatus and although the PIA apparatus was initially used to span the majority of a simple highway bridge crossing, the PIA apparatus (no mechanical amplifier) is often used for comparison to the GWS apparatus. For this comparison, a numerical model of the PIA apparatus was developed. The PIA apparatus is meant to be similar to the RM apparatus used by Patten et al. (1999) on the I-35 bridge crossing over Walnut Creek consisting of five W54x132 girders to span the river.

For response modification, Patten et al. (1998) used an extension weighing 3840 lb with an effective stiffness of 3694.5 ksi. The length of the extension is not reported, but from one of the figures it can be assumed that the length is not longer than 30.3 ft (9.25 m) and should be slightly less because of the length of the actuator. It is assumed that the length of the extension was 29.5 ft and therefore the weight per unit length is approximately 130 lb/ft. The density of steel is approximately 490 lb/ft^3 (7850 kg/m^3) so that the area of the extension is approximately 38.2 in^2. The area of a W54x132 is 38.8 in^2 and it is clear that the area of the extension is on the order of the area of the girder. It should be noted that three RM apparatuses are used to modify the five girders so that the area of steel being used for modification is about 60 percent of the axial area of the girders. The Cedar Avenue Bridge has an area of 288.5 in^2 for each girder near the vulnerable connection; for a similar comparison it may be reasonable to use up to 171.3 in^2 for the total area of RM apparatus axial members.

Since the exact configuration and parameters of the RM apparatuses used by Patten are unknown, an approximation of the RM apparatuses was developed. Therefore, two springs in series, one the RM device and the other the axial stiffness of the extension, are approximated as a two-joint link. The resulting stiffness, k_{eff}, is found through

$$\frac{1}{k_{eff}} = \frac{1}{k_d} + \frac{1}{k_{ext}} = \frac{1}{k_d} + \frac{1}{\frac{EA}{\tilde{L}}} \tag{3.54}$$

where $\tilde{L}$ is the distance between attachment points, A is the cross-sectional area of the extension beam, k_d is the RM device stiffness, and k_{ext} is the extension stiffness. For early comparisons without RM apparatus member flexibility, the extension stiffness is assumed to be infinite so that the effective stiffness was equivalent to the RM device stiffness. For the parameter studies, Eq. 4.54 was utilized to calculate the effective stiffness provided by the two joint link in the SAP2000 model.

When the reduced order model was developed for RM apparatus characteristic optimization, the coupling of RM device stiffness and extension stiffness made manipulation of characteristics difficult. To create the perturbation matrices, a slightly different approach was used. Due to the way the equivalent stiffness was modeled in the two joint link between the attachment points, the matrices cannot be separated into an area change matrix, a device stiffness matrix, and a device damping matrix. Instead, a device damping matrix, an area change matrix for just the attachments, and a stiffness matrix combining the device stiffness and leg stiffness are employed. To achieve this, a stiffness coefficient was created such that

$$k_{PIA} = \frac{k_{d,des}k_{leg,des}}{k_{d,des} + k_{leg,des}} - \frac{k_{d,i}k_{leg,i}}{k_{d,i} + k_{leg,i}} \tag{3.55}$$

where k_{PIA} is the stiffness coefficient for the two joint link, k_d is the RM device stiffness, k_{leg} is the extension stiffness, and the subscripts *des* and *i* stand for the desired and initial values respectively. One problem arose using the effective stiffness approach; while it works in theory for stiffness, the RM device damping is poorly defined. Since the attachment points of the two joint link are actually at the truss joints that attach to the bridge girder, the flexibility of the extension does not get taken into account when damping forces are calculated.

Therefore, due to the damping problems and the convoluted nature of Eq. 4.55, a more straight-forward approach was developed. The premise of the two springs in series was left in place but instead of representing the axial strut (the extension beam) and RM device in series as a two joint link with an effective stiffness, each was modeled

separately. The RM device was modeled as a 24-inch link placed in series with a 697-inch beam between the attachment points (Fig. 4.28). To keep a hinge from forming where the two joint link was connected to the beam, an additional 24 inch member was placed in parallel with the two joint link. This member maintained moment continuity at the extension beam joint, but was given minimal axial area so that its axial stiffness was negligible. Without moment continuity, a hinge forms between the beam and the two joint link that created problems during modal analysis. To provide a fair comparison for the PIA and the GWS models, the PIA leg axial area was modeled as twice that of the GWS leg area to compensate for the extra leg; the attachment members were identical for the GWS and PIA apparatuses.

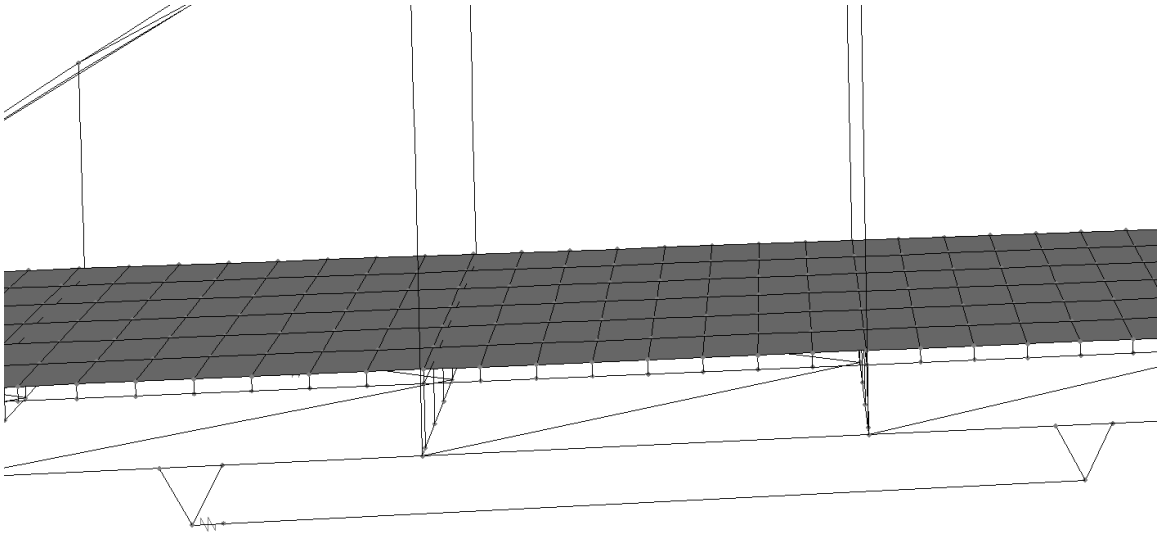

Figure 4.28 PIA apparatus with RM device modeled as 24 inch two joint link

Chapter 5: Response Modification Apparatus Parameter Studies

To understand the effects of the response modification approach utilizing the GWS apparatus, a multitude of parameter studies to be described in this chapter were performed using the various numerical models of the Cedar Avenue Bridge (Fig. 5.1). The parameter studies explored the range of performance of the modification approach by varying the number of RM apparatuses, the length of the RM apparatus, the magnification of the RM apparatus, the size of the RM device damping and stiffness coefficients, the speed of moving truck load, and the cross-sectional area of the RM apparatus members.

(photo credit: Arturo Schultz)

Figure 5.1 Cedar Avenue Bridge northbound span

5.1 One Set of GWS Apparatuses

A pair of GWS apparatuses in different configurations was designed and attached to the steel component Cedar Avenue Bridge model across the vulnerable joints on both

transverse bridge girders (see Fig. 5.2). The joint was chosen because it has the highest moment range (Fig. 5.3) of any of the bridge joints. In this section, the effect of the pair of GWS apparatuses was evaluated when placed across both one connection and two connections (see Fig. 5.4 and Fig. 5.5) on the South end of the bridge. In practice, a similar set of GWS apparatuses would also be placed across joint L3' due to the symmetry of the bridge and moment diagram (Fig. 5.3) but is not attached for the initial response modification exploration.

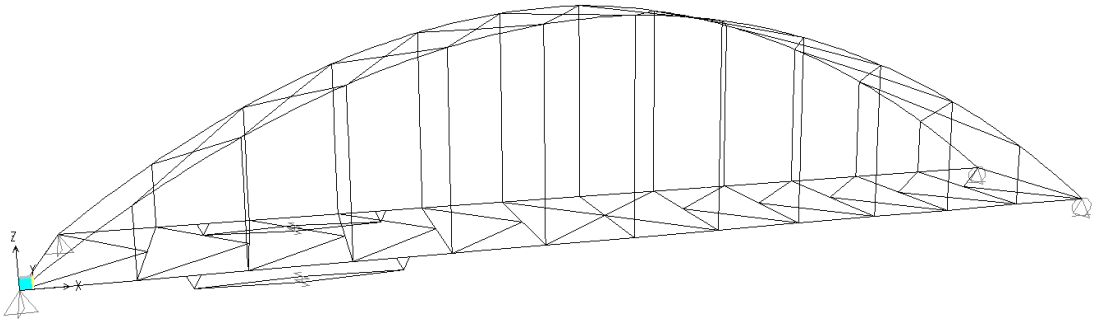

Figure 5.2 Cedar Avenue Bridge steel only model with the GWS apparatuses

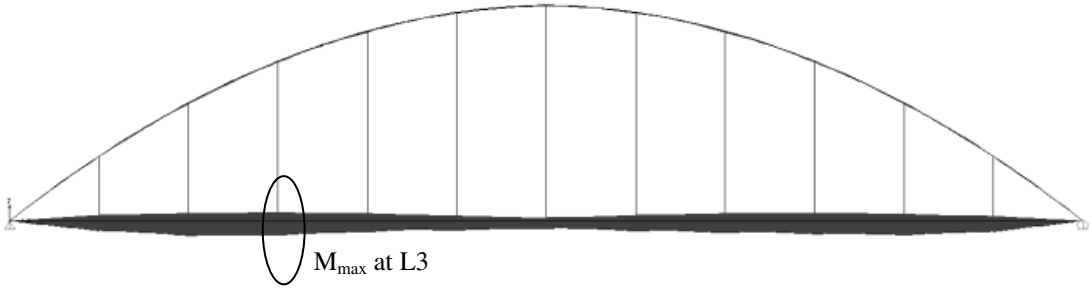

Figure 5.3 Cedar Avenue Bridge moment envelope

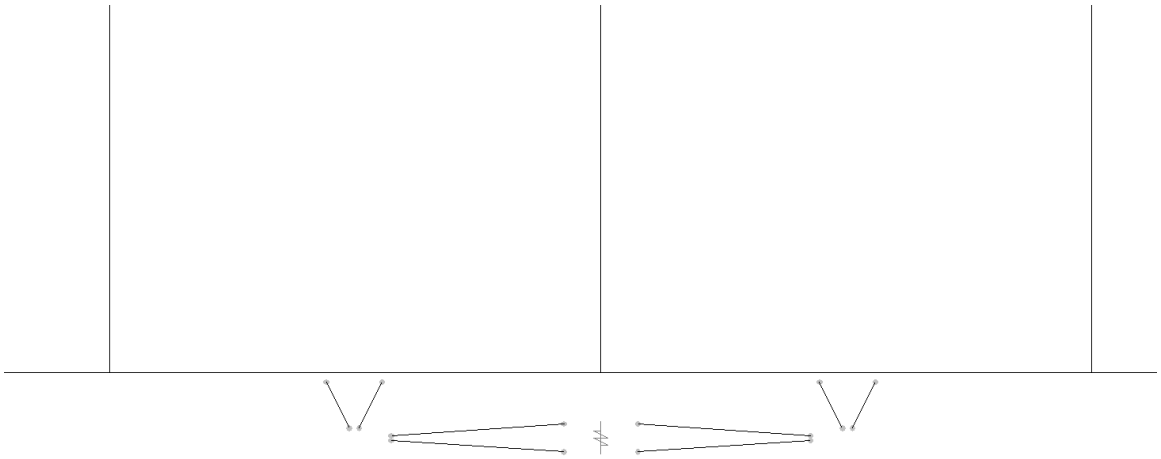

Figure 5.4 Cedar Avenue Bridge with GWS apparatus placed across joint L3

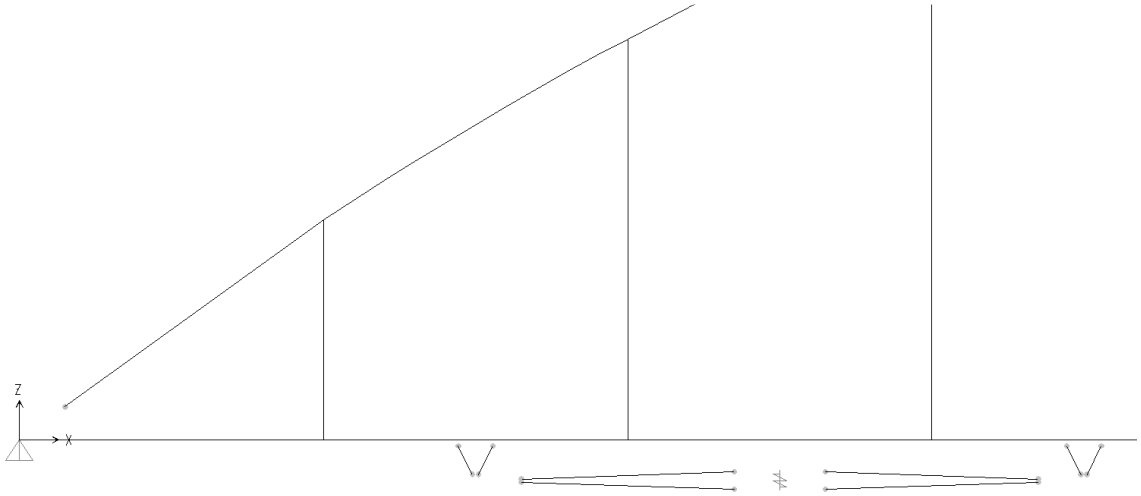

Figure 5.5 Cedar Avenue Bridge with GWS apparatus spanning joints L2 and L3

The damping and stiffness characteristics for the initial RM device that was placed within the scissor jack of the GWS apparatuses were selected to only allow a maximum of 20 tons for the controlling force in the RM device. The value of 20 tons is the force that a typical large scale damping device can exert. A simulation was carried out without a RM device placed in the scissor jack, and maximum displacements and velocities across the scissor jack where the RM device would be placed were calculated. By

equating the maximum force exerted by the RM device to 20 tons (40 kip), the stiffness constant k, for a pure linear stiffness element included in the scissor jack, was calculated to be 110 kip/in. The damping constant c was determined to be 3 kip·s/in when a pure, linear damping element was placed in the scissor jack. This assured that the forces would not be larger than 40 kip and in reality, much less than 40 kip because displacements across the scissor jack will be much smaller when a RM device with stiffness and damping is present. In fact, maximum forces actually exerted by the RM device were found to be only about 4 kip. Analyses were carried out using the aforementioned standard truck loading and only planar degrees of freedom were active.

5.1.1 Varying Connection Type and Magnification

Initial trials were run using different GWS apparatus parameters and connections and the largest positive and negative moments were calculated to obtain moment range. The GWS apparatus connections refer to how the RM apparatus is connected to the deck and can be either ideal moment connections, as seen in Fig. 3.6, or more practical truss connections, as seen in Fig. 3.7. The connection depths resulted in a moment arm of 4 feet from the bridge girder. The depth of the scissor jack was 2 feet and the total length was either 30 feet spanning just joint L3 or 60 feet spanning joints L2 and L3; these sizes resulted in magnification values of 15 or 30 for the GWS apparatuses. Table 5.1 shows the results along with the overall reduction in moment range compared to the Cedar Avenue Bridge without response modification due to an identical vehicle loading. It can be seen from Table 5.1 that longer RM apparatuses with higher magnification, m, lead to a higher moment range reduction. It can also be seen that the moment connection leads to larger reductions in moment range, but it should be noted that a rigid moment connection is more difficult to achieve than a truss connection in practice. Figure 5.6 shows the moment envelope for the GWS apparatuses with truss connections and spanning two joints. Although it is difficult to discern in Fig. 5.6, the moment ranges in the bridge girder have been reduced by almost 40%. As previously discussed, overall reduction in moment range is pertinent because fatigue life is inversely proportional to the cube of the stress range. If it is assumed that the moment range seen by the

connection is proportional to the stress range, a 39 percent reduction in moment range leads to a 346 percent increase in fatigue life of the critical joint. Additionally, a convenient way to reconsider the equation for safe life estimation (Eq. 2.1) is by assuming the bridge has been in service for Y_p years and had an initial safe life Y_1 years. Then the remaining safe life Y_f due to a new stress range is:

$$Y_f = \left(Y_1 - Y_p\right)\left(\frac{1}{\left(1 - \frac{R_{red}}{100}\right)^3}\right) \tag{4.1}$$

where R_{red} is the percent moment reduction. This assumes that there are no changes in the daily truck traffic or number of cycles and that the effective stress range is the moment range obtained from simulations. For example, if Y_p = 30 years, initial safe life was Y_1 = 50 years, and R_{red} = 39.3%, then the remaining fatigue safe life would be Y_f = 89 years; this is a safe life increase of 69 years.

Table 5.1 Moment envelope at the critical joint on the Cedar Avenue Bridge with different scissor jack configurations

Connection type	*m*	*k* (kip/in)	*c* (kip·s/in)	Moment (kip·in)			Reduction (%)	Safe life increase (%)
				Max	Min	Range		
-	-	-	-	11654	-6827	18481	-	-
Moment	30	110	3	6811	-4412	11223	39.3	346.5
Truss	30	110	3	7669	-4792	12461	32.6	226.2
Moment	15	110	3	7346	-4524	11870	35.8	277.4
Truss	15	110	3	8434	-5145	13579	26.5	152.1

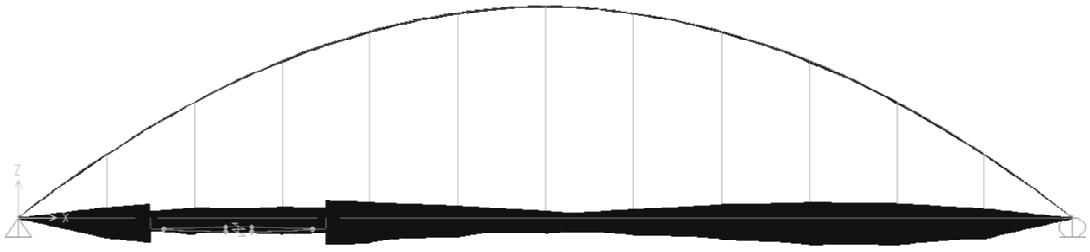

Figure 5.6 Moment range diagram for the Cedar Avenue Bridge with a single pair of GWS apparatuses across the critical region

The first brief application of the response modification methodology on the numerical model of the Cedar Avenue Bridge demonstrates the efficacy of the GWS apparatus approach, specifically the novel use of a mechanical amplifier, the scissor jack, for reducing moment ranges seen by a connection or member in a bridge structure. By reducing the moment range, bridge life can be safely extended in structures with a finite fatigue life. Since the fatigue life is inversely proportional to the cube of the stress range, even small reductions in ranges can have a large effect on fatigue life. Assuming the connections in the Cedar Avenue Bridge had a finite fatigue life due to their stress concentrations, the GWS apparatuses could safely extend fatigue life by 346 percent giving bridge owners time to allocate funds to replace a bridge that has reached its design life limit.

5.1.2 Varying RM Device Characteristics

In addition to examining the effects of the attachment type and the magnification of the RM apparatus and its length, the effects of varying RM device damping and stiffness characteristics were investigated. Using the same 2D steel component only numerical model of the Cedar Avenue Bridge, different pairs of stiffness and damping coefficients were chosen for the RM device and analyses using a single truck traveling at 65 mph were carried out. The pair of GWS apparatuses utilized for this section used the practical truss connections and the best configuration found in the previous section: rigid members; a 60-foot length; and magnification of 30. The results from the parameter study are summarized in Table 5.2. The base characteristics of stiffness of 110 (kip/in) and damping of 3 (kip·s/in) provide a large moment range reduction. Notice that by increasing stiffness tenfold, from 1100 to 11000 (kip/in) only a one-tenth of a percent increase in reduction is attained when damping is 27 (kip·s/in). However, when RM device damping is 0.33 (kip·s/in), increasing RM device stiffness from 1.1 to 11 (kip/in), another tenfold increase, the moment range percent reduction jumps from 11.6 to 30.7 percent. It seems that a critical value for either RM device damping or RM device stiffness exists such that any further damping or stiffness increases provide little benefit.

Additionally, notice that due to the inverse cubic relationship between stress range and safe life, small increases in moment reduction can lead to much larger safe life increases.

Table 5.2 Moment ranges for the 2D steel component Cedar Avenue Bridge model

RM device		Moment (kip·in)				Safe life increase (%)
k (kip/in)	*c* (kip·s/in)	Max	Min	Range	% red	
-	-	11650	-6828	18478	-	-
110	3	6792	-4370	11162	39.6	353.7
110	1	6792	-4368	11160	39.6	353.9
110	0.33	6792	-4374	11166	39.6	353.2
110	9	6789	-4378	11167	39.6	353.1
110	27	6765	-4384	11149	39.7	355.3
110	81	6705	-4351	11056	40.2	366.8
11000	27	6613	-4317	10930	40.8	383.2
1100	27	6630	-4322	10952	40.7	380.3
11	27	6996	-4289	11285	38.9	339.0
1.1	27	7048	-4072	11120	39.8	358.8
1.1	0.33	10510	-5818	16328	11.6	44.93
11	0.33	7975	-4829	12804	30.7	200.6
1100	0.33	6630	-4323	10953	40.7	380.1
11000	0.33	6613	-4317	10930	40.8	383.2

5.1.3 Varying Truck Speeds

Another important parameter in the RM apparatus analyses involves not the RM apparatus characteristics themselves, but the speed of the vehicle that is driving across the bridge. Again using the 2D steel component only numerical model of the Cedar Avenue Bridge, analyses were performed for varying truck speeds. Speeds were allowed to vary from 40 mph to 75 mph. The speed limit on the bridge is 65 mph, but an on ramp precedes the bridge such that many trucks may be traveling more slowly. The RM device used was the base device with stiffness of 110 (kip/in) and damping of 3 (kip·s/in) which had provided adequate moment reduction in the preceding parameter study. The GWS apparatuses had a magnification of 30 and a length of 60 feet, spanning both joints L2 and L3. Figures 5.7 and 5.8 show the maximum and minimum moments at joint L3 for the various truck speeds at 5 mph intervals. These initial studies show that the maximum

and minimum ranges are dependent on truck speed. A range of 5.5 percent exists for the maximum moment and 10.6 percent for minimum moment.

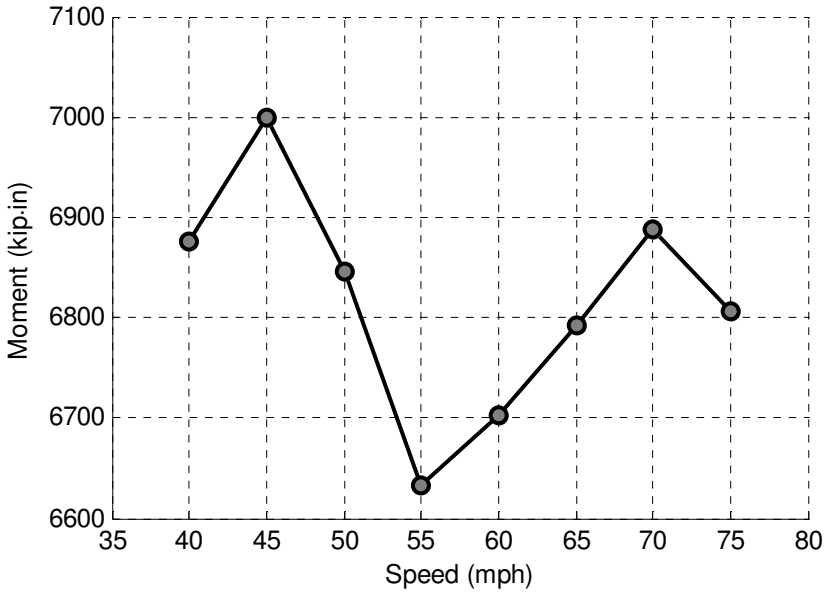

Figure 5.7 Maximum moment at joint L3 for various truck speeds

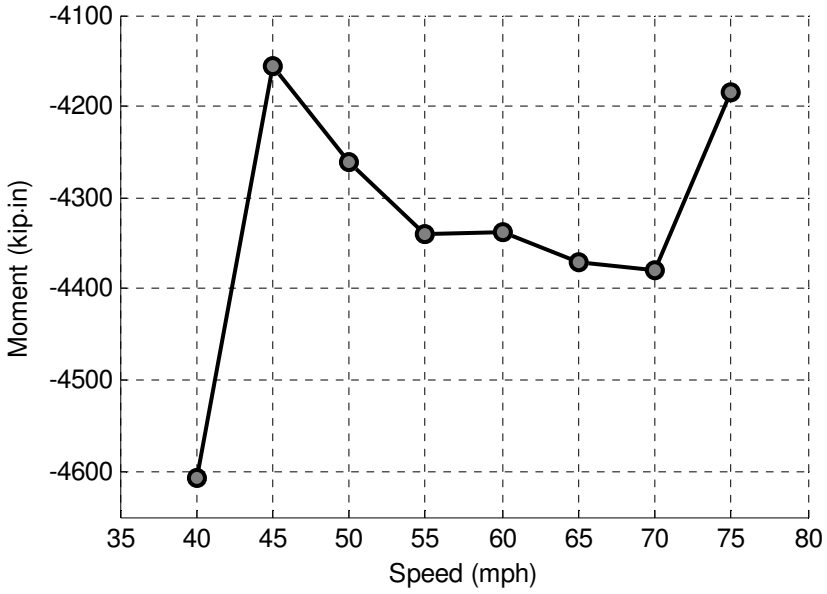

Figure 5.8 Minimum moment at joint L3 for various truck speeds

5.1.4 Three Dimensional Analyses

The previous parameter studies used the 2D steel component Cedar Avenue Bridge. While this was convenient for the parameter study of vehicle speed, a more comprehensive approach allowing unconstrained degrees of freedom was carried out to ensure more realistic modeling. Similar parameter studies were carried out for the 3D steel component Cedar Avenue Bridge model with the corrected box girder torsional rigidity. These studies looked at the length of the GWS apparatuses, the magnification, and also compared the GWS apparatus to the PIA apparatus described in Section 4.2.6. Tables 5.3 and 5.4 show the deflection and moment ranges at joint L3 respectively. It is clear that the overall deflections and ranges are much larger for the 3D model than the 2D model. However, overall percent deflection and percent moment reduction remain similar. Additionally, analyses run on the numerical model utilizing PIA apparatuses are reported in Table 5.3 and 5.4 and are denoted by having length but no magnification. The PIA apparatuses used the same RM device as the GWS apparatuses. While the PIA apparatuses would perform much better with a larger and stiffer RM device, it is clear that the GWS apparatuses outperform the PIA apparatus with identical RM devices. The parameter study confirms that longer RM apparatuses and larger magnification values perform better than shorter RM apparatuses and smaller magnification values. The study also confirms that the GWS apparatuses outperform the PIA apparatuses with identical RM devices and that the GWS apparatuses allow for much smaller RM devices to be used for response modification.

Table 5.3 Deflection ranges for the 3D steel component Cedar Avenue Bridge model

Length (ft)	*m*	Deflection (in)			
		Max	Min	Range	% red
-	-	0.33	-0.54	0.88	-
60	30	0.28	-0.41	0.69	21.1
60	15	0.28	-0.43	0.71	19.2
60	-	0.33	-0.54	0.87	0.7
30	30	0.32	-0.47	0.79	10.2
30	15	0.31	-0.48	0.79	9.9
30	-	0.33	-0.54	0.87	0.2

Table 5.4 Moment ranges for the 3D steel component Cedar Avenue Bridge model

Length (ft)	*m*	Moment (kip·in)				Safe life increase (%)
		Max	Min	Range	% red	
-	-	14300	-9296	23596	-	
60	30	8352	-5272	13624	42.3	419.5
60	15	8928	-5628	14556	38.3	326.0
60	-	14100	-8884	22984	2.6	8.20
30	30	8725	-5850	14575	38.2	324.3
30	15	9533	-6283	15816	33.0	232.1
30	-	14140	-9012	23152	1.9	5.86

Assuming the connections in the Cedar Avenue Bridge have a finite fatigue life due to their stress concentrations, the combination of the RM device and the scissor jack mechanical amplifier reduced moment range, and in turn, stress levels, in the box girder to floor beam joints by as much as 42.3 percent. Using the fatigue life estimation described herein these reductions translate into fatigue life extensions of over 420 percent. If an initial fatigue design life of 50 years is assumed, safe life can be extended by more than 70 years, thus giving bridge owners ample time to allocate funds to replace a bridge that has reached its design life limit.

5.2 Multiple Sets of GWS Apparatuses

While the use of a single set of RM apparatuses shows great promise as evidenced by the aforementioned example, it is hypothesized that the judicious use of multiple RM apparatuses will only further reduce the bridge response due to typical, service loads and thus even further extend the lifetime of the bridge. This section will investigate the application of multiple sets of RM apparatuses (Fig. 5.9) on the Cedar Avenue Bridge model and will compare these to the previous results.

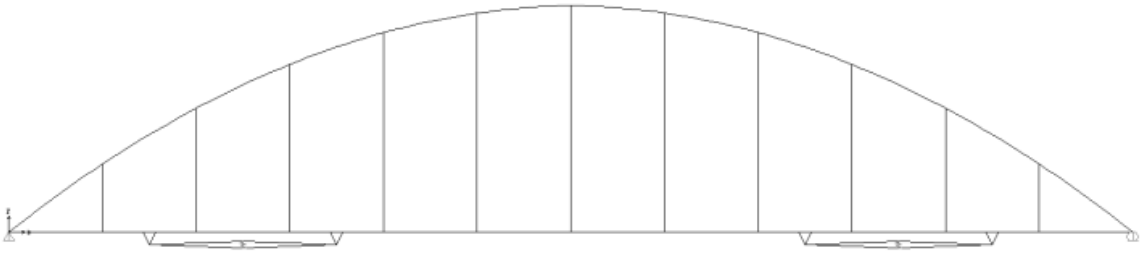

Figure 5.9 Cedar Avenue Bridge model with multiple RM apparatuses

5.2.1 Four RM Apparatuses

While RM apparatuses attached on one end of the bridge reduced moment ranges by over 40 percent, it is clear that due to the symmetric nature of the bridge moment envelope, moment range reduction at the joint on the opposite end also needs to take place so that the structure's service life is not limited by the other connection. Therefore, four RM apparatuses placed in two pairs on either end of the bridge would seem to be a natural extension of the previous work and may also further reduce deflections and moment ranges encountered by the bridge vulnerabilities.

Numerical analyses were completed using the 3D steel component numerical model in the finite element program SAP2000 and the moment ranges for the bridge structure with multiple response modification apparatuses with different geometric configurations was calculated. For comparison, the moment ranges were also computed for the Cedar Avenue Bridge with four PIA apparatuses, which lack a mechanical amplifier. The efficacy of the addition of multiple GWS apparatuses to reduce the stress ranges experienced by a detail for extending the fatigue life of the bridge is demonstrated in the results. As seen in Table 5.5, the deflections at the joint under consideration were reduced by 12 to 28 percent depending on the length and magnification factor of the GWS apparatus. In addition, the RM apparatus with the amplifier clearly outperforms a response modification apparatus alone which has length but no magnification value, *m*. It is interesting to note that, for overall deflection range reduction, doubling the length of the RM apparatus is more beneficial than doubling the magnification factor. Also, comparing the deflections in Table 5.5 for the model with multiple apparatuses to those in Table 5.5 for the simple model with RM apparatuses on one end shows much larger

reductions in deflection for the case with multiple RM apparatuses. The larger reductions in deflection are due to increased stiffness in the entire bridge when multiple RM apparatuses are attached thus causing less overall deflection at the joint under consideration. Again, the GWS apparatus outperforms the PIA apparatus with an identical RM device.

Table 5.5 Deflection ranges for the Cedar Avenue Bridge model not including the bridge deck with various apparatuses

Length (ft)	*m*	Deflection (in)							
		2 apparatuses				4 apparatuses			
		Max	Min	Range	% red	Max	Min	Range	% red
-	-	0.33	-0.54	0.88	-	0.29	-0.54	0.83	-
60	30	0.28	-0.41	0.69	21.1	0.22	-0.38	0.60	28.2
60	15	0.28	-0.43	0.71	19.2	0.23	-0.39	0.62	25.3
60	-	0.33	-0.54	0.87	0.7	0.28	-0.54	0.82	1.2
30	30	0.32	-0.47	0.79	10.2	0.26	-0.45	0.72	13.8
30	15	0.31	-0.48	0.79	9.9	0.26	-0.47	0.73	11.9
30	-	0.33	-0.54	0.87	0.2	0.28	-0.54	0.82	0.9

While the examination of deflections is interesting, more importantly the moment ranges at joint L3 were reduced by 34 to 42.5 percent (see Table 5.6) for the short RM apparatus with the small magnification factor and long RM apparatus with the large magnification factor respectively. It is clear that when the RM apparatus has a larger magnification value, *m*, better performance is achieved. Interestingly, in contrast to the deflection reduction results, when the RM apparatus is longer much smaller differences in the moment range are observed and it is seems that the magnification factor is also an important factor for moment range reduction. Doubling the length of the RM apparatus led to a 5 percent increase in moment reduction and doubling the magnification also led to a 5 percent increase in moment reduction. Although minor, for both the GWS apparatuses and the PIA apparatuses, the longer RM apparatuses do have slightly better performance due to the larger changes in rotation the further apart the attachment points are along the girder. In all cases, the GWS apparatuses significantly outperforms the PIA apparatus. Comparing the moment range reductions in Table 5.6 for the single pair of RM apparatuses model to the reductions for the multiple RM apparatuses model, it is

interesting to note that no large differences in moment range reduction are present which is quite different from the overall deflection comparison. Therefore, in terms of moment range reductions, the RM apparatuses are very localized in their effect, which means that an RM apparatus on one end of the bridge is not having a large effect on the stress range at a vulnerable connection on the other end of the bridge. However, to safely extend the service life of the bridge, it is still necessary to consider each localized vulnerable connection.

Table 5.6 Moment ranges for the Cedar Avenue Bridge model

Length (ft)	*m*	2 apparatuses					4 apparatuses				
		Moment (kip·in)			% red	Safe life increase (%)	Moment (kip·in)			% red	Safe life increase (%)
		Max	Min	Range			Max	Min	Range		
-	-	14300	-9296	23596	-	-	14150	-8498	22648	-	-
60	30	8352	-5272	13624	42.3	419.5	8036	-4985	13020	42.5	426.3
60	15	8928	-5628	14556	38.3	326.0	8588	-5252	13839	38.9	338.3
60	-	14100	-8884	22984	2.6	8.20	13899	-8208	22108	2.4	7.5
30	30	8725	-5850	14575	38.2	324.3	8557	-5174	13730	39.4	348.8
30	15	9533	-6283	15816	33.0	232.1	9371	-5610	14982	33.9	245.5
30	-	14140	-9012	23152	1.9	5.86	14109	-8264	22373	1.2	3.7

The moment envelope for the Cedar Avenue Bridge with multiple sets of GWS apparatuses is shown in Fig. 5.10. When this moment envelope is compared to that of the Cedar Avenue Bridge with no RM apparatuses (Fig. 5.11), the reduction in moment range between the attachment points of the RM apparatuses is quite apparent. Additionally, it is also obvious that multiple RM apparatuses decrease the moment range across other joints with initially large moment ranges as well.

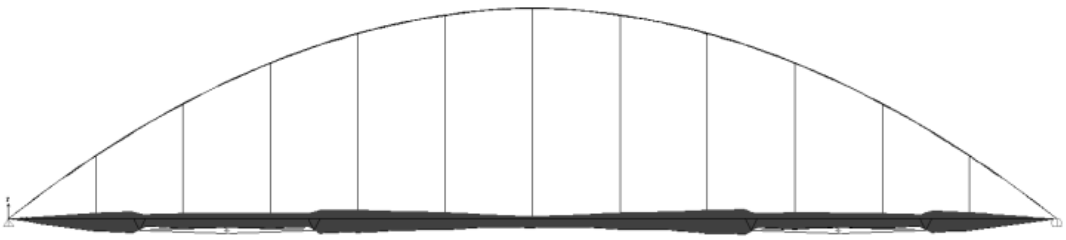

Figure 5.10 Moment envelope for Cedar Avenue Bridge with multiple apparatuses

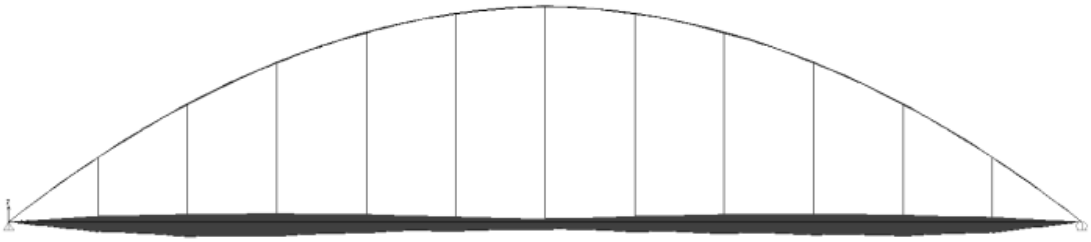

Figure 5.11 Moment envelope for Cedar Avenue Bridge with no modification

Using the moment range reductions at the considered joint in Table 5.6, the fatigue life extension of the particular connections can again be evaluated if the moment range is assumed to be proportional to the stress range experienced by the detail. Since the fatigue life is inversely proportional to the cube of the stress range, the 42.5 percent moment range reduction for the longer apparatus with larger magnification factor leads to a 426 percent increase in fatigue life. Currently, for the Cedar Avenue Bridge, the connection type does not fit into one of the categories defined by AASHTO and, for a thorough safe life analysis, stress concentration values would need to be further investigated. It would be necessary to do a refined analysis of each troublesome hanger to find exactly what stress concentrations will be seen in the vicinity of the problematic details, but this is outside the scope of this dissertation.

By assuming an original fatigue life for the Cedar Avenue Bridge joint under consideration of 50 years, bridge safe life extension can again be evaluated. Since the Cedar Avenue Bridge was built in 1979 making it 31 years old and assuming that the original safe life of the connection was 50 years, the remaining safe life for a 42.5 percent stress range reduction has been extended from 19 to 100 years meaning a safe life extension of 81 years for the connection under consideration. The results for the rest of the cases are given in Table 5.7.

Table 5.7 Remaining safe life for the Cedar Avenue Bridge with different RM apparatuses

Length (ft)	*m*	2 apparatuses			4 apparatuses		
		Safe life increase (%)	Remaining life (yr)	Safe life extension	Safe life increase (%)	Remaining life (yr)	Safe life extension
-	-	-	19	-	-	19	-
60	30	420.6	98.9	79.9	426.3	100.0	81.0
60	15	325.7	80.9	61.9	338.3	83.3	64.3
60	-	8.2	20.6	1.6	7.5	20.4	1.4
30	30	323.7	80.5	61.5	348.8	85.3	66.3
30	15	232.5	63.2	44.2	245.5	65.6	46.6
30	-	5.9	20.1	1.1	3.7	19.7	0.7

From the parameter study in this section, it can be seen that the use of multiple RM apparatuses greatly decreases overall deflections. Although the multiple RM apparatuses do not provide a large increase in overall moment range reduction at the vulnerable joints, it still increases the overall fatigue service life of the bridge by decreasing the moment range at other limiting vulnerable connections. It is also an indication that the moment reduction remains localized at the joint so that targeted moment reduction at specific vulnerabilities is the best approach. However, it is possible that other locations on the bridge actually limit the fatigue service life of the bridge and would need to be investigated. Additionally, it is also clear that the longer the length of the RM apparatus and the larger the magnification factor, *m*, the greater the safe life extension. However, it should also be noted that, while the RM apparatus theoretically extends the remaining life for up to 81 years, the components of the apparatus itself would need to last that long as well and would need to be evaluated. When the same RM device used in the GWS apparatus is used in the PIA apparatus, the safe life extension is barely increased. The RM apparatuses without mechanical amplification (PIA apparatus) would need a much larger RM device with larger stiffness and/or damping, to increase the safe life extension to the number of years calculated for the RM apparatus with mechanical amplification (GWS apparatus). In the end, judicious use of multiple response apparatuses at targeted vulnerabilities seems to achieve the best results for safe bridge life extension.

5.2.2 Flexible RM Apparatuses

While the use of the GWS apparatuses has been shown to increase safe life, this section will investigate the inclusion of flexibility in the RM apparatus members. Previous studies assumed that all RM apparatus members are rigid, an ideal case. Other characteristics previously explored using the rigid members including RM device stiffness, RM device damping, and scissor jack geometry will also be further investigated to evaluate the reduction in moment range at the potential vulnerabilities when flexibility of the members is considered. In addition to looking at the effects of these properties, both the bridge deck and structural damping were also added to the structure to ensure the robustness of the results.

To further study the apparatus geometry, three different RM apparatus were chosen each with the same magnification value of 30. The varying lengths, $2l_0$, l_0, and $l_0/2$, were based on the distance l_0 between two joints on the Cedar Avenue Bridge. These lengths are given in Table 5.8 with the sizes and stiffness of the members within the RM apparatus that will be in axial tension and compression shown. Analyses were carried out for models using the three different geometries with and without structural damping as well as using various cross-sectional areas for the axial members. Results are given in Tables 5.9-5.14 for the three different RM apparatus configurations, with and without damping. The results from the tables are summarized in Fig. 5.12 and Fig. 5.13. For the majority of cases, damping in the superstructure seemed to only have a small effect on performance of the RM apparatuses. It is interesting to note that the most significant factor determining the performance of the RM apparatus is the cross-sectional area of the members since the previous analyses assumed ideally rigid members being placed in the scissor jack for simplicity. The rigid RM apparatuses are the absolute maximum performance that can be achieved. The RM apparatuses with the largest cross-sectional area would still need much more area to approach the performance of the rigid RM apparatus. It is again confirmed that the larger the RM apparatus, meaning the attachment points are further apart, the better the performance will be. Although the shorter length RM apparatuses have larger member stiffnesses due to their shorter

member lengths, the longer RM apparatuses still performed better. Lastly, the GWS apparatuses vastly outperformed the PIA apparatuses with identical RM devices.

Table 5.8 Apparatus member sizes, lengths, and stiffnesses

Apparatus length	Leg length (in)	Jack length (in)	Leg stiffness/area (kip/in^3)
Short	89.55	179	323.8
Medium	179.35	358.5	161.7
Long	358.70	717	80.85

Table 5.9 Moment ranges at L3 connection for long apparatuses without damping

Apparatus members	Area (in^2)	Leg stiffness (kip/in)	Range (kip·in)	Maximum (kip·in)	Minimum (kip·in)	Reduction (%)	Safe life increase (%)
None	-	-	22766	14220	-8546	-	-
Rigid	-	Infinite	13500	8281	-5219	40.7	379.6
W4x13	3.83	309.6	22271	13990	-8281	2.17	6.8
W8x35	10.3	832.7	21477	13540	-7937	5.66	19.1
W8x67	19.7	1592.7	20585	13000	-7585	9.58	35.3
W12x120	35.3	2853.9	19555	12330	-7225	14.1	57.8
W14x145	42.7	3452.2	19169	12120	-7049	15.8	67.5

Table 5.10 Moment ranges at L3 connection for long apparatuses with damping

Apparatus members	Area (in^2)	Leg stiffness (kip/in)	Range (kip·in)	Maximum (kip·in)	Minimum (kip·in)	Reduction (%)	Safe life increase (%)
None	-	-	21608	13800	-7808	-	-
Rigid	-	Infinite	12301	7837	-4464	43.1	442.0
W4x13	3.83	309.6	21137	13510	-7627	2.18	6.8
W8x35	10.3	832.7	20434	13070	-7364	5.43	18.2
W8x67	19.7	1592.7	19584	12540	-7044	9.37	34.3
W12x120	35.3	2853.9	18492	11850	-6642	14.4	59.5
W14x145	42.7	3452.2	18068	11580	-6488	16.4	71.0

Table 5.11 Moment ranges at joint L3 for medium apparatuses without damping

Apparatus members	Area (in^2)	Leg stiffness (kip/in)	Range (kip·in)	Maximum (kip·in)	Minimum (kip·in)	Reduction (%)	Safe life increase (%)
None	-	-	22766	14220	-8546	-	-
Rigid	-	Infinite	13707	8627	-5080	39.8	358.2
W4x13	3.83	309.6	22354	13960	-8394	1.81	5.6
W8x35	10.3	832.7	21798	13620	-8178	4.25	13.9
W8x67	19.7	1592.7	21079	13160	-7919	7.41	26.0
W12x120	35.3	2853.9	20187	12600	-7587	11.3	43.4
W14x145	42.7	3452.2	19821	12370	-7451	12.9	51.5

Table 5.12 Moment ranges at L3 connection for medium apparatuses with damping

Apparatus members	Area (in^2)	Leg stiffness (kip/in)	Range (kip·in)	Maximum (kip·in)	Minimum (kip·in)	Reduction (%)	Safe life increase (%)
None	-	-	21608	13800	-7808	-	-
Rigid	-	Infinite	13240	8392	-4848	38.7	334.7
W4x13	3.83	309.6	21266	13570	-7696	1.58	4.9
W8x35	10.3	832.7	20737	13230	-7507	4.03	13.1
W8x67	19.7	1592.7	20076	12800	-7276	7.09	24.7
W12x120	35.3	2853.9	19204	12230	-6974	11.1	42.5
W14x145	42.7	3452.2	18866	12010	-6856	12.7	50.2

Table 5.13 Moment ranges at L3 connection for short apparatuses without damping

Apparatus members	Area (in^2)	Leg stiffness (kip/in)	Range (kip·in)	Maximum (kip·in)	Minimum (kip·in)	Reduction (%)	Safe life increase (%)
None	-	-	22766	14220	-8546	-	-
Rigid	-	Infinite	15388	9562	-5826	32.4	223.8
W4x13	3.83	309.6	22446	14000	-8446	1.40	4.3
W8x35	10.3	832.7	22100	13760	-8340	2.93	9.3
W8x67	19.7	1592.7	21613	13450	-8163	5.06	16.9
W12x120	35.3	2853.9	20945	13000	-7945	8.00	28.4
W14x145	42.7	3452.2	20660	12830	-7830	9.25	33.8

Table 5.14 Moment ranges at L3 connection for short apparatuses with damping

Apparatus members	Area (in^2)	Leg stiffness (kip/in)	Range (kip·in)	Maximum (kip·in)	Minimum (kip·in)	Reduction (%)	Safe life increase (%)
None	-	-	21608	13800	-7808	-	-
Rigid	-	Infinite	14941	9383	-5558	30.9	202.5
W4x13	3.83	309.6	21379	13640	-7739	1.06	3.2
W8x35	10.3	832.7	21021	13400	-7621	2.72	8.6
W8x67	19.7	1592.7	20569	13100	-7469	4.81	15.9
W12x120	35.3	2853.9	19942	12680	-7262	7.71	27.2
W14x145	42.7	3452.2	19679	12500	-7179	8.93	32.4

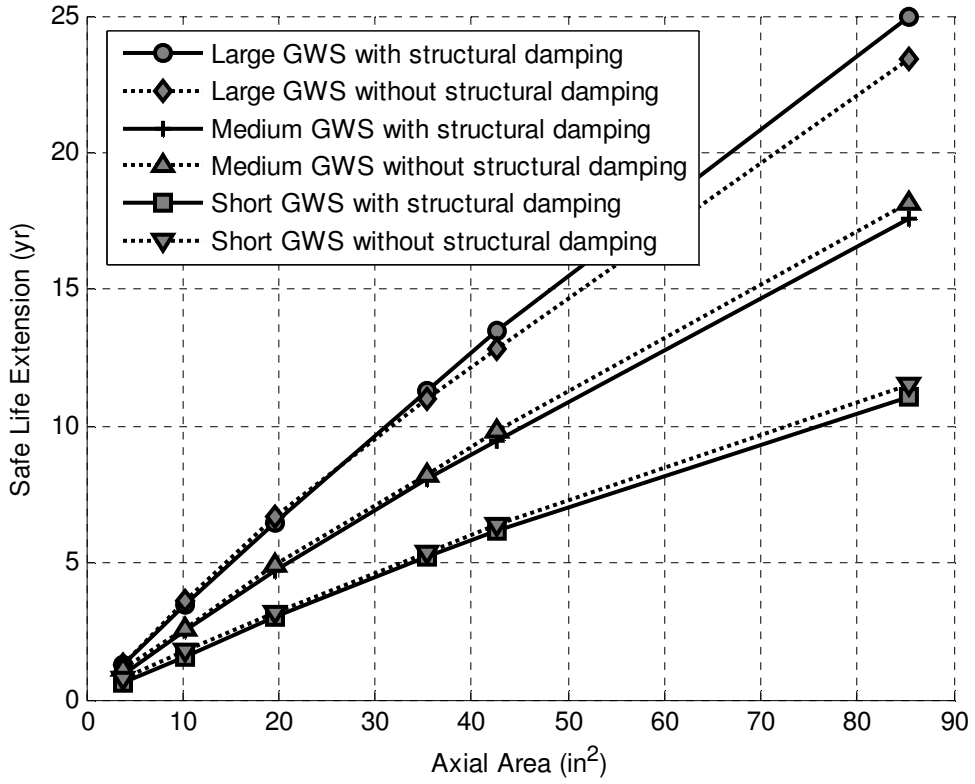

Figure 5.12 Safe life extension for varying lengths of GWS apparatuses and member axial area for the Cedar Avenue Bridge with and without structural damping

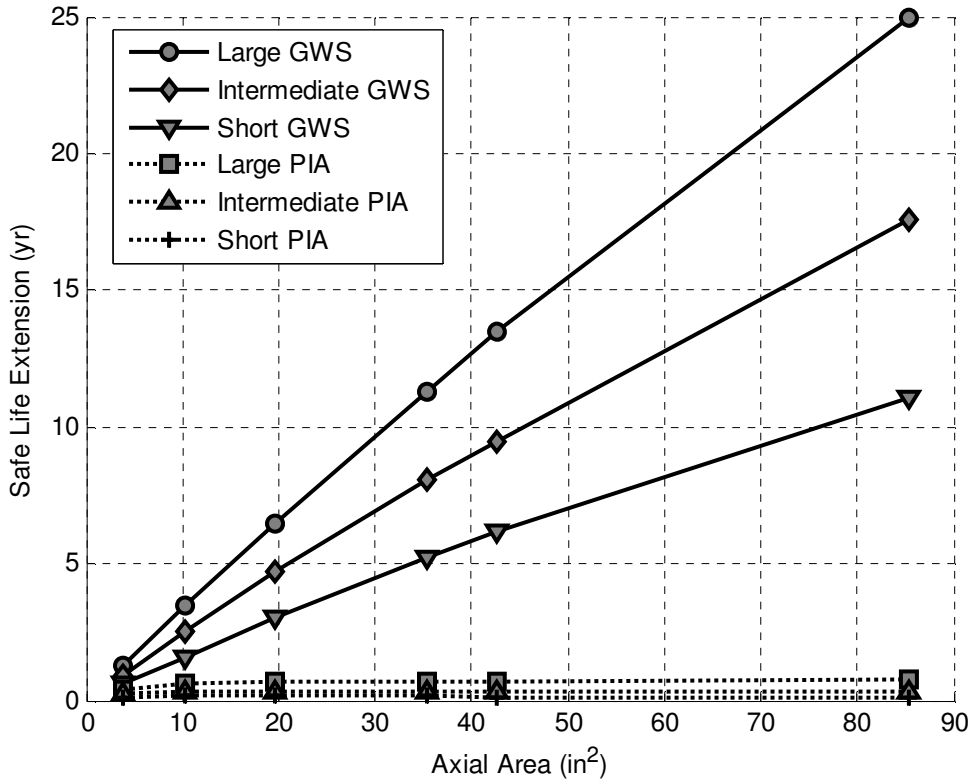

Figure 5.13 Safe life extension for varying lengths of RM apparatuses and member axial area for the Cedar Avenue Bridge

Table 5.15 shows the effect of different stiffness and damping properties of the RM device. It can be seen that changing one or the other by a factor of 100 has a slight effect on the overall performance and increasing both by a factor of 100 has about the same effect as just one. This confirms the previous assertion that the stiffness of the members (mainly the area) and the size of the RM apparatus (the distance between attachment points) has the largest effect on the performance of the GWS apparatus. To fully investigate these RM apparatuses, the cost of the materials should be taken into account; RM apparatus members with larger cross-sectional area have increased cost for the steel. Table 5.16 shows one possible way to compare the costs of the different GWS apparatuses. It can be seen that the weight of steel divided by the amount of moment reduction is the lowest for the short RM apparatus using the W4x13 section and therefore most cost effective for a percent reduction. However, depending on the specific nature of

the bridge vulnerability in detail, it may be necessary to use a configuration with higher cost to provide more moment reduction such as the short apparatus using the W14x145 sections. Since safe life extension is the ultimate goal and not overall moment reduction, Table 5.17 shows perhaps a better way to compare the costs of the different GWS apparatuses. The weight of the steel divided by the amount of safe life extension is still best for the smallest RM apparatus with the smallest members, but the other member sizes are much closer in relative difference.

Table 5.15 Moment ranges at L3 connection for various device parameters

Apparatus members	Area (in^2)	Device stiffness (kip/in)	Device damping (kip·s/in)	Range (kip·in)	Maximum (kip·in)	Minimum (kip·in)	Reduction (%)	Safe life increase (%)
None	-	-		22766	14220	-8546	-	-
Rigid	-	110	3	15388	9562	-5826	32.4	223.8
W14x145	42.7	110	3	20660	12830	-7830	9.25	33.8
W14x145	42.7	11000	3	20602	12790	-7812	9.51	34.9
W14x145	42.7	110	300	20608	12800	-7808	9.48	34.8
W14x145	42.7	11000	300	20602	12790	-7812	9.51	34.9

Table 5.16 Comparison of cost per percent reduction for different RM apparatus characteristics

Apparatus length	Pounds / percent reduction				
	W4x13	W8x35	W8x67	W12x120	W14x145
Long	766.4	827.9	919.2	1069.4	1137.4
Medium	564.5	596.8	649.5	741.3	785.3
Short	475.9	499.8	540.6	603.8	630.1

Table 5.17 Comparison of cost per percent life extension for different RM apparatus characteristics

Apparatus length	Pounds/ percent life extension				
	W4x13	W8x35	W8x67	W12x120	W14x145
Long	244.4	246.6	250.9	259.1	262.2
Medium	182.3	183.1	186.6	194.4	198.3
Short	155.3	157.6	163.1	171.1	173.7

From the analyses performed in this section, it seems that the most important characteristic of the RM apparatus is the member cross-sectional area followed by the overall length between the attachment points of the RM apparatus. Additionally, the smallest sized RM apparatuses seem to be the most cost effective but would need to be analyzed on a case by case basis to verify that they provide adequate lifetime extension.

5.2.3 Varying Truck Speeds

To study the effect of varying truck speeds, a reduced order model was utilized. The reduced order model used in this section was slightly different than the more comprehensive one described in the modeling section. Since member flexibility was not being investigated, all RM apparatus members were modeled as rigid for this simpler reduced order model and the model only used the first 13 vertical modes (no additional static load modes). The simpler reduced order model was sufficient for capturing the effects of changes in truck loading speed, but was not capable of capturing changes in flexibility of the RM apparatus members or changes in RM device characteristics. The model maintained the base RM device characteristics of 110 kip/in and 3 kip·s/in for stiffness and damping respectively. Truck speeds were varied from 12 mph up to 92 mph. Analyses were run for a total of 15 seconds to allow the slowest trucks time to cross the bridge. Fig. 5.14 shows the moment at the vulnerable joint L3W for a given time history for a selection of truck speeds.

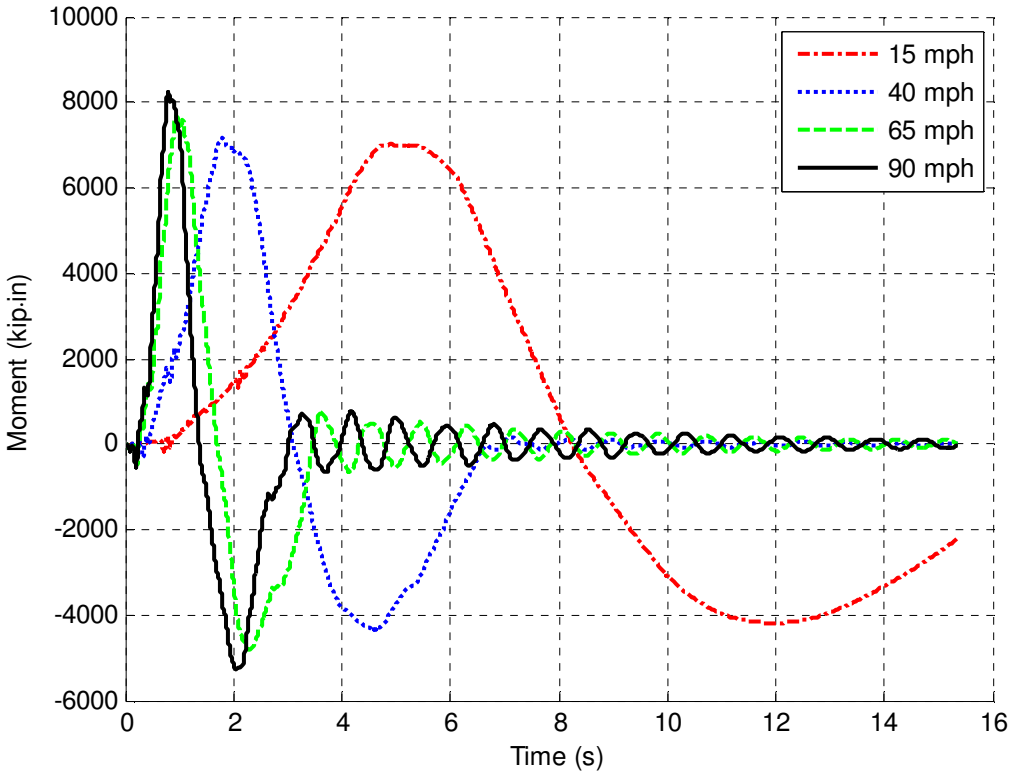

Figure 5.14 Moment time history at joint L3W for various truck speeds

Notice that the moment starts positive when the load is near the vulnerable joint and turns negative as the load crosses the bridge and reaches the opposite symmetric joint. The results show that increased response can occur at faster truck speeds. Fig. 5.15 shows the general trend toward increases in both the maximum moment and minimum moment for higher truck speeds. However, when the maximum and minimum are combined for overall moment range, Fig. 5.16 shows there is more variation in the results. From the smallest moment range at 15 mph to the largest moment range at 92 mph there is a 21 percent increase. This trend is similar to the results obtained by Fryba (1999) for a simple beam subjected to a moving sprung mass (a mass on a spring). The general trend is increased response for increased speed, but local peaks exist within the trend. Fryba (1999) uses a more complicated loading model, which includes the interaction of the stiffness of the vehicle. Neglecting this interaction means that some

bridge vehicle dynamics are lost and load amplification is possibly being missed in these simulations. Additionally, Fryba (1999) poses a critical speed for simple beams such that

$$c_{cr} = \frac{2f_{(j)}l}{j} \tag{4.2}$$

where $f_{(j)}$ is the jth natural frequency of the beam and l is the length of the beam. For the bridge structure, the stiffer floor beams can act like a support as can other stiffer components. Table 5.18 shows some possible critical speeds for the first two fundamental frequencies for varying support lengths. These lengths correspond to: (1) support points for the bridge deck, (2) distance between floor beams, (3) length of the bridge. Due to the flexible nature of long span bridges, these speeds fall well within the realm of typical highway truck speeds.

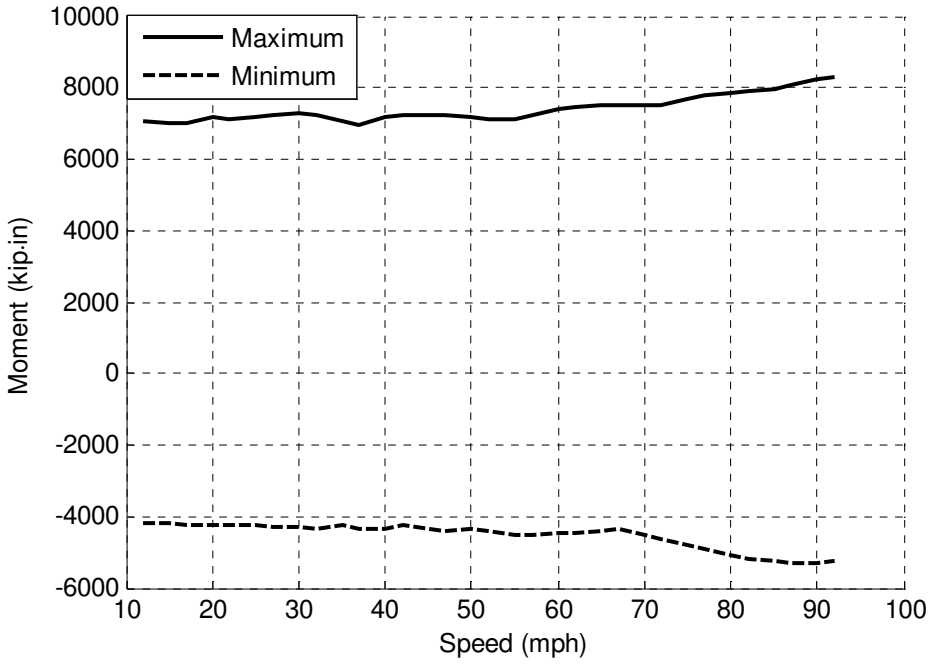

Figure 5.15 Moment envelope at joint L3W for various truck speeds

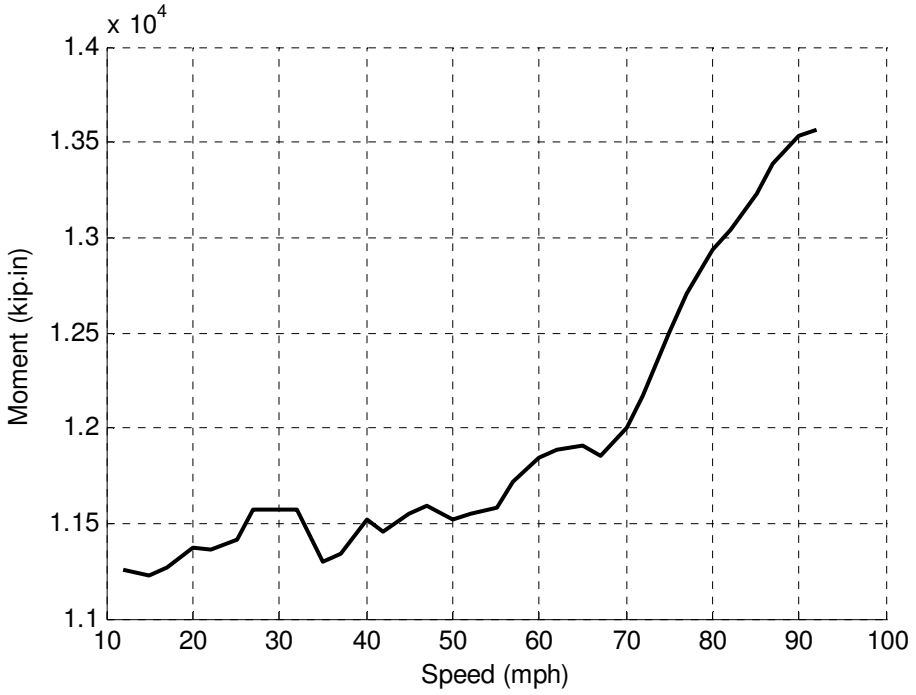

Figure 5.16 Moment range at joint L3W for various truck speeds

Table 5.18 Critical speeds for a moving sprung mass on a simple beam

Frequency (cyc/s)	Length (in)	Critical speed (mph)
1.64	44.8	8.35
1.64	358.5	66.8
1.64	4302	802
2.26	44.8	5.75
2.26	358.5	46.0
2.26	4302	552

Overall, the results from these different parameter studies have led to a better understanding of the advantages and challenges of using the GWS apparatus as a way to safely extend bridge life. The initial parameter studies utilizing a single pair of RM apparatuses on one end of the Cedar Avenue Bridge showed that both length and magnification have a large effect on GWS apparatus performance. Wider and shallower GWS apparatuses have better performance than narrower and taller apparatuses utilizing identical RM devices. Larger RM device characteristics are helpful for PIA apparatus performance, but only provide minimal performance increases for GWS apparatuses.

Adding the bridge deck and damping to the numerical models had little effect on overall performance. An additional set of RM apparatuses added to the other end of the Cedar Avenue Bridge provided significant reductions in displacement at the L3W vulnerable joint, but minimal increase in performance in terms of moment range reduction; the GWS apparatus provides very localized moment reduction. Member flexibility had a very large effect on overall moment range reduction. Large member cross sections are necessary to approach rigid RM apparatus member performance. Finally, truck speed studies showed that amplification can occur at specific loading speeds. In general, the faster the truck speed, the larger the amplification; however, some variability of maximum and minimum moment ranges was experienced within the general trend. While the investigation of changes in RM device characteristics, RM apparatus characteristics, member flexibility, and truck loading speed has provided insight into the approach, ultimately an optimized solution will be the most beneficial for safe life extension.

Chapter 6: Response Modification Apparatus Optimization

The previous parameter studies provided insight into the abilities of the GWS apparatuses for the safe extension of bridge life. However, the RM apparatus characteristics were never optimized to provide the best performance. This section explores the optimization of passive RM apparatuses to achieve specific design goals for a single truck crossing the Cedar Avenue Bridge as well as for five trucks crossing the bridge in succession. The optimization studies were carried out using the reduced order model comprised of vertical modes and static load modes of the final Cedar Avenue Bridge numerical model described in section 4.2.5. The optimization of RM apparatus characteristics was completed for the GWS apparatus as well as the PIA apparatus for comparison.

6.1 Single Truck Loading

The design optimization of the RM apparatuses was carried out using the optimization and uncertainty quantification software DAKOTA (Adams et al. 2009) interfaced with the reduced order numerical model of the Cedar Avenue Bridge in MATLAB. The numerical bridge model was subjected to a truck loading consisting of a single fatigue truck for a duration of 5.12 seconds traveling at 1144 in/s (65 mph). The truck takes 4.22 seconds to fully cross the bridge. The loading for the reduced order model is slightly different than for the full order model in SAP2000 as explained in the reduced order model section. Instead of using two point loads for each axle only one is utilized to simplify the loading.

In formulating the design optimization problems, bounds on the design characteristics were first chosen. The area of members was limited to a selection from the W12 family of wide flange sections. The maximum member size was chosen to be the largest

member providing less than 25 percent of the 288.5 in^2 axial area of the box girder, 67.7 in^2. The minimum was chosen to be the smallest W12 cross section, 11.7 in^2; a representative sample was taken for the areas in between and the range of options is shown in Table 6.1.

Table 6.1 Available wide flange sections for optimizations

Section	W12x40	W12x58	W12x87	W12x120	W12x152	W12x190	W12x230
Area (in^2)	11.7	17	25.6	35.2	44.7	55.8	67.7

For the RM device characteristics, the coefficients for stiffness and damping were allowed to be greater than or equal to zero. Since damping and stiffness coefficients can vary widely for different RM devices, no explicit upper bounds were placed on these coefficients; instead, the maximum force that the RM device can provide was limited to 2.5 tons, implicitly restricting the maximum RM device damping and stiffness coefficients. The value of 2.5 tons was chosen to achieve the goal of a small RM device. Lastly, a buckling force limit was placed on the compression members, but this constraint was found to be never active during optimizations. Moment ranges at joints L3W, L6W, and L3W' were used as outputs to compare the RM apparatus modified structures to the bridge without response modification; the baseline moment range used for optimization at the unmodified vulnerable joint L3W was equal to 20,653 kip·in. Prior to the formulation of the optimization problems, a brief parameter study of RM device stiffness and damping was carried out to gain insight into what the optimal characteristics may be. Fig. 6.1 displays the variation of the moment range for select values of RM device stiffness and damping for a pair of GWS apparatuses applied to both ends of the Cedar Avenue Bridge numerical model. While difficult to discern in the figure, the Cedar Avenue Bridge modified with the GWS apparatus performs best when RM device stiffness is zero and damping is nonzero.

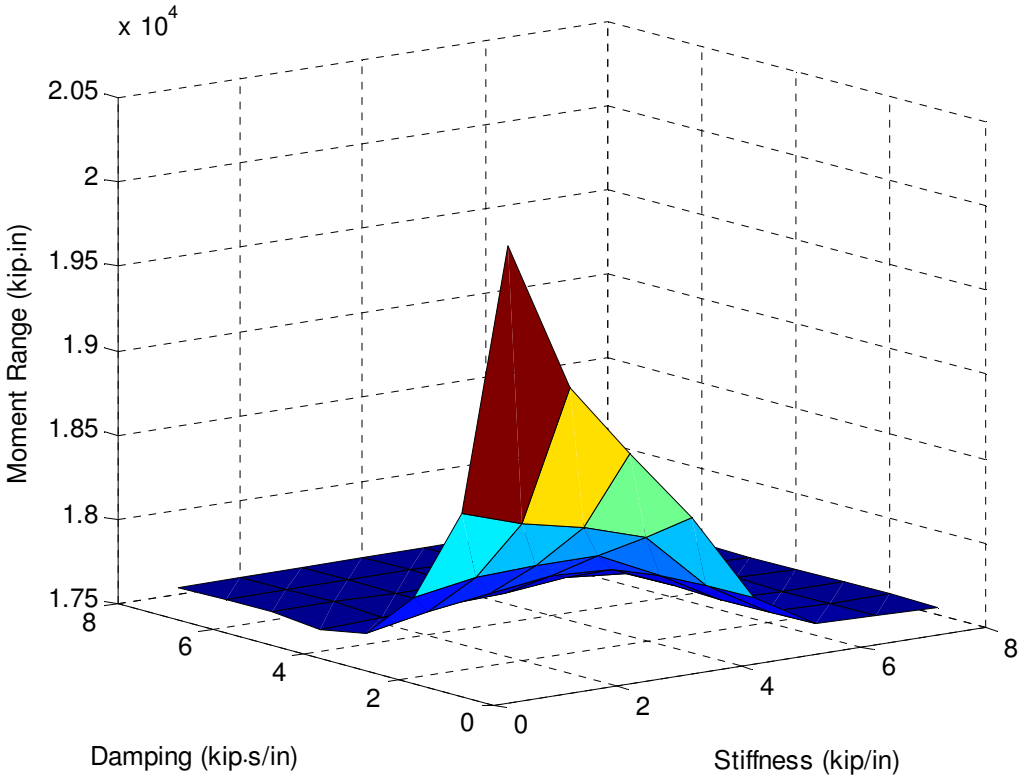

Figure 6.1 Moment range for given values of stiffness and damping (GWS)

Two constrained design optimization problems were formulated to compare performance of the optimized GWS and PIA apparatuses. The first optimization formulation sought to minimize the moment range (maximize safe life) at L3W for a fixed RM apparatuses member axial area while varying both the RM device damping and stiffness coefficients. The minimization was subjected to the 2.5 ton RM device force constraint and the buckling force constraint. The only constraint that was active during optimizations was the 2.5 ton RM device constraint when testing the PIA apparatuses. Tables 6.2 and 6.3 show the results for both the GWS and PIA apparatuses respectively. For the GWS apparatus, optimal RM device stiffness was always zero and larger member axial area resulted in larger optimal damping values, and, as expected, larger safe life

increases. Fig. 6.2 shows a quadratic relationship between the area and the optimal damping values for the GWS apparatus. Conversely, for the PIA apparatus, larger member area resulted in smaller optimal RM device stiffness and damping and slightly smaller safe life increases. Fig. 6.3 shows an inverse quadratic relationship for the area and the optimal damping values for the PIA. This trend is most likely due to the force limitation placed on the RM device, as it was active in all PIA apparatus optimizations. Also, due to the force limitation of the RM device, the GWS apparatus vastly outperforms the PIA apparatus for safe life extension.

Table 6.2 Optimal GWS apparatus RM device damping and stiffness characteristics for a given member cross-section

W12x	Area (in^2)	c (kip·s/in)	k (kip/in)	F_{device} (kip)	Moment range (kip·in)	Reduction (kip·in)	Reduction (%)	Safe life increase (%)
40	11.7	4.0	0	0.55	19519	1134.2	5.5	18.5
58	17	5.4	0	0.77	18934	1719.4	8.3	29.8
87	25.6	7.7	0	1.1	18172	2481.1	12.0	46.8
120	35.2	10	0	1.4	17525	3128.4	15.2	63.7
152	44.7	12	0	1.6	16995	3657.5	17.7	79.4
190	55.8	76	0	2.0	16531	4122.4	20.0	95.0
230	67.7	200	0	2.2	16142	4511.2	21.8	109.5

Table 6.3 Table 2 Optimal PIA apparatus RM device damping and stiffness characteristics for a given member cross-section

W12x	Area (in^2)	c (kip·s/in)	k (kip/in)	F_{device} (kip)	Moment range (kip·in)	Reduction (kip·in)	Reduction (%)	Safe life increase (%)
40	11.7	72	20	5.0	20398	254.8	1.23	3.8
58	17	67	15	5.0	20443	210.0	1.02	3.1
87	25.6	63	13	5.0	20484	169.5	0.82	2.5
120	35.2	62	8	5.0	20512	141.1	0.68	2.1
152	44.7	61	7	5.0	20526	127.1	0.62	1.9
190	55.8	61	4	5.0	20539	113.5	0.55	1.7
230	67.7	60	5	5.0	20545	108.2	0.52	1.6

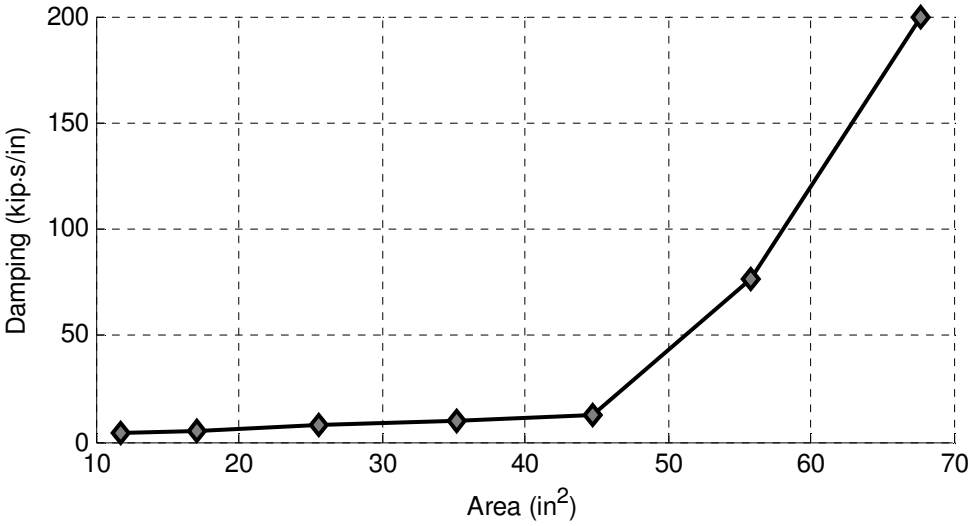

Figure 6.2 Optimal RM device damping for maximal safe life for a given member area for the GWS apparatus

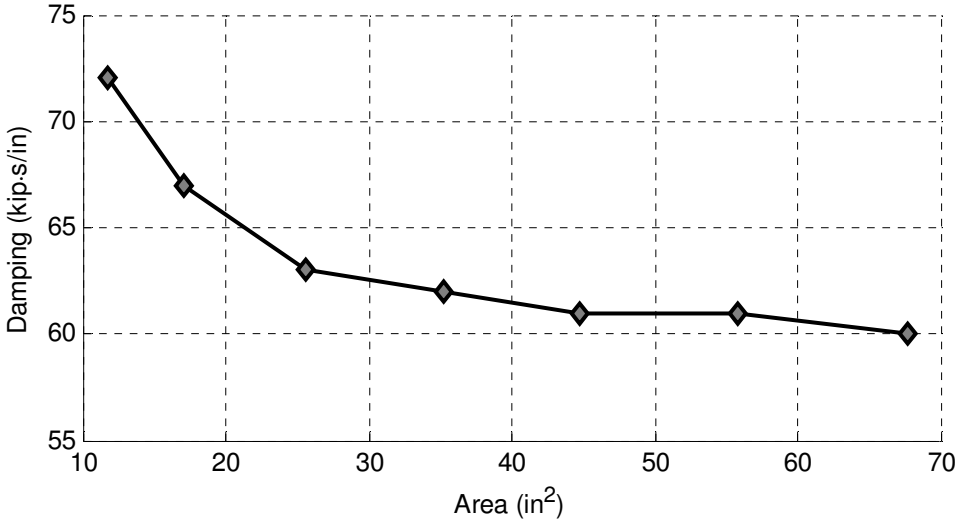

Figure 6.3 Optimal RM device damping for maximal safe life for a given member area for the PIA apparatus

If the force limitation is relaxed, Table 6.4 shows the optimal PIA characteristics for varying maximum levels of RM device forces. To achieve the same life extension for the optimized W12x120 GWS apparatus, the PIA apparatus would require a RM device with a force capability of over 40 kip and damping coefficient of over 3,709 kip·s/in. The maximum RM device force for the GWS apparatus was only 1.4 kip and the damping coefficient was 10.1 kip·s/in. Since large RM devices are generally more expensive, may not fit the apparatus properly, and would add more weight to the bridge, minimizing the size of the RM device available to the GWS apparatus is desirable. Additionally, while 20-ton MR dampers have been investigated, these devices have been characterized with damping coefficients significantly smaller than 3700 kip·s/in (Yang et al. 2004).

Table 6.4 Optimal PIA damping and stiffness for a given area and a varying device force constraint

RM device force max (kip)	Area (in^2)	c (kip·s/in)	k (kip/in)	Moment range (kip·in)	Reduction (kip·in)	Reduction (%)	Safe life increase (%)
10	35.2	145	5	20193.7	459.3	2.2	6.98
20	35.2	398	7	19560.4	1092.6	5.3	17.71
30	35.2	930	5	18621.8	2031.2	9.8	36.42
40	35.2	3710	0	17557.1	3095.9	15.0	62.78

The second optimization formulation sought to minimize the cross-sectional area of the RM apparatus members to minimize the weight of the RM apparatus while still maintaining a desired safe life increase. The design variables considered consisted of the cross-sectional area of the RM apparatus members and RM device damping (optimal RM device stiffness is zero). The minimization was subject to the two previous constraints on maximum RM device force and buckling load with an additional equality constraint fixing the desired percent safe life extension. The optimization was repeated for eight different levels of safe life extension for only the GWS apparatus as the PIA apparatus was unable to attain these safe life increases for any choice of RM apparatus characteristics when limited to the 5 kip RM device force limitation. Table 6.5 summarizes the RM apparatus characteristics resulting from these eight optimizations.

Table 6.5 Optimal GWS damping, stiffness, and member cross section for a given safe life requirement

Safe life increase	Area (in^2)	c (kip·s/in)	k (kip/in)	Moment range (kip·in)	Reduction (kip·in)	Reduction (%)
30%	17.54	2.62	0	18923.5	1729.5	8.37
40%	22.32	3.25	0	18461.7	2191.3	10.61
50%	27.74	3.62	0	18042.0	2611.0	12.64
60%	33.08	9.40	0	17658.0	2995.0	14.50
70%	38.90	11.1	0	17304.8	3348.2	16.21
80%	45.04	12.4	0	16978.2	3674.8	17.79
90%	52.16	21.5	0	16675.0	3978.0	19.26
100%	60.17	45.8	0	16392.3	4260.7	20.63

To achieve higher safe life values, increases in both damping and area are optimal. Fig. 6.4 displays the variation in the optimal axial area for a given safe life increase. It seems that safe life increase varies linearly with an increase in cross-sectional area. However, as was seen in the parameter studies, the rigid RM apparatus members provide a limit to the overall performance. At some point these values would start to level off and reach the maximum value achieved by rigid RM apparatus members.

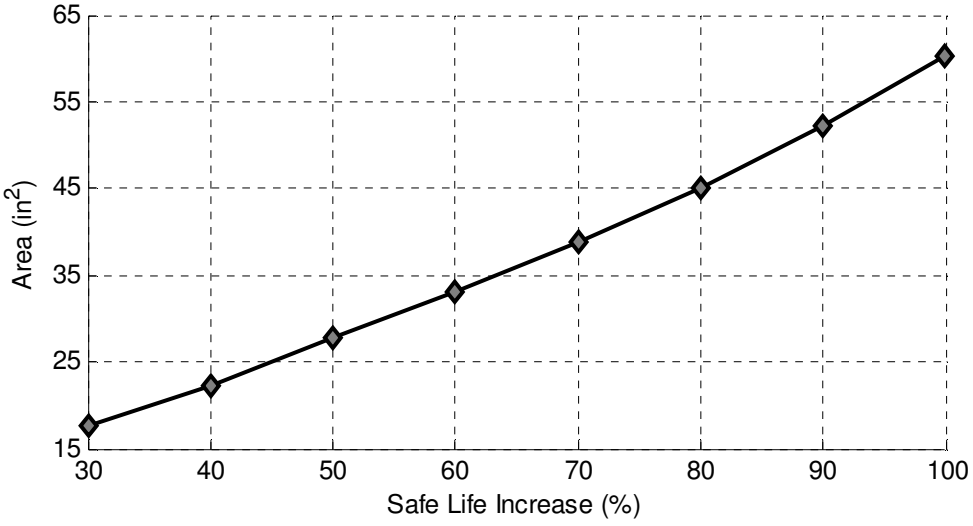

Figure 6.4 Optimal area for GWS apparatus members for a given safe life

In addition to optimizing the cross-sectional area and the RM device characteristics for overall moment range, optimizations of RM apparatus characteristics for the maximum moment and the minimum moment separately may provide further insight into the GWS apparatus approach. Since the minimum moment is achieved when the truck is not directly over the vulnerable joint L3W, it may be beneficial to employ different RM device characteristics than those optimal for when the truck load is directly over the vulnerable joint. The optimizations were formulated identically to the previous optimizations for given member cross-sectional areas except, now instead of total moment range, maximum moment and minimum moment are considered separately. The optimization formulations sought to minimize the maximum moment or minimize the absolute value of the negative moment for a fixed member axial area while varying both the RM device damping and stiffness. The minimizations were subjected to the 2.5 ton RM device force constraint and the buckling force constraint (neither was active). Tables 6.6 and 6.7 show the results for the GWS apparatuses for minimum and maximum moment respectively. The initial minimum moment at joint L3W was -7493 kip·in and reductions up to 24 percent were achieved. The initial maximum moment at joint L3W was 13160 kip·in and reductions up to 22 percent were achieved. Interestingly, the minimum moment optimizations required small damping coefficients with no stiffness for the optimal RM device. Conversely, the maximum moment optimizations required larger damping coefficients with some stiffness for the optimal RM device. Table 6.8 compares the maximum moment, minimum moment, and overall moment range optimums. The overall moment range optimums lie in between the maximum and minimum optimums. This leads to the conclusion that *a RM device which can change properties depending on the location of the moving load may be advantageous*. Instead of the 21.8 percent reduction achieved for the total moment range optimization it may be possible to get closer to the 24 percent reduction achieved for the minimum moment optimization.

Table 6.6 Optimal GWS apparatus RM device damping and stiffness characteristics for minimum moment

W12x	Area (in^2)	c (kip·s/in)	k (kip/in)	F_{device} (kip)	Moment (kip·in)	Reduction (kip·in)	Reduction (%)	Safe life increase (%)
40	11.7	1.06	0	0.44	-6935	558.4	7.45	26.2
58	17	1.47	0	0.63	-6646	846.6	11.3	43.3
87	25.6	2.12	0	0.91	-6292	1200	16.0	68.8
120	35.2	3.16	0	1.2	-6019	1474	19.7	93.0
152	44.7	6.59	0	1.5	-5895	1598	21.3	105
190	55.8	7.36	0	1.8	-5801	1692	22.6	115
230	67.7	8.14	0	2.0	-5687	1806	24.1	129

Table 6.7 Optimal GWS apparatus RM device damping and stiffness characteristics for maximum moment

W12x	Area (in^2)	c (kip·s/in)	k (kip/in)	F_{device} (kip)	Moment (kip·in)	Reduction (kip·in)	Reduction (%)	Safe life increase (%)
40	11.7	215.5	29.5	0.62	12501	659.4	5.01	16.7
58	17	294.75	34.75	0.85	12168	992.0	7.54	26.5
87	25.6	396.5	62.25	1.2	11713	1447	11.0	41.8
120	35.2	501.5	203.25	1.5	11300	1860	14.1	58.0
152	44.7	569.75	210.25	1.8	10948	2212	16.8	73.7
190	55.8	664.25	220	2.0	10602	2558	19.4	91.3
230	67.7	818	244.75	2.3	10305	2855	21.7	108

Table 6.8 Summary of optimal characteristics

W12x	Area (in^2)	Maximum moment		Minimum moment		Moment range	
		c (kip·s/in)	k (kip/in)	c (kip·s/in)	k (kip/in)	c (kip·s/in)	k (kip/in)
40	11.7	215.5	29.5	1.06	0	4.0	0
58	17	294.75	34.75	1.47	0	5.4	0
87	25.6	396.5	62.25	2.12	0	7.7	0
120	35.2	501.5	203.25	3.16	0	10	0
152	44.7	569.75	210.25	6.59	0	12	0
190	55.8	664.25	220	7.36	0	76	0
230	67.7	818	244.75	8.14	0	200	0

6.2 Multiple Truck Loading

While the optimization of the GWS apparatus' performance to a single truck loading scenario is instructive, a situation where multiple trucks are loading the bridge in succession would cause much larger moment ranges at the vulnerable connections and may excite different bridge vehicle dynamics. To study this phenomenon, a modified loading scheme of five trucks driving across the bridge was implemented. Each fatigue truck was traveling 65 mph and followed the preceding truck at exactly one truck length (44 feet). The analyses were conducted for 7 seconds to allow all trucks to exit the bridge. Table 6.9 and 6.10 show the results for the GWS apparatuses for a given cross-sectional area and a given safe life respectively. Similar safe life reduction and RM device damping and stiffness coefficients trends were seen for the multiple truck loading scenario as the single truck scenario. Small RM device damping coefficients and zero stiffness coefficients were observed. As axial area increased, optimal RM device damping coefficients generally increased as well. Due to the much larger loads, larger cross-sectional areas for the multiple truck scenario than for the single truck loading were necessary for similar safe life increase.

Table 6.9 Optimal GWS apparatus RM device damping and stiffness characteristics for a given member cross section with multiple truck loading

W12x	Area (in^2)	c (kip·s/in)	k (kip/in)	F_{device} (kip)	Moment range (kip·in)	Reduction (kip·in)	Reduction (%)	Safe life increase (%)
40	11.7	13.0	0	0.63	24124	1076.1	4.3	14.0
58	17	11.0	0	0.85	23472	1728.5	6.9	23.8
87	25.6	15.3	0	1.2	22535	2664.9	10.6	39.8
120	35.2	16.0	0	1.5	21781	3419.3	13.6	54.9
152	44.7	18.6	0	1.7	21172	4038.0	16.0	68.9
190	55.8	20.7	0	2.0	20539	4661.4	18.5	84.7
230	67.7	19.5	0	2.2	20139	5061.1	20.1	95.9

Table 6.10 Optimal GWS damping, stiffness, and member cross section for a given safe life requirement with multiple truck loading

Safe life increase	Area (in^2)	c (kip·s/in)	k (kip/in)	Moment range (kip·in)	Reduction (kip·in)	Reduction (%)
30%	20.7	5.5	0	23090	2110.2	8.37
40%	26.2	6.7	0	22526	2673.6	10.61
50%	32.1	10.8	0	22014	3185.8	12.64
60%	39.0	17.1	0	21546	3654.3	14.50
70%	45.4	18.7	0	21115	4085.4	16.21
80%	52.5	20.0	0	20716	4483.8	17.79
90%	59.7	18.6	0	20346	4853.8	19.26
100%	71.1	20.3	0	20001	5198.7	20.63

Fig. 6.5 and Fig. 6.6 compare the optimal RM apparatus characteristics for the single truck and multiple truck loading scenarios. The multiple truck loading scenario results in a more constant value for optimal RM device damping characteristics. This may be because the much larger loading requires larger axial areas for similar performance and the quadratic damping value relationship seen for the single truck loading has not yet been activated. It may also be due to the fact that for the multiple truck loading scenario, minimum moment more heavily dominates the overall moment range and so damping values remain lower. Fig. 6.6 shows that the multiple truck scenario leads to larger cross-sectional areas for safe life extension but with a linear trend similar to the single truck loading scenario. The last data point shows the start toward a quadratic trend; if the data continued, the curve would trend toward the safe life extension limit seen for rigid RM apparatus members (a rigid member can be approximated as infinite area).

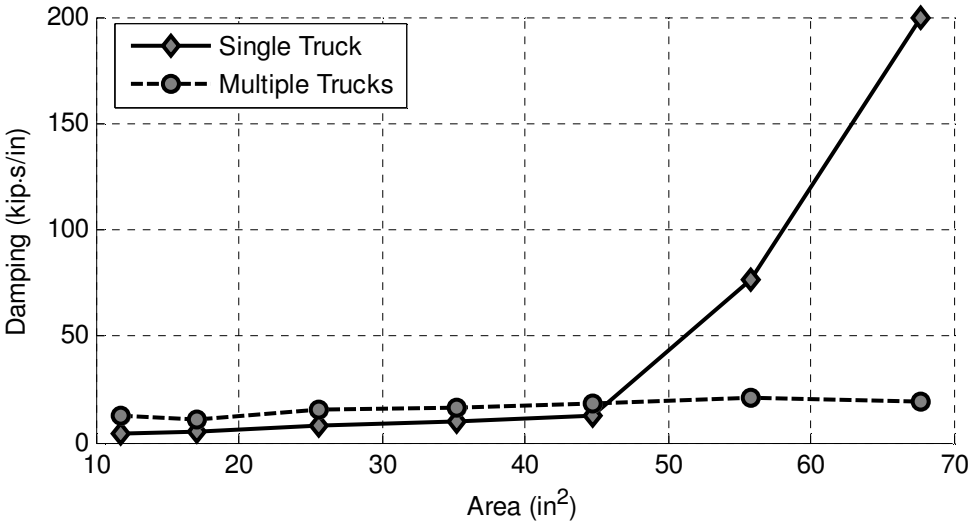

Figure 6.5 Optimal RM device damping for maximal safe life for a given member area for the GWS apparatus for various loading scenarios

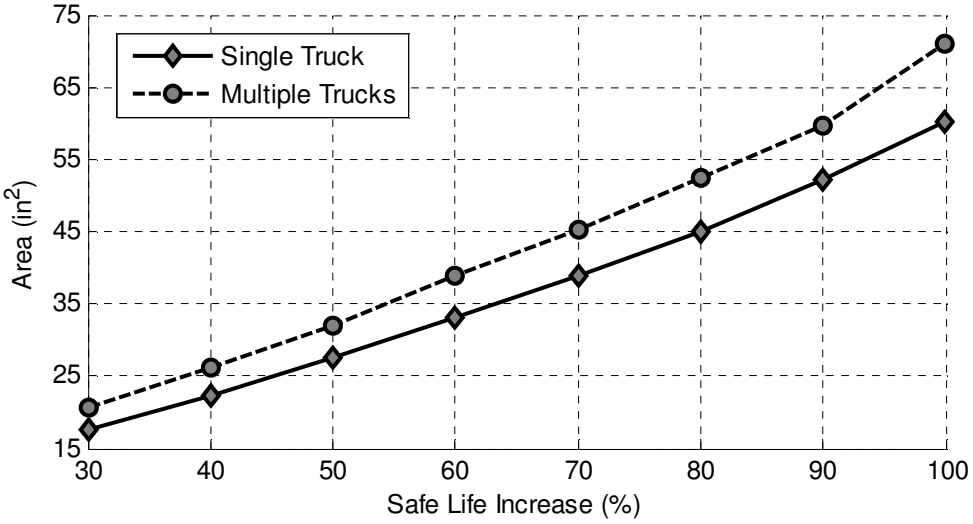

Figure 6.6 Optimal area for GWS apparatus members for a given safe life for various loading scenarios

The optimization of the GWS response modification apparatus confirms the assertion that response modification can effectively extend fatigue safe life of existing steel bridges. Enabled by the development of an accurate, computationally efficient reduced order model, multiple design optimizations were performed. Larger safe life increases

require more axial apparatus member area, larger damping coefficients, and larger force demands on the RM devices. Interestingly, small RM device stiffness coefficients with some amount of damping are optimal. It is recommended that for passive RM devices a pure damper be used in GWS apparatuses. For RM apparatus members with axial area less than 25 percent of the axial area of the bridge girder, safe life extension of over 100 percent was achieved for the GWS apparatus. The PIA apparatus requires extremely large RM device forces and damping characteristics to achieve similar performance to the GWS apparatus. Similar safe life reduction and RM device damping and stiffness coefficients trends were seen for the multiple truck loading scenarios as for the single truck scenarios.

Chapter 7: Frequency Response of Modified Structures

Due to the dynamic nature of bridge loading, varying magnitudes of amplification can occur at different loading frequencies. At certain resonant frequencies, the dynamic amplification can occur that may negate the advantages of the RM apparatus applied to a bridge structure. If a particular loading is detected at a problematic frequency, these resonant frequencies may be able to be manipulated by varying the parameters of the RM device so that large amplifications will not occur. A beam model (Fig. 7.1) was used to study a simple example of how the dynamic characteristics of the beam are changed by the addition of the GWS apparatus. A small parameter study was carried out considering the dynamic effects of different RM device characteristics for a beam structure. Additionally, frequency responses were carried out for the Cedar Avenue Bridge numerical models as well.

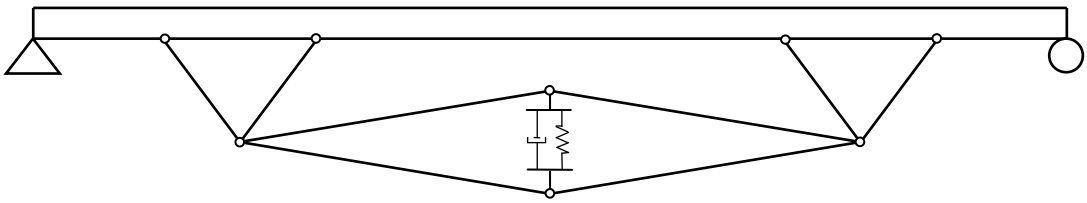

Figure 7.1 Response modification apparatus on a simple beam

7.1 Simple Beam

A finite element numerical model of a beam with a RM apparatus was developed in SAP2000 using frame elements, which used a 10 element W40x324 beam (I = 25,600 in^4, E = 29,000 ksi) to span a length of 50 feet between simple supports and rigid elements (E=1x10^{10}ksi) for all members of the GWS apparatus. The RM apparatus spanned the entire length of the beam and had a magnification factor of 25 and the RM device had a

stiffness of k = 15 kip/in and damping of c = 10 kip·s/in. All connections within the RM apparatus were pin connections except for the connections to the wide flange beam section which was modeled as a rigid moment connection. Using this SAP2000 finite element model, mass and stiffness matrices were exported and used to obtain the state space representation in MATLAB. Frequency response analyses for a load at midspan and the displacement at midspan were carried out for the beam without the GWS apparatus as well as with the GWS apparatus utilizing a RM device with fixed passive damping and stiffness. The magnitude of the transfer function, a mathematical relationship between an input that can vary with frequency and an output, between load and displacement is plotted on a log-log scale in Fig. 7.2; it is clear that when the GWS apparatus is present significant reductions (60 percent) occur at smaller frequencies but amplification at higher frequencies can occur. In addition, at certain higher frequencies, deflections of the beam with the GWS apparatus can exceed the deflections of the beam without the GWS apparatus.

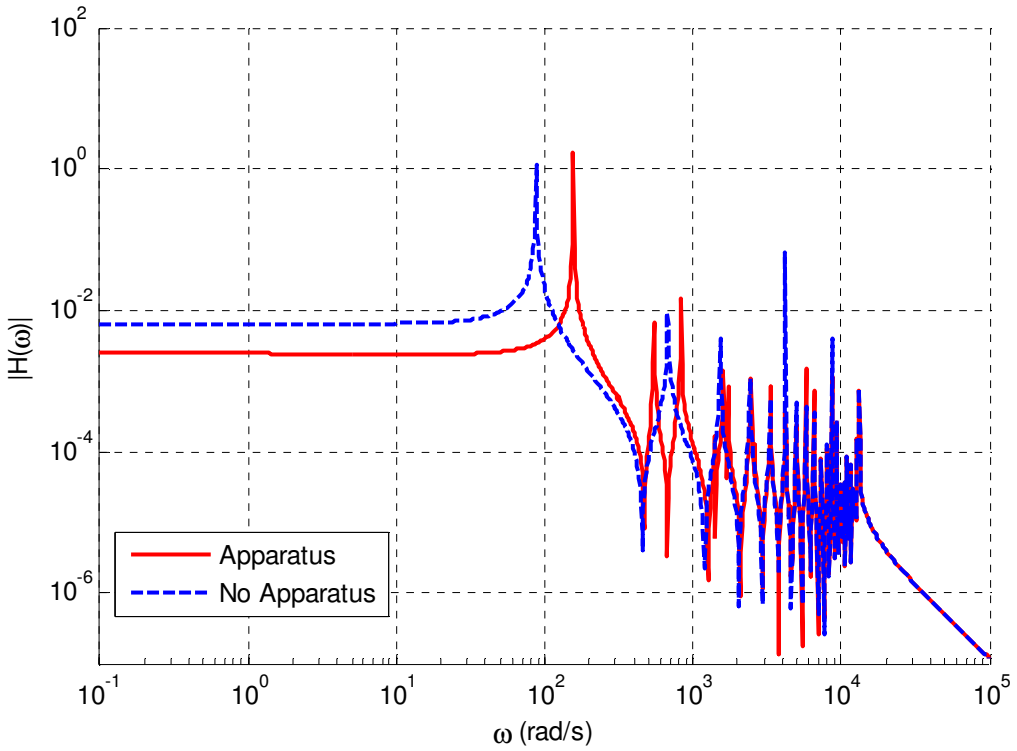

Figure 7.2 Deflection magnitude of beam loaded at the center with an oscillating point load

To further investigate the dynamic effects, a parameter study was carried out for a similar simply supported W33x201 beam of 50 feet modeled with 50 frame elements in SAP2000 and modified with a GWS apparatus located centrally of length 25 feet and of magnification 12.5. The scissor jack was attached using truss attachments instead of the rigid moment connection with a moment arm from the centroid of the beam of 2 feet. All members within the GWS apparatus were flexible and had the same cross-sectional area as the beam. A 10 kip sinusoidal point load was applied at midspan. Structural damping of 2 percent of the first two vertical modes was added to the model. The RM device had initial damping and stiffness characteristics of c = 10 kip·s/in and k = 10 kip/in respectively. The mass and stiffness matrices from the simple beam model were transferred from SAP2000 to MATLAB. To change the RM device characteristics, the stiffness and damping matrices were directly adjusted and no reduced order model was used. A wide range of stiffness and damping characteristics and loading frequencies were tested. Fig. 7.3 through Fig. 7.5 show the moment range trend for increasing levels of stiffness in the RM device. The initial unmodified system has two resonant peaks. In Fig. 7.3, it can be seen that for k = 0 (kip/in), c = 0.05 (kip·s/in) the first peak and second peaks are significantly reduced but the resonant frequencies barely change. As damping increases, the first peak is initially decreased but then begins to grow and shift to the right; the second peak decreases and then completely disappears. The best performance seems to be for k = 0 (kip/in), c = 0.15 (kip·s/in) where the response is relatively flat for lower frequencies with a drop-off in the high frequency region. In Fig. 7.4, for k = 10 (kip/in), only the first shifted peak seems to be active with the second peak having been completely reduced. Again, for increasing damping the shifted first peak initially decreases but then grows and shifts to the right. In Fig. 7.5, stiffness is so large that basically all levels of damping have reached the limit of the shifted first peak.

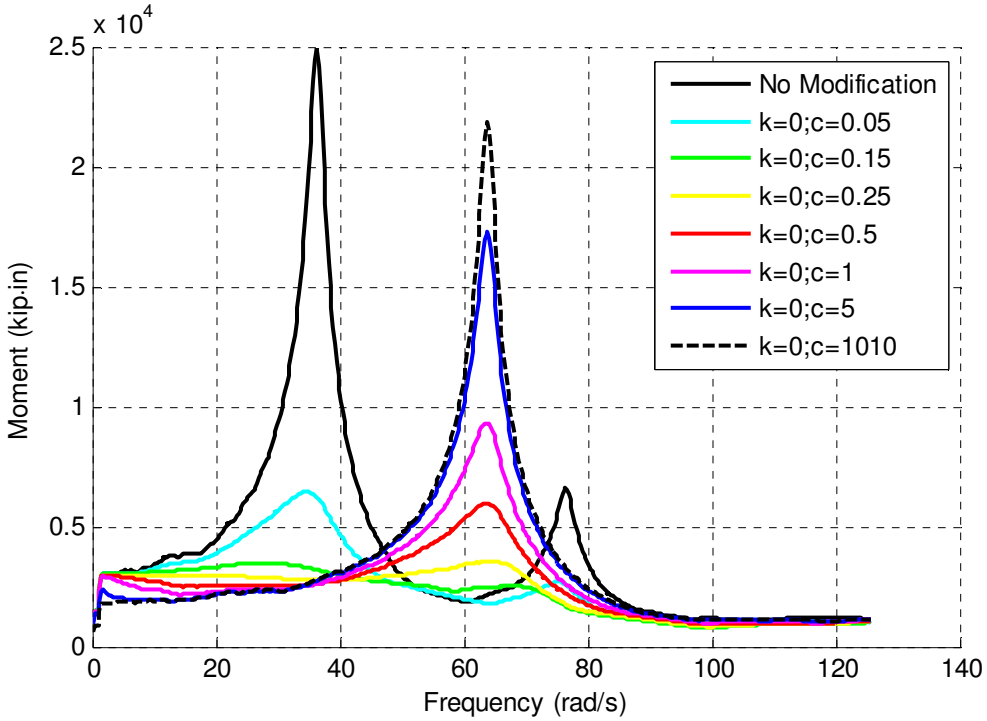

Figure 7.3 Moment range of a response modified beam employing an RM device with no stiffness and varying levels of damping

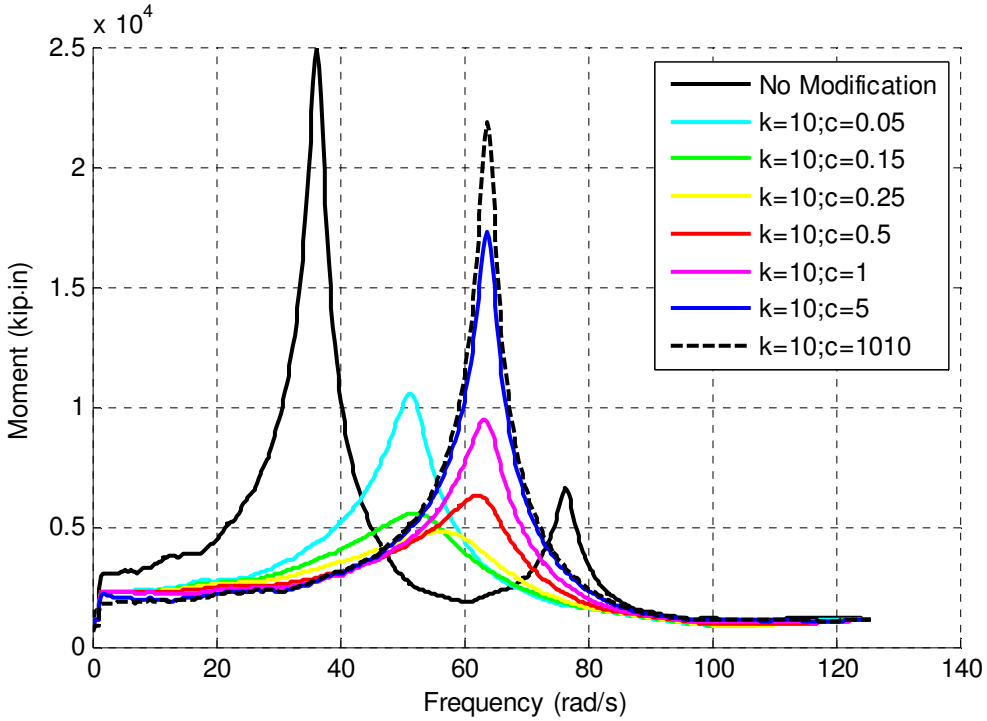

Figure 7.4 Moment range of a response modified beam employing an RM device with small stiffness and varying levels of damping

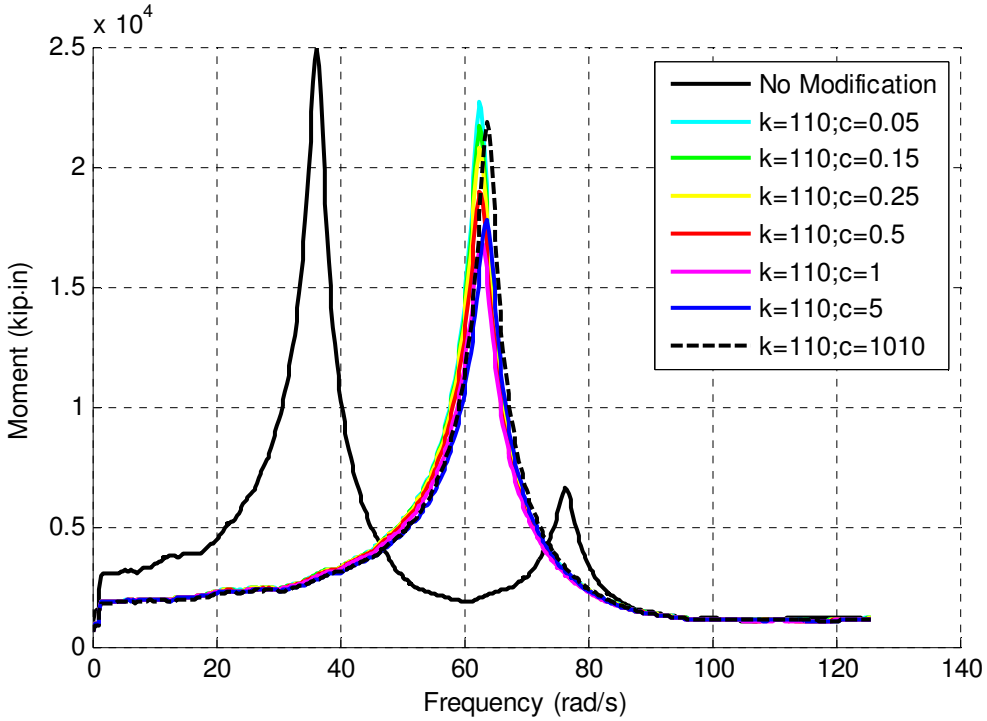

Figure 7.5 Moment range of a response modified beam employing an RM device with large stiffness and varying levels of damping

Fig. 7.6 through Fig. 7.8 show the moment range trend for increasing levels of damping in the RM device. The initial unmodified system again has two resonant peaks. In Fig. 7.6 it can be seen that for c = 0.05 kip·s/in and up to k = 1 kip/in the first peak and second peaks are significantly reduced but the resonant frequencies barely change. As stiffness increases, the first peak is initially decreased but then begins to grow and shift to the right; the second peak decreases and then completely disappears. In Fig. 7.7, for c = 0.2 kip·s/in up to k = 1 kip/in the response is very flat and then drops off near the frequency of the shifted first peak. Again, for increasing stiffness the shifted first peak initially decreases but then grows and shifts to the right. In Fig. 7.8, damping is so large that basically all levels of stiffness shifted the first peak, but only the larger stiffness values cause large resonance. It seems that there is an optimal level of stiffness and damping. Too much of either one causes larger resonances at certain frequencies.

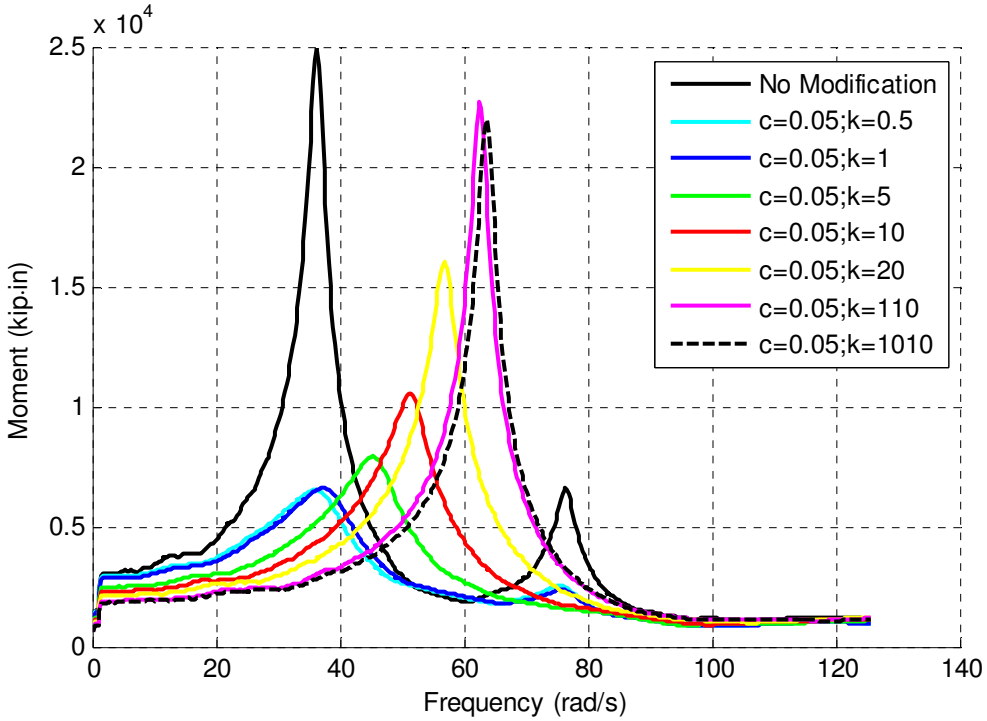

Figure 7.6 Moment range of a response modified beam employing an RM device with small damping and varying levels of stiffness

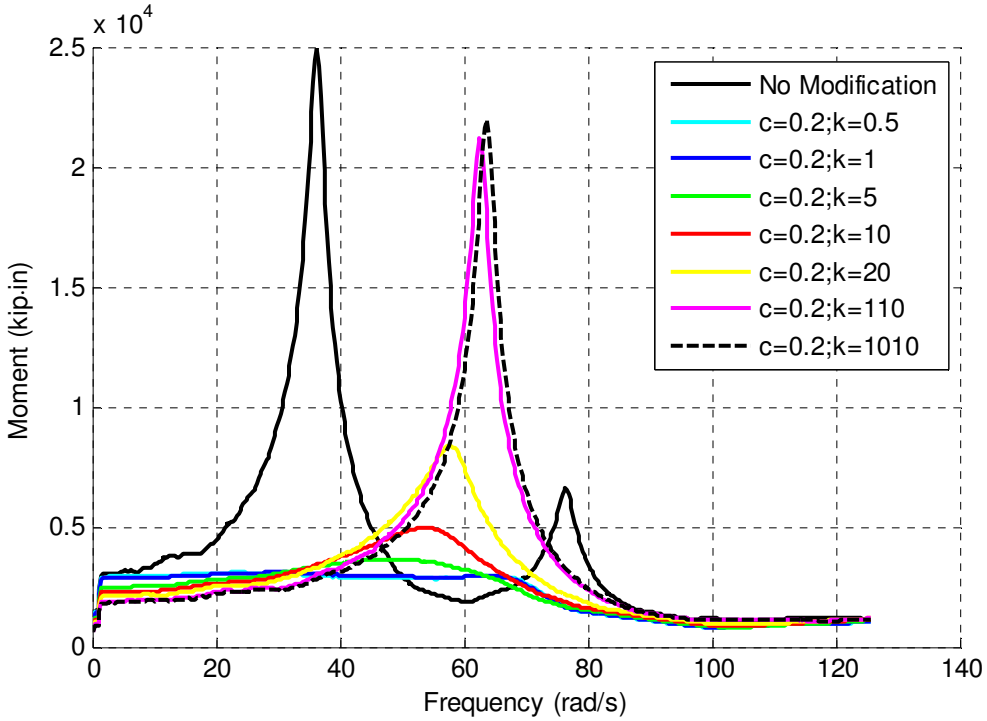

Figure 7.7 Moment range of a response modified beam employing an RM device with medium damping and varying levels of stiffness

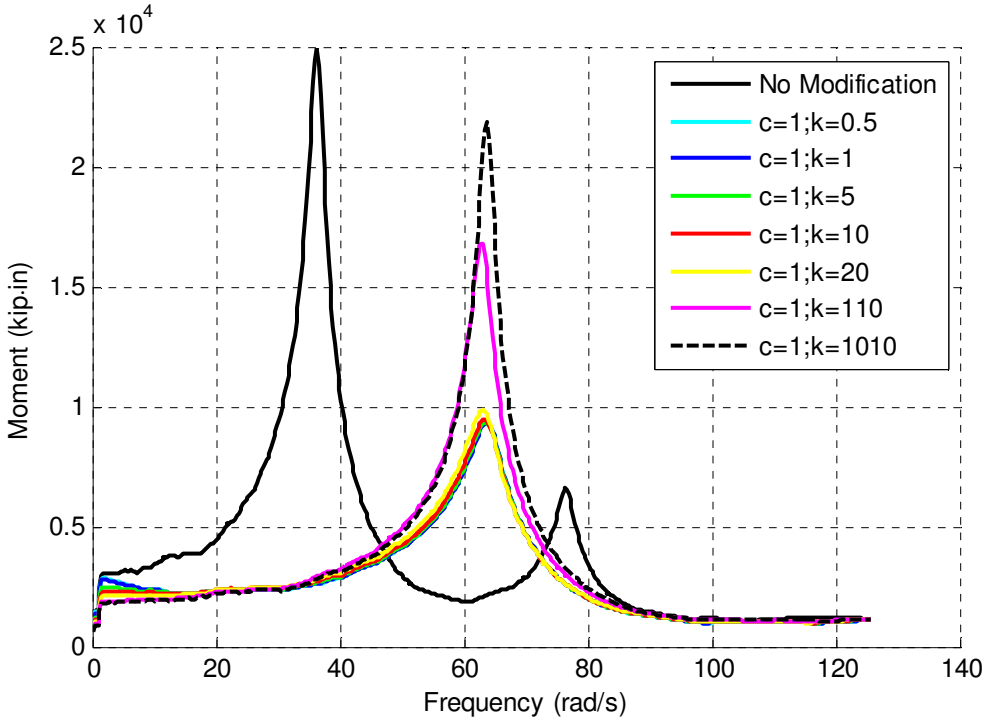

Figure 7.8 Moment range of a response modified beam employing an RM device with large damping and varying levels of stiffness

Fig. 7.9 shows the stiffness and damping values from the sets shown in Fig. 7.3 through Fig. 7.8 for selected frequencies that have the lowest moment range. It seems that for the majority of frequencies, low values of stiffness and damping perform the best.

Figure 7.9 RM device coefficients for minimum moment range for selected loading frequencies

Fig. 7.10-7.14 show the moment range at a particular loading frequency for a variety of RM device coefficient combinations. The first two figures show that for lower frequencies large RM device damping and large RM device stiffness perform the best. However, at certain larger frequencies, the best performance occurs at smaller values of RM device damping and RM device stiffness. Notice in Fig. 7.12-7.14 the dips in moment range that occur with small values of damping and stiffness. It is clear that variability exists between different loading frequencies. Very small damping and stiffness coefficients for the RM device work well for the higher frequencies (Fig. 7.12, Fig. 7.13) but are a poor choice for the lower frequencies (Fig. 7.10, Fig. 7.11); however, even another high frequency has some variability for small coefficient values (Fig. 7.14).

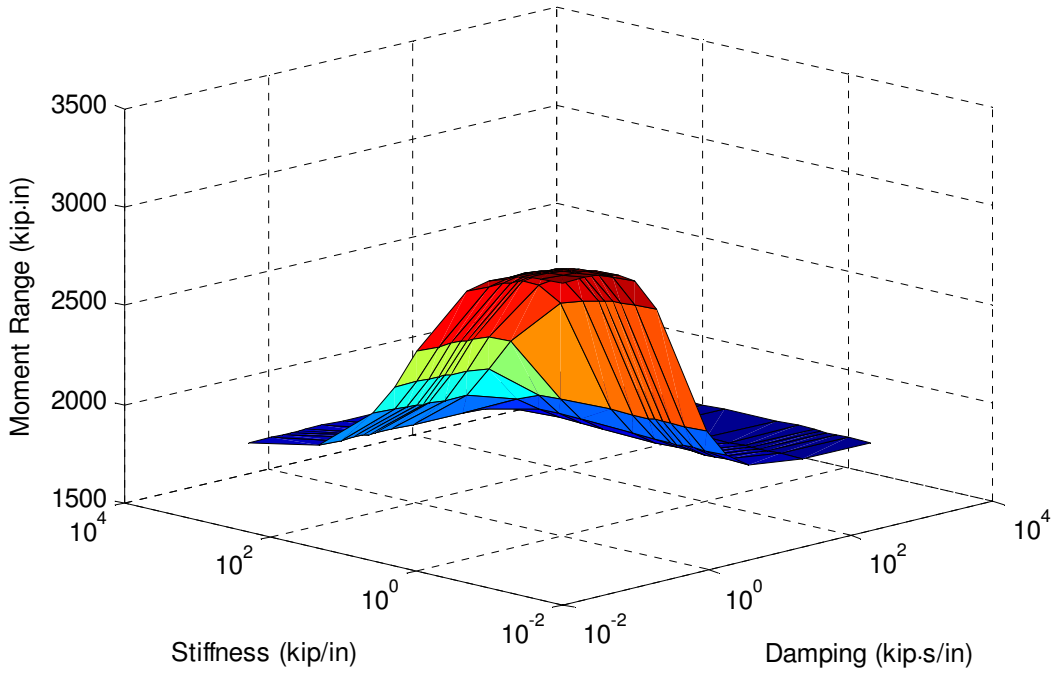

Figure 7.10 Moment range of a response modified beam for an oscillating load of 4.021 rad/s

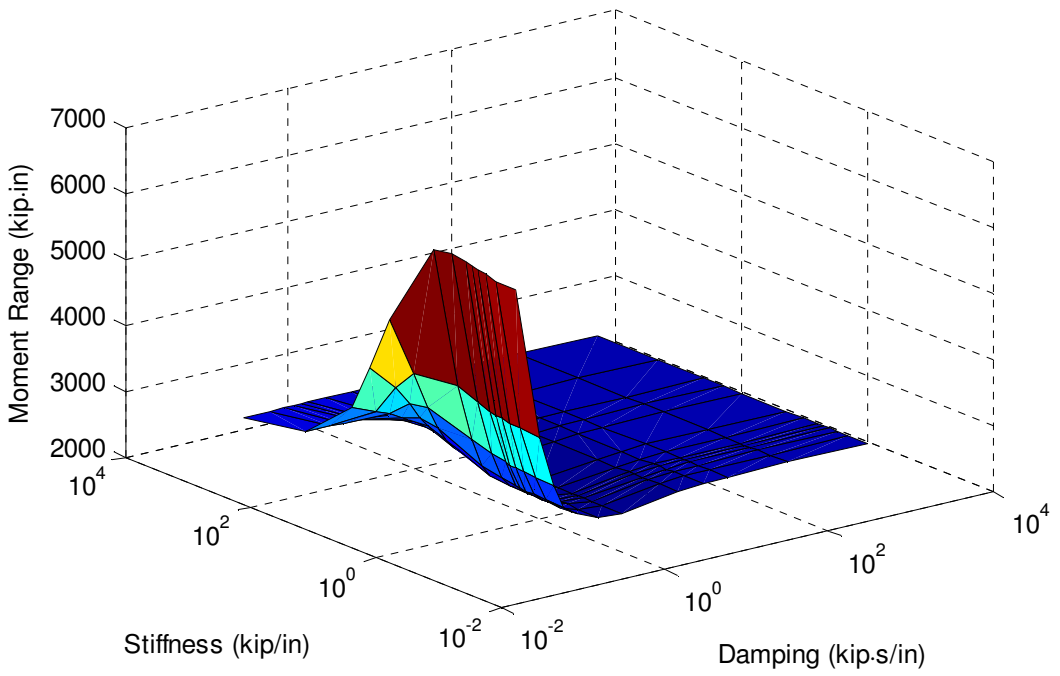

Figure 7.11 Moment range of a response modified beam for an oscillating load of 36.19 rad/s

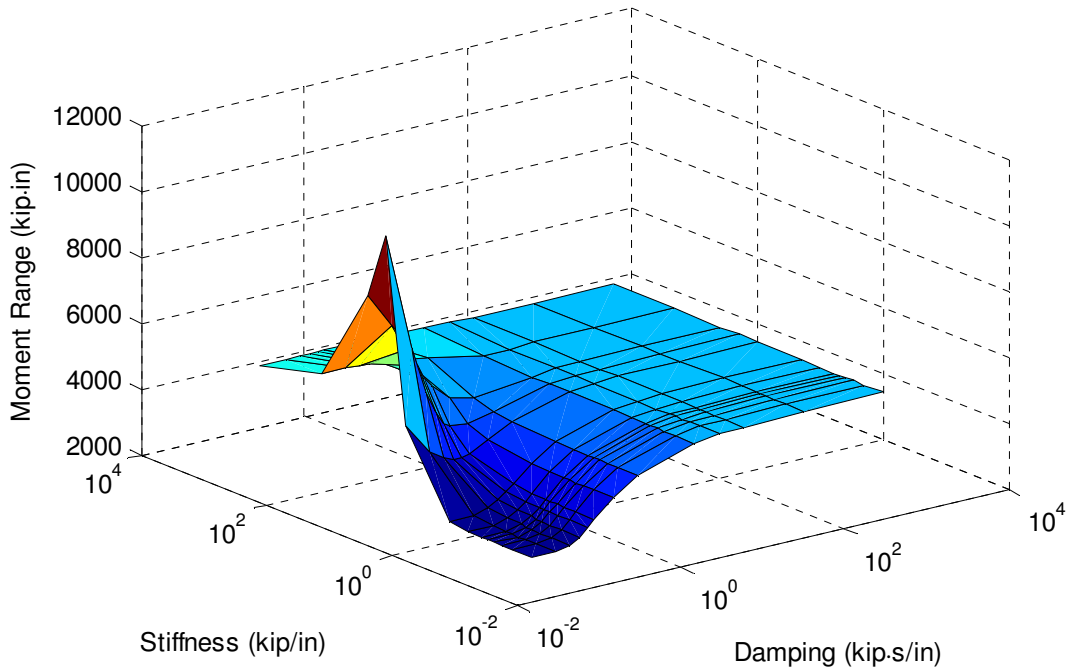

Figure 7.12 Moment range of a response modified beam for an oscillating load of 51.02 rad/s

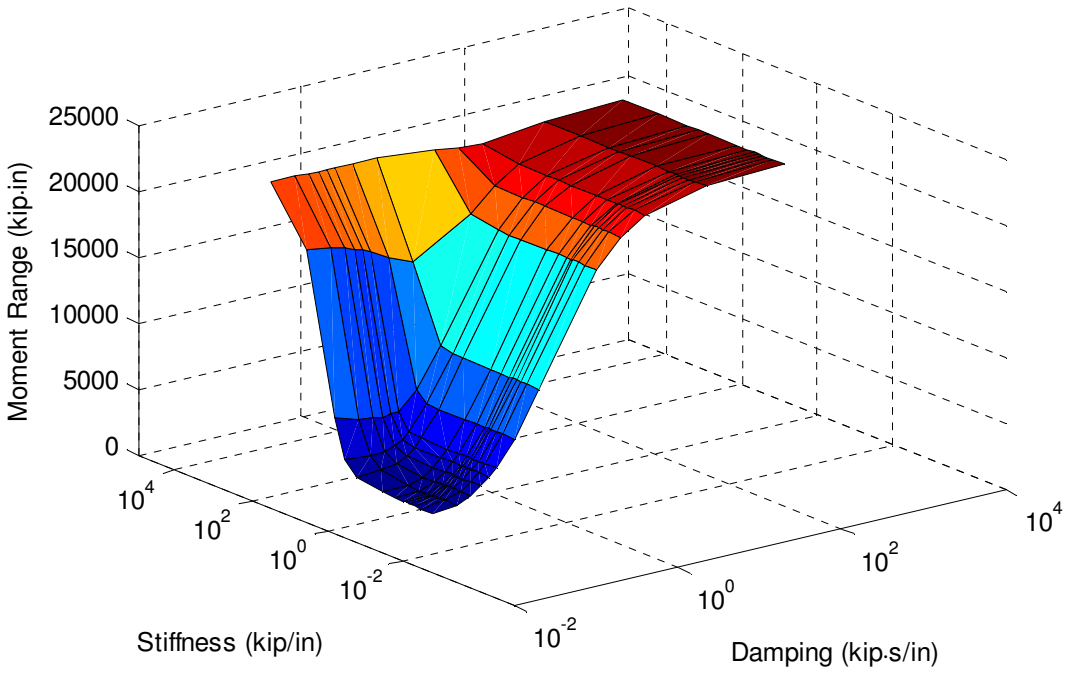

Figure 7.13 Moment range of a response modified beam for an oscillating load of 63.84 rad/s

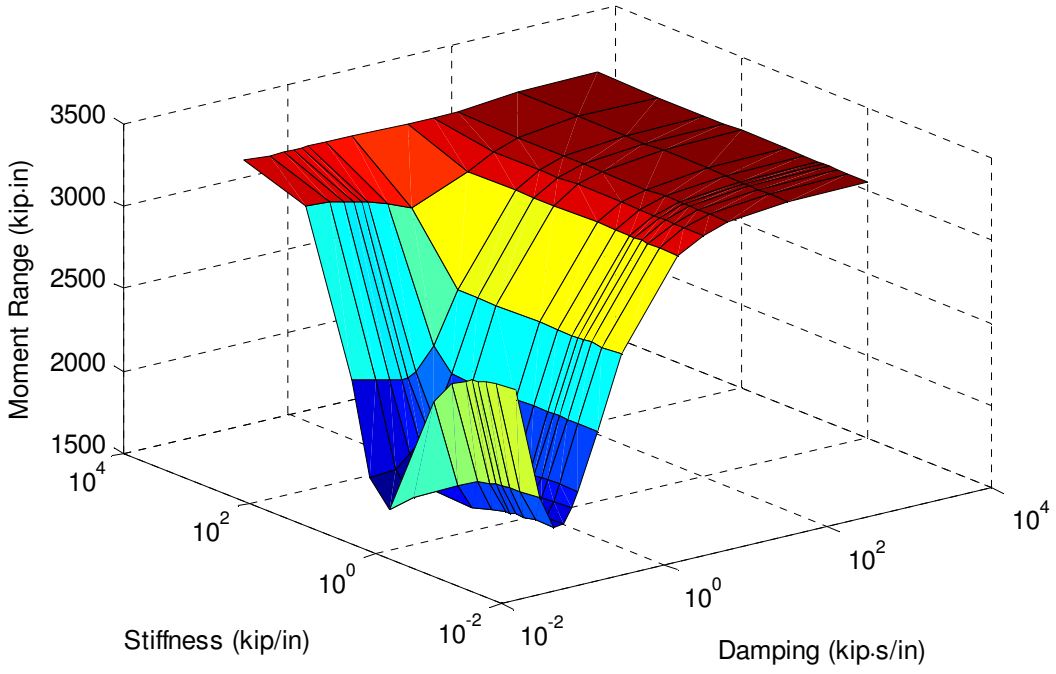

Figure 7.14 Moment range of a response modified beam for an oscillating load of 76.4 rad/s

While passive RM devices can often be selected to provide adequate response reduction if the loading is known, the ability of the RM device to adapt to various loading scenarios seems necessary to take full advantage of the GWS apparatuses. This section has shown that extending the response modification framework to include semi-active RM devices whose properties can be modified to manipulate structural response may be of interest. These properties can theoretically be governed by a control algorithm which incorporates real-time data of loadings subjected on the bridge potentially measured using accelerometers, WIM (weigh-in-motion) technologies, or other bridge health monitoring equipment. Therefore, to further ensure response reduction over a larger range of loading frequencies and truck speeds, a semi-active RM device with properties that can be manipulated depending on loading conditions might prove to be advantageous.

7.2 Cedar Avenue Bridge

After finding that semi-active RM devices might be useful on a simple beam model, the Cedar Avenue Bridge numerical model is the next logical investigation. To carry out frequency response analyses, the model had to be transferred from SAP2000 into MATLAB, and the mass and stiffness matrices had to be transformed due to the zeros in the mass matrix discussed in section 4.2.5. This approach was carried out on both the model with the bridge deck and without the bridge deck. Only a comprehensive transfer function on the full order model without the bridge deck was obtained due to the large size of the model with the bridge deck and memory constraints. The frequency response plot for displacement at the vulnerable joint and a load at midspan for the steel component Cedar Avenue Bridge numerical model can be seen in Fig. 7.15. Similar to the simple beam model, it is clear that the additional stiffness in the bridge from the RM apparatuses shifts the response plot and even increases the response at some frequencies as well as adding other resonant modes.

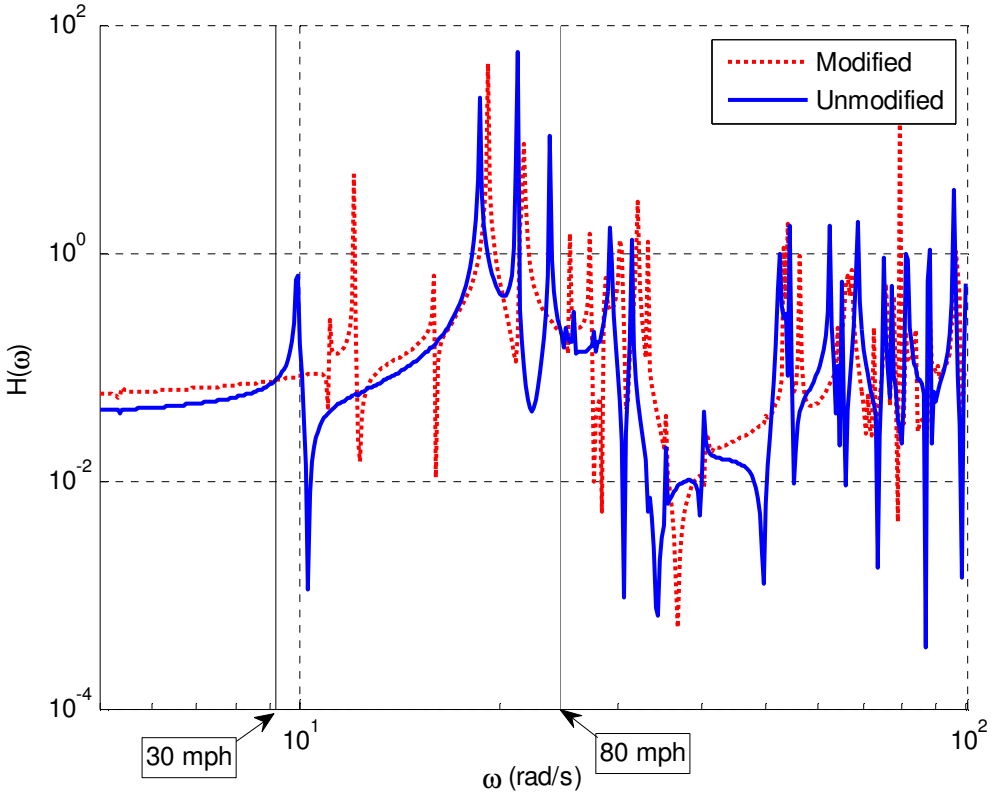

Figure 7.15 Bridge frequency response for deflection at the L3 joint and 72 kip load at midspan for the Cedar Avenue Bridge numerical model without bridge deck

To evaluate the frequency response plot with the addition of the bridge deck, the reduced order model was utilized. Fig. 7.16 shows the reduced order models both with and without the GWS apparatuses. Additionally, a few points were run for the full order model modified with GWS apparatuses to verify the ability of the reduced order model to predict the frequency response behavior. It can be seen that the first peak is unaffected by the GWS apparatuses and the second peak is shifted to the right. It may be that due to the placement of the GWS apparatuses, some modes of the numerical model are unaffected by the additional localized stiffness while others (the second peak) can be easily manipulated. While this could be an issue, the frequency response plots are using displacement as the magnitude as opposed to moment range. The displacement is a global phenomenon while the moment range within RM apparatuses is much more localized (as shown in the parameter studies). Also note the relative smoothness of Fig. 7.16 compared to Fig. 7.15; two causes are likely: (1) spurious modes of the numerical

model were not constrained for the steel component numerical model and (2) Fig. 7.16 is on a much smaller frequency scale. Lastly, a similar frequency comparison for moment range was completed using the reduced order model and a sinusoidal point load at midspan. Fig. 7.17, Fig. 7.18, and Fig. 7.19 show that for various levels of RM device damping, amplification can occur. At lower frequencies (Fig. 7.18) more damping reduced response by 10 percent. However, at higher frequencies (Fig. 7.19) increased RM device damping caused extremely large amplification while lower RM device damping showed little amplification.

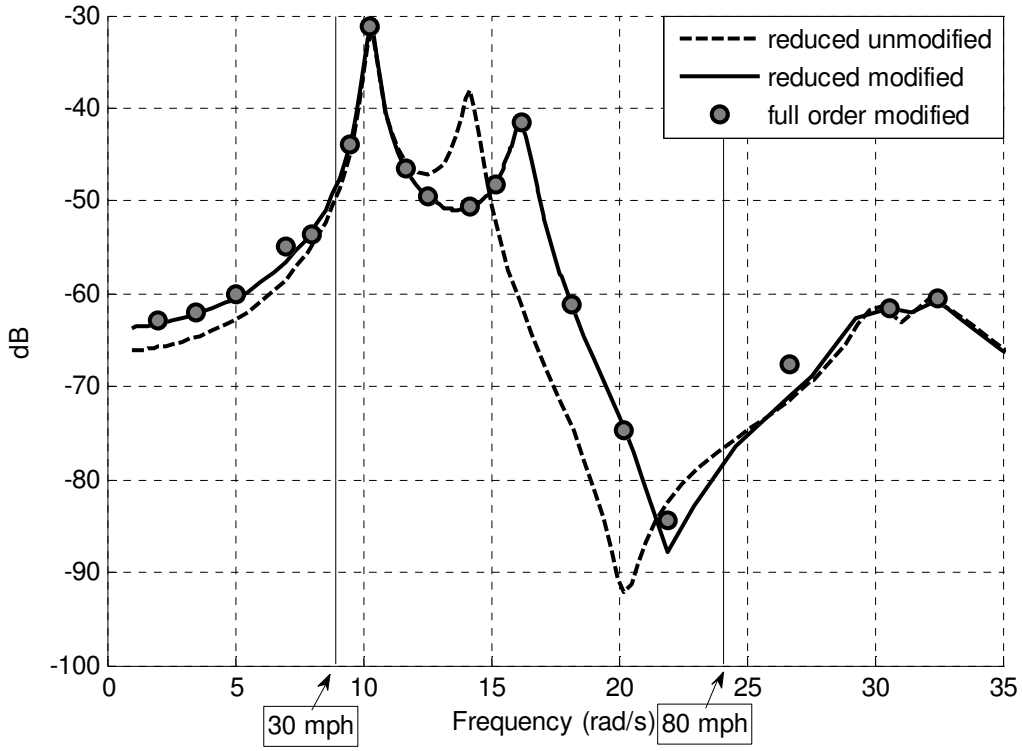

Figure 7.16 Bridge frequency response for deflection at the L3 joint and load at midspan for the Cedar Avenue Bridge numerical model with bridge deck

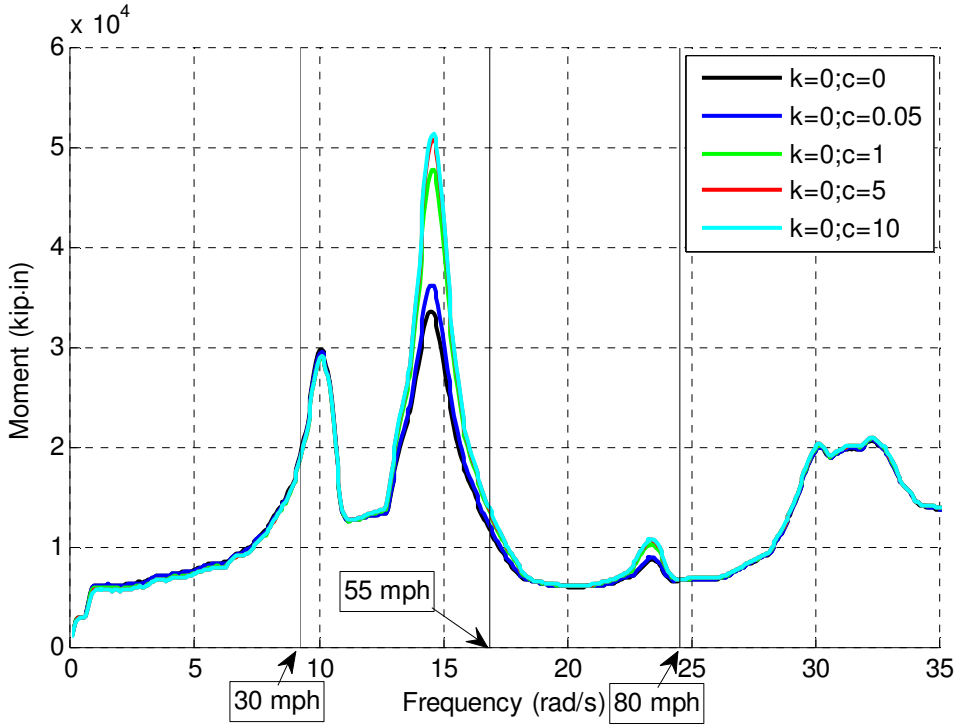

Figure 7.17 Bridge frequency response for moment range at the L3 joint and load at midspan for various RM device damping coefficients

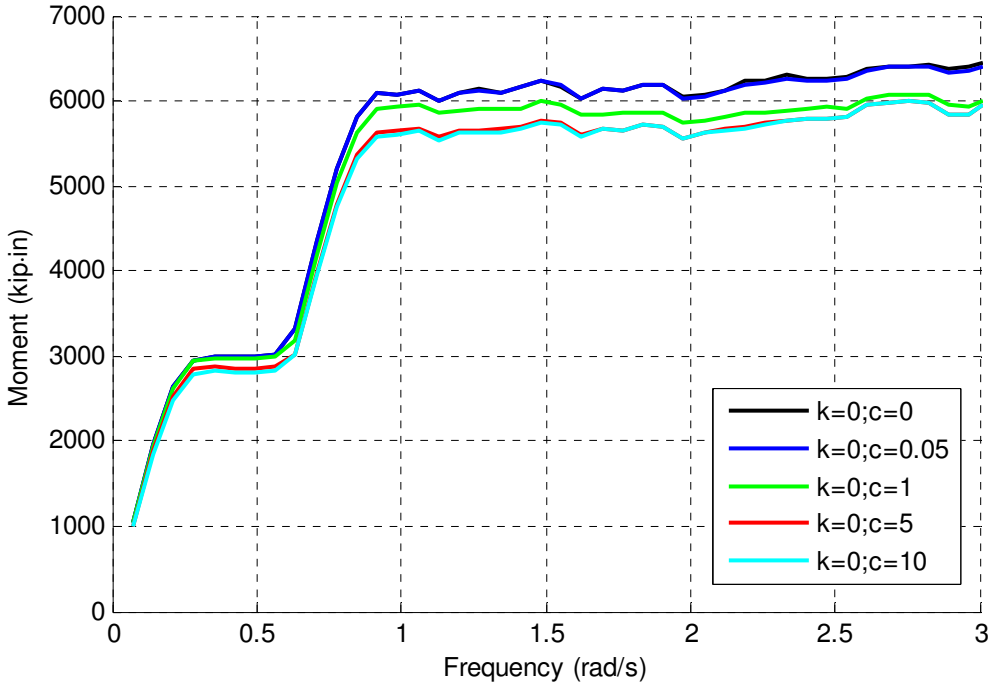

Figure 7.18 Bridge frequency response for moment range for various RM device damping coefficients at low frequencies

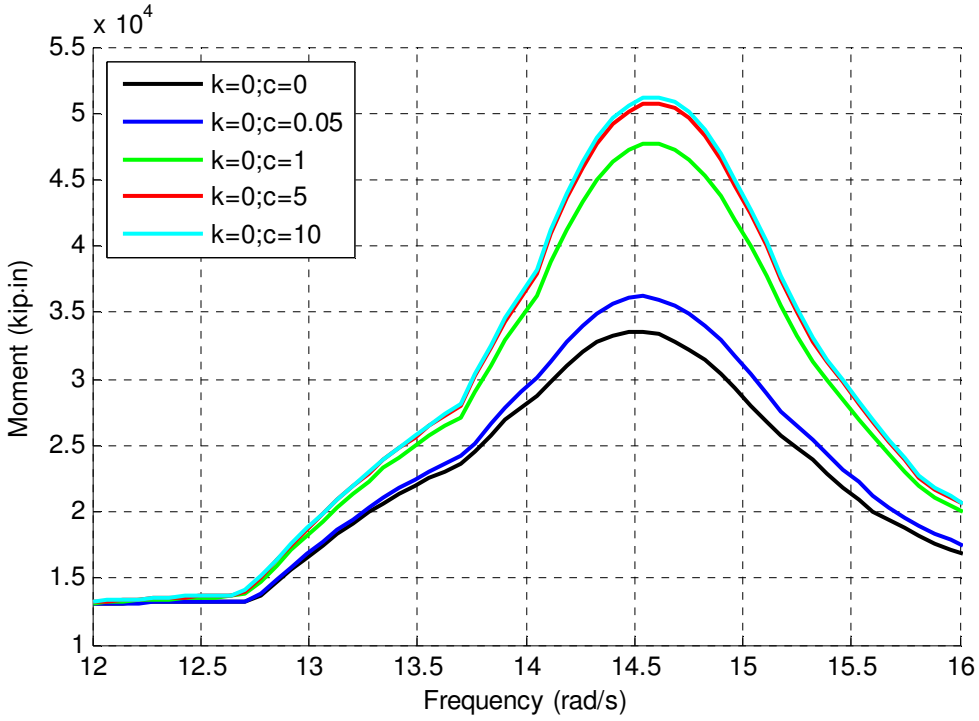

Figure 7.19 Bridge frequency response for moment range for various RM device damping coefficients at amplified frequencies

Fig. 7.20, Fig. 7.21, and Fig. 7.22 show that for various levels of RM device stiffness, amplification can occur. At lower frequencies (Fig. 7.18) more stiffness reduced response by 10 percent. However, at higher frequencies (Fig. 7.19) increased RM device stiffness caused extremely large amplification while lower RM device stiffness showed little amplification.

While these frequency response plots are interesting, ultimately it is vehicle speeds and dynamics that will need to excite these modes. One possible way to evaluate the resonant effects of heavy truck vehicle speeds has been denoted with solid vertical lines in the figures and it seems that the resonant frequencies fall in the range of typical vehicle speeds. Table 7.1 shows equivalent natural frequencies, similar to the critical speeds introduced by Fryba (1999), for varying truck speeds where L (ft) is the assumed distance between point loads, which is calculated based on four possible assumptions: (1) L = 358.5 which is the whole length of the bridge so one truck on the bridge at a time repeating; (2) L = 30 feet which is the distance between the two heavy axles for the case

of a the AASHTO truck; (3) L = 44 feet which is the distance between the front axle and the rear axle; and (4) L = 14 feet which is the distance between the front axle and the first heavy axle. Case two is the most severe case due to the heaviest loads and has frequencies that lie within the largest amplifications in the frequency response plot.

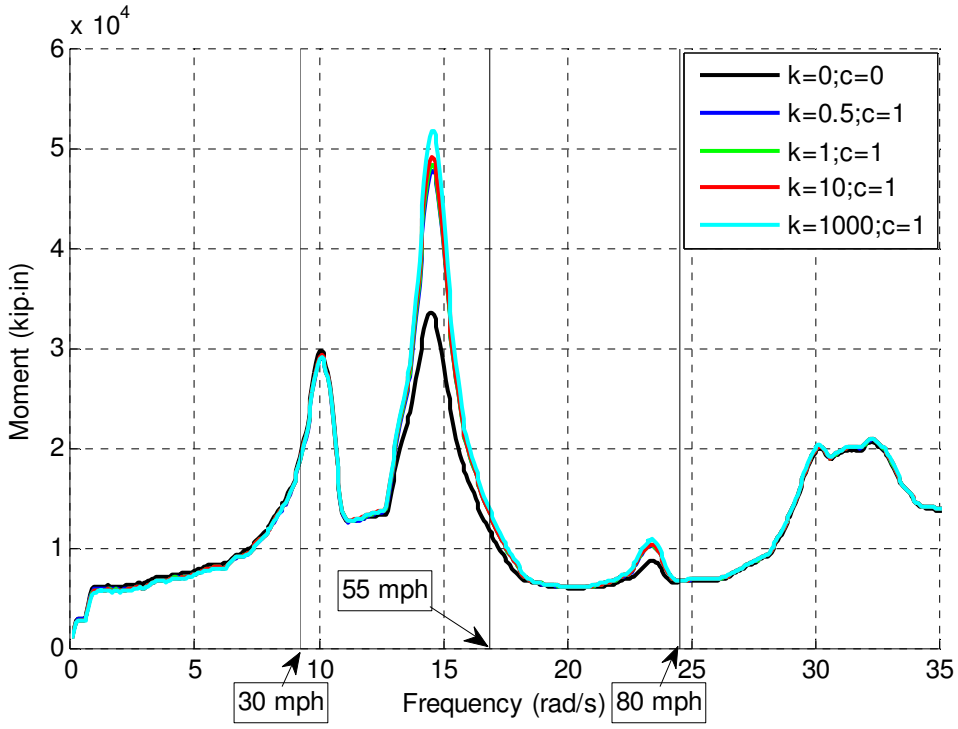

Figure 7.20 Bridge frequency response for moment range at the L3 joint and load at midspan for various RM device stiffness coefficients

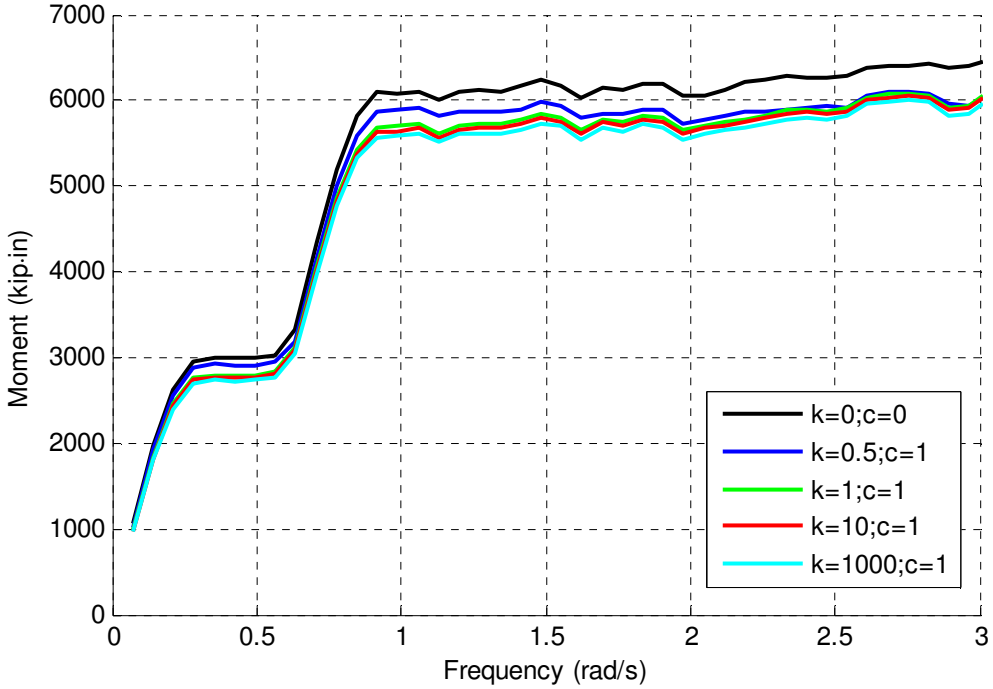

Figure 7.21 Bridge frequency response for moment range for various RM device stiffness coefficients at low frequencies

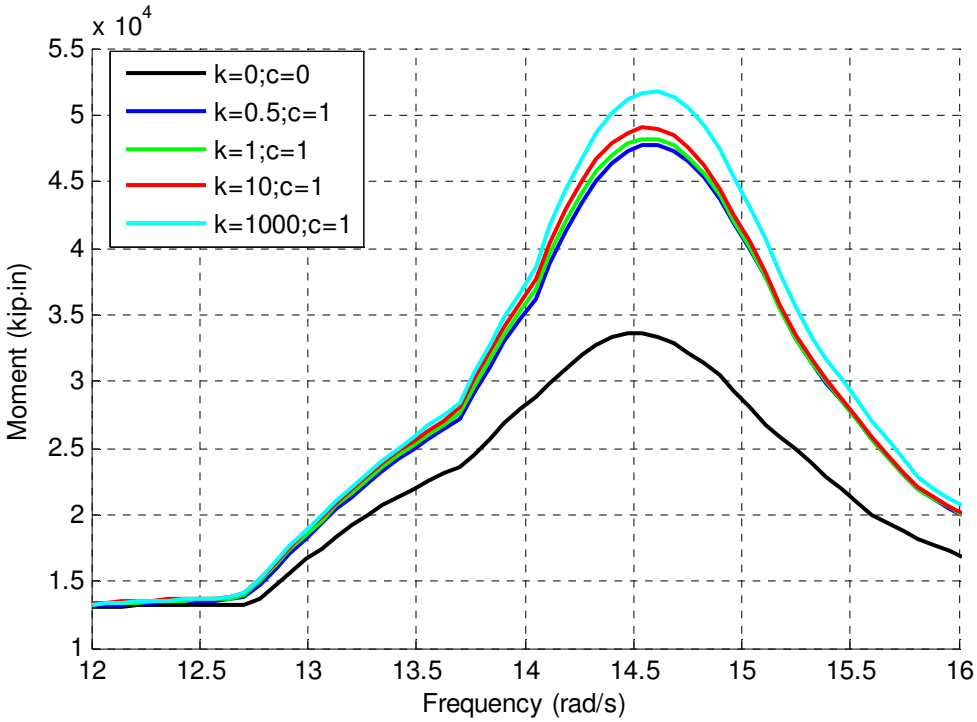

Figure 7.22 Bridge frequency response for moment range for various RM device stiffness coefficients at amplified frequencies

Table 7.1 Fatigue truck loading frequencies

L (ft)	Frequency (rad/s)		
	55 mph	60 mph	80 mph
358.5	1.41	1.54	2.06
30	*16.89*	*18.43*	*24.57*
44	11.52	12.57	16.76
14	36.20	39.49	52.66

Table 7.2 shows the reductions and amplifications from Fig. 7.15 that can be caused by the GWS apparatus for vehicles traveling at varying speeds. It is shown that for certain loading frequencies the response is decreased up to 100% using the GWS apparatuses but for other loading frequencies that the response can be increased by 8700% over the original bridge structure. Table 7.3 shows selected reductions and amplifications from Fig. 7.16. Similar to the numerical model without the bridge deck, both reductions and amplifications can be seen. Therefore, being able to change the properties of the RM device to shift the frequency response plot is attractive; semi-active RM devices would be useful to fully take advantage of the GWS apparatuses.

Table 7.2 Fatigue truck loading deflections for varying frequencies for steel component numerical model

mph	L (ft)	Frequency (rad/s)	Modified displacement magnitude (in)	Unmodified displacement magnitude (in)	Decrease (%)
32.4	30	9.95	0.082	0.634	87
39.3		12.08	4.95	0.0563	-8629
51.8		15.92	0.635	0.154	-312
60.7		18.66	1.05	22.6	95
62.5		19.19	46.19	0.927	-4877
69.3		21.28	0.186	59.1	100
70.7		21.73	8.89	0.101	-8757

Table 7.3 Fatigue truck loading deflections for varying frequencies for numerical model with bridge deck

mph	L (ft)	Frequency (rad/s)	Modified displacement magnitude (in)	Unmodified displacement magnitude (in)	Decrease (%)
33.5	30	10.3	1.98	1.86	-6.4
46.2		14.2	0.211	0.893	76
52.7		16.2	0.610	0.00510	-1100
65.8		20.2	0.132	0.00179	-635
74.9		23	0.00523	0.00828	37

From this section, frequency response analyses of both a simple beam model and the numerical model of the Cedar Avenue Bridge have shown that amplification of the bridge response can occur at some frequencies. These studies have shown that it may be advantageous to outfit the GWS apparatuses with semi-active RM devices that have the ability to adapt. By changing stiffness and damping characteristics, this section has shown that a variety of responses can be induced.

Chapter 8: Summary and Conclusions

With a large number of bridges reaching the end of their intended design life, options for safe bridge life extension are becoming vital for maintaining our infrastructure. Bridge health monitoring and structural response modification techniques are one possible method for the safe extension of bridge life. To accomplish successful response modification of bridge structures, the classification of common bridge vulnerabilities, bridge loading models, available bridge monitoring systems, and RM devices must be well understood. Once these are known for a specific bridge candidate, response modification can be carried out to safely extend the life of these structures. The proposed response modification approach, utilizing a RM device and a mechanical amplifier to provide additional stiffness and damping, has been well described and thoroughly analyzed for passive response modification. The GWS apparatus allows for much smaller RM devices and provides a localized approach for specific vulnerabilities compared to approaches without the mechanical amplifier.

Due to the complexities of bridge failures, bridge vulnerabilities are not always easy to identify and classify. However, previous major bridge collapses have been reviewed and many common steel details with fatigue vulnerabilities have been identified as candidates for response modification and bridge health monitoring to safely extend bridge life. The mathematical concepts for the stress concentrations around cover plates and web gaps have been presented along with the equations for fatigue life adopted by AASHTO.

Bridge loading models can be defined in multiple ways. To extend bridge fatigue life, loading the bridge with an AASHTO specified truck is the most logical choice to allow for safe bridge life extension calculations. Because fatigue life is based on millions of loadings at a typical value, a standard truck loading is appropriate. Other models such

as WIM may be beneficial and would be especially helpful for bridges that see typical truck loads that are higher than the AASHTO specified truck.

The various applications of different bridge health monitoring systems have been categorized and useful systems have been categorized. These systems can be used to analyze bridge responses to vehicle loading and verify that stress reduction has been achieved for safe life extension. The systems could ultimately be linked to a control computer and used for feedback to control the RM device, allowing for optimized stress range reduction at the vulnerable element for variable loading situation. For control purposes, multiple systems would be necessary to provide both global bridge response measurements for feedback control and local stress range readings for stress verification.

Response modification devices relevant to bridge health monitoring and structural response modification techniques have been identified. Passive, semi-active, and active devices can all be used in a bridge setting, but the best candidates are passive and semi-active devices due to their minimal power consumption. These RM devices can be used to provide added stiffness and damping to allow for safe bridge life extension. The addition of a mechanical amplifier, the scissor jack, has been explored to allow for larger control forces by amplifying the typically small displacements seen in bridge applications as well as amplifying the forces from the RM device. The mathematical relationships for the scissor jack magnification of both beam displacements and RM device forces have been derived and presented. Demonstrated on a simple beam numerical model, the RM apparatus with the mechanical amplifier outperforms an RM apparatus without the mechanical amplifier when the same RM device is used for each.

The Cedar Avenue Bridge, a fracture critical tied-arch bridge, was chosen to demonstrate the efficacy of the GWS apparatus approach on an in-service fracture critical bridge. Due to the stress concentrations experienced at the hanger - bridge girder - floor beam connection detail, fatigue cracking is a concern. By reducing the moment range, bridge life can be safely extended in structures with a finite fatigue life. Since the fatigue life is inversely proportional to the cube of the stress range, even small reductions in ranges can have a large effect on fatigue life. To demonstrate the approach, a numerical model of the bridge was developed which evolved during the course of the research.

Table 8.1 provides a brief description of the various bridge models and their uses. A steel component only bridge model was initially used for analyses. Improvements including the addition of the concrete bridge deck, global Rayleigh damping, six degree of freedom per joint analysis capabilities, inclusion of flexible RM apparatus members, as well as other minor adjustments were made.

Table 8.1 Various Cedar Avenue Bridge numerical model descriptions and uses

Bridge Model	Description	Uses
2D Steel Component Model	Numerical model incorporates steel components of the Cedar Avenue Bridge. RM apparatus members are rigid. A single pair of RM apparatuses is placed on one end of the bridge. Degrees of freedom are constrained to planar motion. The truck loading is modeled as 6 moving point loads.	initial parameter studies; truck speed studies
3D Steel Component Model	Numerical model incorporates steel components of the Cedar Avenue Bridge with revised girder torsional rigidity. RM apparatus members are rigid. Both a single pair of RM apparatuses placed on one end of the bridge and two sets placed on symmetric ends are modeled. Displacement and rotation in all three dimensions is allowed. The truck loading is modeled as 6 moving point loads.	initial parameter studies; frequency analyses
3D Bridge Deck Model	Numerical model incorporates steel components and the concrete deck of the Cedar Avenue Bridge. RM apparatus members have flexibility. Two sets of RM apparatuses placed on symmetric ends are modeled. Displacement and rotation in all three dimensions is allowed. The truck loading is modeled as 6 moving point loads. Global damping is included.	parameter studies; frequency analyses
Simple Reduced Order Model	Model uses the first 9 vertical modes of the 3D Bridge Deck model to create a reduced order model. Model predicts displacement and moment at the critical joint well. Model has poor performance for changes in RM device characteristics or member stiffness. The truck loading is modeled as 3 moving point loads. Global damping is included.	truck speed studies
Reduced Order Model	Model uses vertical modes, static deflection shapes due to point loads, and member stiffness change shapes of the 3D Bridge Deck model to create a 53 DOF reduced order model. Model predicts displacement and moment well at multiple locations for changes in RM device characteristics and member stiffness. The truck loading is modeled as 3 moving point loads. Global damping is included.	RM apparatus characteristics optimizations; frequency analyses

Additionally, the final 35,402 degree of freedom numerical model was reduced down to a 53 degree of freedom model for RM apparatus optimization analyses. The reduced order model achieved a speedup of 11 to 200 times for surveyed RM apparatus characteristics.

The response modification methodology was carried out on the numerical bridge models and demonstrates the efficacy of the GWS apparatus for reducing moment ranges seen by a vulnerable connection or member in a bridge structure. Numerous parameter studies showed the advantages and disadvantages of the GWS apparatus. Ultimately, a wide but shallow (large magnification value) GWS apparatus performs the best. Longer (length between the attachment points) RM apparatuses have better performance and larger cross-sectional axial areas provide more safe life extension. Adding the bridge deck and damping to the numerical models had little effect on overall performance. Additional RM apparatuses provide better displacement performance, but the moment effects of the RM apparatuses are localized between the attachment points; supplementary RM apparatuses away from the point of interest provide little benefit for moment reduction. Increasing damping and stiffness coefficients for the RM device beyond a certain threshold provides little improvement. Comparing the GWS apparatus to the PIA apparatus, for identical RM device characteristics, the GWS apparatus outperforms the PIA apparatus (an RM apparatus without a mechanical amplifier). The GWS apparatus allows for a much smaller RM device in terms of damping and stiffness coefficients as well as force capabilities. For a cost analysis, the weight of the steel divided by the amount of safe life extension is most efficient for the smallest RM apparatus with the smallest member cross-sectional area; however, the amount of safe life extension will most likely not be adequate and a larger less efficient GWS apparatus will probably be necessary. Finally, truck speed studies showed that amplification can occur at specific loading speeds. In general, the faster the truck speed, the larger the amplification, but variability of maximum and minimum moment ranges was experienced within the general trend.

In addition to performing multiple parameter studies, optimizations of the RM apparatuses were also completed. To minimize the moment range at the critical joint, a small amount of damping and no stiffness was optimal for a passive RM device installed

in the GWS apparatus; smaller cross-sectional areas required smaller damping coefficients. Considering maximum moment and minimum moment separately, the minimum moment optimizations required small damping coefficients with no stiffness for the optimal passive RM device. Conversely, the maximum moment optimizations required larger damping coefficients and stiffness coefficients for the optimal RM device. Similar safe life reduction and RM device damping and stiffness coefficients trends were seen for the multiple truck loading scenarios as for the single truck scenarios. For multiple trucks, a passive RM device with some damping and no stiffness is also optimal; smaller cross-sectional areas generally required smaller damping coefficients. Ultimately, GWS apparatus optimization studies showed safe life increases of over 100 percent for cross-sectional areas of less than 25 percent of the bridge girder cross-section. When limited to an RM device force of 2.5 tons, PIA apparatuses could only achieve safe life extension of under 4 percent. Forces of over 20 tons were necessary to achieve even a 63 percent safe life increase for the PIA apparatuses.

Due to the truck speed results and maximum and minimum moment optimization results, further study of the bridge dynamics was warranted. From the frequency response plots of a simple beam modified by the GWS apparatus, it is clear that, even with the RM apparatus, some loading frequencies may increase response compared to the unmodified structure. For the simple beam structure, low values of stiffness and damping perform the best for many loading frequencies (similar to the optimized passive RM devices for the Cedar Avenue Bridge). An optimal set of damping and stiffness coefficients provided adequate response for a variety of loading frequencies, but large stiffness or damping coefficients leads to large response amplification. Frequency response studies of both the Cedar Avenue Bridge steel component model and the numerical model with bridge deck modified with multiple GWS apparatuses also showed that response can be amplified with the RM apparatuses at certain loading frequencies. Due to the truck speed findings, optimization discrepancies, and frequency analyses, a semi-active RM device which can change properties depending on the location and speed of the moving load may be advantageous. Optimization of multiple trucks traveling at different speeds other than 65 mph, which may activate other bridge vehicle dynamics

would provide insight into whether or not semi-active control may provide increased benefit. In addition, improving the loading model to accurately represent typical truck loading with random input noise from the road roughness as well as vehicle dynamics will also activate bridge-vehicle interaction. Ultimately, design and testing of a small scale semi-active apparatus would allow for a good comparison of passive and semi-active RM device applications.

Ultimately, for the design of a passive GWS apparatus, a long and slender RM apparatus is recommended for safe life extension. A RM device with a small damping coefficient and no stiffness should be employed for a passive system. For the modeling of a passive system, a simple bridge model should be sufficient for GWS apparatus implementation. The more complicated model including structural damping and the bridge deck yielded very similar results. The cross-sectional area of the RM apparatus members will need to be sufficiently large to provide adequate safe life extension and will have to be evaluated on a case-by-case basis. An initial starting point of around 25 percent of the cross-sectional area of the member being modified should provide a good starting point for design.

In conclusion, bridge health monitoring and structural response modification techniques are a promising solution to address the aging bridge infrastructure in the United States. These techniques can reduce stress ranges at vulnerable bridge details by providing an alternate load path. By reducing and monitoring these stress ranges, safe life extension of vulnerable details can be accomplished in a safe and effective manner. The application of the GWS apparatus, a RM device augmented by a mechanical amplifier, has been investigated analytically and applied to a numerical model of an in-service vulnerable bridge. The bridge safe life has been theoretically extended by over 100 percent using GWS apparatus members of less than 25 percent of the cross-sectional area of the bridge girder and an optimized passive RM device. The GWS apparatus out performs the PIA apparatus when both employing a similar RM device and allows for a much smaller RM device.

Bibliography

Adams, B.M., Bohnhoff, W.J., Dalbey, K.R., Eddy, J.P., Eldred, M.S., Gay, D.M., Haskell, K., Hough, P.D., and Swiler, L.P. (2009). "DAKOTA, A Multilevel Parallel Object-Oriented Framework for Design Optimization, Parameter Estimation, Uncertainty Quantification, and Sensitivity Analysis: Version 5.0 User's Manual." *Sandia Technical Report SAND2010-2183*, Sandia National Laboratories, Albuquerque, NM.

Akesson, B. (2008). *Understanding Bridge Collapses*, Taylor and Francis, London, UK.

Altay, A.K., Arabbo, D. S., Corwin, E. B., Dexter, R. J., French C.E. (2003). "Effects of Increasing Truck Weight on Steel and Prestressed Bridges." *Final Report 2003-16*, Mn/DOT, St. Paul, MN, 129 pp.

American Association of State Highway and Transportation Officials (AASHTO). (2008). *Manual for Bridge Evaluation*, 1st Ed., AASHTO, Washington, DC.

AASHTO. (2010). *LRFD Bridge Design Specifications*, 5th Ed., AASHTO, Washington, D.C.

American Society of Civil Engineers (ASCE). (2013). *2013 Report Card for America's Infrastructure.* Reston, VA.

Andrawes, B., DesRoches, R. (2005). "Unseating Prevention for Multiple Frame Bridges using Superelastic Devices." *Smart Mater. Struct.*, **14**(3), S60-S67.

Berglund, E., Schultz, A.E. (2002) "Analysis Tools and Rapid Screening Data for Assessing Distortional Fatigue in Steel Bridge Girders." *Final Report 2002-06*, Mn/DOT, St. Paul, MN, 94 pp.

Biezma, M.V., Schanack, F. (2007). "Collapse of Steel Bridges." *J. Perform. Constr. Facil.*, **21**(5), 398-405.

Billah, K.Y., Scanlon, R.H. (1991). "Resonance, Tacoma Narrows Bridge Failure, and Undergraduate Physics Textbooks." *Am. J. Phys.*, **59**(2), 118-124.

Bolandhemmat, H., Clark, C.M., Golnaraghi, F. (2010). "Development of a systematic and practical methodology for the design of vehicles semi-active suspension control system." *Vehicle Syst. Dyn.*, **48**(5), 567-585.

Carlson, J.D., Catanzarite, D.M., St. Clair, K.A., (1996). "Commercial magneto-rheological fluid devices." *Int. J. Mod. Phys. B.*, **10**(23-24), 2857-2865.

Cheng, F. Y., Jiang, H., Lou, K. (2008). *Smart Structures - Innovative Systems for Seismic Response Control*, CRC Press, Boca Raton, FL, 652 pp.

Christenson et al. 2009. Unpublished Manuscript. University of Connecticut. Private Communication.

Chung, H.-Y., Manuel, L. and Frank, K.H. (2003). "Reliability-Based Optimal Inspection for Fracture-Critical Steel Bridge Members," Paper No. 03-4296, *Transportation Research Record*, Vol. 1845.

Das, A. K., Dey, S. S. (1992). "Effects of tuned mass dampers on random response of bridges." *Comput. Struct*., **43**(4), 745-750.

Dyke, S.J., Spencer, B.F., Sain, M.K., Carlson, J.D. (1996). "Modeling and control of magnetorheological dampers for seismic response reduction." *Smart Mater. Struct*., **5**(5), 565-575.

Enright, M. P., Frangopol, D. M. (2000). "Survey and Evaluation of Damaged Concrete Bridges." *J. Bridge Eng.*, **5**(1), 31-38.

Erkus, B., Abé, M., Fujino, Y. (2002) "Investigation of semi-active control for seismic protection of elevated highway bridges." *Eng. Struct*., **24**(3), 281-293.

Federal Highway Administration (FHWA). (2012). "Deficient Bridges by State and Highway System 2012." <http://www.fhwa.dot.gov/bridge/nbi/no10/defbr12.cfm> (Oct. 2, 2013).

Fisher, J. W., Kaufmann, E. J., Wright, W., Xi, Z., Tjiang, H., Sivakumar, B., Edberg, W. (2001). "Hoan Bridge forensic investigation failure analysis." *Final Report*. Wisconsin Department of Transportation and FHWA.

Fryba, Ladislav. (1999). *Vibration of Solids and Structures under Moving Loads*. Thomas Telford Ltd., Prague, Czech Republic.

Gastineau, A. J., Johnson, T., Schultz, A. E. (2009). "Bridge Health Monitoring and Inspection Systems - A Survey of Methods," *Final Report 2009-29*, Mn/DOT, St. Paul, MN, 194 pp.

Gastineau, A.J., Wojtkiewicz, S.F., Schultz, A.E. (2011a). "Fatigue Life Extension of Vulnerable Steel Bridges using a Response Modification Approach," *Proceedings of the 8th International Conference on Structural Dynamics, EURODYN 2011*, Leuven, Belgium, July 4-6, 2011.

Gastineau, A., Wojtkiewicz, S., Schultz, A. (2011b). "Innovative Technologies for Lifetime Extension of an Aging Inventory of Vulnerable Bridges," *Final Report CTS 11-27*, Center for Transportation Studies, University of Minnesota, 28 pp.

Gastineau, A., Schultz, A., Wojtkiewicz, S. (2011c). "Response Modification for Enhanced Operation and Safety of Bridges," *Final Report CTS 11-14*, Center for Transportation Studies, University of Minnesota, 54 pp.

Gastineau, A.J., Wojtkiewicz, S.F., and Schultz, A.E. (2012a). "Response Modification Approach for Safe Extension of Bridge Life." *J. Bridge Eng.*, **17**(4), 728-732.

Gastineau, A.J., Wojtkiewicz, S.F., Schultz, A.E. (2012b). "Extending the fatigue life of steel bridges using a response modification system," *Proceedings of Structural Faults and Repair 2012*, Edinburgh, Scotland, 3-5 July.

Gastineau, A.J., Wojtkiewicz, S.F., and Schultz, A.E. (2013). "Lifetime Extension of a Realistic Model of an In-Service Bridge through a Response Modification Approach." *J. Eng. Mech.*, Advance online publication. doi: 10.1061/(ASCE) EM.1943-7889.0000611

Green, D., Unruh, W.G. (2006). "The Failure of the Tacoma Bridge: A Physical Model." *Am. J. Phys*., **74**(8), 706-716.

Hao, S. (2010). "I-35W Bridge Collapse." *J. Bridge Eng.*, **15**(5), 608-614.

Hilber, H.M, Hughes, T.J.R., Taylor, R.L. (1977). "Improved Numerical Dissipation for Time Integration Algorithms in Structural Dynamics." *Earthquake Eng. Struct. Dyn.*, **5**, 282-292.

Housner, G., Bergman, L., Caughey, T., Chassiakos, A., Claus, R., Masri, S., Skelton, R., Soong, T., Spencer, B., and Yao, J. (1997). ”Structural Control: Past, Present, and Future.” *J. Eng. Mech.*, **123**(9), 897–971.

Jajich, D., Schultz, A.E., Bergson, P. M., Galambos, T. V. (2000). “Distortion-Induced Fatigue in Multi-Girder Steel Bridges.” *Final Report 2000-16*, Mn/DOT, St. Paul, MN, 283 pp.

Johnson, K. (2013). "Washington State Bridge Collapse Could Echo Far Beyond Interstate." *The New York Times*. <www.nytimes.com> (Oct. 4, 2013).

Keating, P.B., Fisher, J.W. (1986). "Evaluation of Fatigue Tests and Design Criteria on Welded Details." NCHRP Report 286, Transportation Research Board, National Research Council, Washington D.C., 66 pp.

Kim, J. M., Feng, M. Q., Shinozuka, M. (2000). “Energy dissipating restrainers for highway bridges,” *Soil Dyn. Earthq. Eng.*, **19**(1), 65-69.

Larsen, A. (2000). "Aerodynamics of the Tacoma Narrows Bridge: 60 Years Later." *Struc. Eng. Intern.*, **10**(4), 243-248.

Lee, H.S., Choi, S.B. (2000). "Control and response characteristics of magneto-rheogical fluid damper for passenger vehicles." *J. Intel. Mat. Syst. and Str.*, **11**(1), 80-87.

Lewis, P. R., Reynolds, K. (2002). "Forensic engineering: A reappraisal of the Tay Bridge disaster." *Interdiscipli. Sci. Rev.*, **29**(2), 177-191.

Li, H., Schultz, A. E. (2005). “Rapid Assessment of Girder Differential Deflection and Distortional Fatigue Stress in Multi-Girder Steel Bridges.” *Final Report 2005-38*, Mn/DOT, St. Paul, MN, 130 pp.

Liao, M., Okazaki, T., Ballarini, R.., Schultz, A. E., Galambos, T.V. (2011). **“**Nonlinear finite-element analysis of critical gusset plates in the I-35W bridge in Minnesota.” *J. Struct. Eng.*, **137**(1), 59-68.

Lichtenstein, A., (1993). “The Silver Bridge collapse recounted.” *J. Perform. Constr. Fac.*, **7**(4), 249-261.

Lindberg, A. Y., Schultz, A. E. (2007). “Incorporation of Fatigue Detail Classification of Steel Bridges into the Minnesota Department of Transportation Database.” *Final*

Report 2007-22, Minnesota Department of Transportation (Mn/DOT), St. Paul, MN, 191 pp.

Lindblom, M. (2013). "NTSB Update: Trucker in Bridge Collapse Felt Crowded, Moved Right." *The Seattle Times.* < www.seattletimes.com > (Oct. 4, 2013).

MATLAB Release 2011a, The MathWorks, Inc., Natick, Massachusetts, United States.

Mertz, D. (2012). "Steel Bridge Design Handbook: Design for Fatigue." *Technical Report FHWA-IF-12-052 – Vol. 12*, FHWA, Washington D.C., 31 pp.

Miao, T. J., Chan, T. H. T. (2002). "Bridge Live Load Models from WIM Data." *Eng. Struct.*, **24**(8), 1071–1084.

Miller, R., Masri, S., Dehghanyar, T., Caughey, T. (1988). "Active vibration control of large structures." *J. Eng. Mech.*, **114**(9), 1542-1570.

Miner, M. A. (1945). "Cumulative Damage in Fatigue." *J. Appl. Mech.*, **12**(3), A159-A164.

Moses, F., Schilling, C.G., Raju, K.S. (1987). "Fatigue Evaluation Procedures for Steel Bridges." NCHRP Report 299, Transportation Research Board, National Research Council, Washington D.C., 94 pp.

Nowak, A. (1991). "Bridge Live-Load Models." *J. Struct. Eng.*, **117**(9), 2757-2767.

Nowak, A. (2003). "Bridge Load Models." *Proceedings of the 2003 ASCE/SEI Structures Congress and Exposition: Engineering Smarter,* May 29-31, ASCE-SEI.

O'Conner, J. S. (2000). "Bridge Safety Assurance Measures Taken in New York State." *Transport. Res. Rec.*, **1696**, 187-192.

Patten, W. N., Sack, R. L., He, Q. (1996). "Controlled Semiactive Hydraulic Vibration Absorber for Bridges." *J. Bridge Eng.*, **122**(2), 187-192.

Patten, W.N., Sun, J., Song, G. (1998). "Prototype Testing of Intelligent Stiffener for Bridges at I-35 Walnut Creek Bridge." *Transport. Res. Rec.*, **1624**, 160-165.

Patten, W. N., Sun, J., Li, G., Kuehn, J., Song, G. (1999). "Field Test of an Intelligent Stiffener for Bridges at the I-35 Walnut Creek Bridge." *Earthquake Eng. Struct. Dyn.*, **28**(2), 109-126.

Petroski, H. (2007). "Engineering: Why Things Break." *Am. Sci.*, **95**(3), 206-209 .

Petroski, H. (2009). "Tacoma Narrows Bridges." *Am. Sci.*, **97**(3), 103-107.

Phares, B. M., Wipf, T. J., Greimann, L. F., Lee, Y. (2005a). “Health Monitoring of Bridge Structures and Components Using Smart-Structure Technology - Volume I”. *Final Report WHRP-05-03*, Wisconsin Department of Transportation (WisDOT), Madison, WI, 53 pp.

Phares, B. M., Wipf, T. J., Greimann, L. F., Lee, Y. (2005b). “Health Monitoring of Bridge Structures and Components Using Smart-Structure Technology - Volume II”. *Final Report WHRP-05-03*, WisDOT, Madison, WI, 202 pp.

Przemieniecki, J.S., (1968). *Theory of Matrix Structural Analysis*. McGraw-Hill, New York, NY.

"Quebec Bridge Disaster." (1908). *The Engineering Record*, **57**, 504-510.

Reissner, H. (1943). "Oscillations of Suspension Bridges." *T. ASME* **65**, A23-A32.

Richland Engineering Limited. “Truss Gusset Plate Failure, Analysis, Repair and Retrofit: Interstate 90 Bridge over Grand River.” *Final Report*, 15 Apr 1997.

SAP2000 v14.2.3, Computers and Structures, Inc., Berkeley, California, United States.

Schilling, C.G., Klippstein, K.H., Barsom, J.M., Blake, G.T. (1978). "Fatigue of Welded Steel Bridge Members Under Variable-Amplitude Loadings." NCHRP Report 188, Transportation Research Board, National Research Council, Washington D.C., 113 pp.

Schultz, A.E., Thompson, D.J. (2010). “Development of an Advanced Structural Monitoring System.” *Final Report 2010-39*, Mn/DOT, St. Paul, MN, 66 pp.

Severtson, B., Beukema, F., Schultz, A. E. (2004). “Rapid Assessment of Distortional Stresses in Multi Girder Steel Bridges.” *Final Report 2004-48*, Mn/DOT, St. Paul, MN, 134 pp.

Sigaher, A., Constantinou, M. (2003). “Scissor-Jack-Damper Energy Dissipation System.” *Earthquake Spectra*, **19**(1), 133–158.

Simulink 7 Reference Accessed June 2010 <http://www.mathworks.com/help/pdf_doc/simulink/slref.pdf>

Siwiecki, K. J., Derby, T. F. (1972). “The full-scale experimental verification of an analytical model for evaluating methods of suppressing excessive bridge vibrations.”

Tech. Rep. DOT-FH-11-7799, U.S. Dept. of Transportation, Washington, D. C., 149 pp.

Soong, T., Spencer, B., (2002). "Supplemental energy dissipation: state-of-the-art and state-of-the-practice." *Eng. Struct.*, **24**(3), 243–259.

Spencer, B.F., Dyke, S.J., Sain, M.K., Carlson, J.D. (1997). "Phenomenological model of a magnetorheological damper." *J. Eng. Mech.*, **123**(3), 230-238.

Spencer, B.F., Nagarajaiah, S., (2003). "State of the Art of Structural Control." *J. Struct. Eng.*, **129**(7), 845-856.

Subramanian, N. (2008). "I-35W Mississippi River Bridge Failure - Is it a Wake Up Call?" *Indian Concrete Journal.*, **82**(2), 29-38.

Symans, M.D., Constantinou, M.C. (1999) "Semi-active control systems for seismic protection of structures: a state-of-the-art review." *Eng. Struct.*, **21**(6), 469-487.

Takamori, H., Fisher, J.W., (2000). "Tests of large girders treated to enhance fatigue strength." *Transport. Res. Rec.*, **1696**, 93-99.

Vukobratovic, M. K. (2000). "Active structures in advanced engineering – an overview," *Int. J. Comput. App. T.*, **13**(1-2), 10-24.

Yang, G., Spencer, B., Carlson, J., Sain, M. (2002). "Large-scale MR fluid dampers: modeling and dynamic performance considerations," *Eng. Struct.*, **24**(3), 309-323.

Yang, J.N., Agrawal, A.K. (2002). "Semi-active hybrid control systems for nonlinear buildings against near-field earthquakes." *Eng. Struct.*, **24**(3), 271-280.

Yao, James T.P., (1972) "Concept of Structural Control." *J. Struct. Div.*, **98**(7), 1567-1574.